UNIVERSITÀ DI PISA

SCUOLA DI DOTTORATO IN INGEGNERIA "LEONARDO DA VINCI"

Corso di Dottorato di Ricerca in

Ingegneria Industriale (A) - Programma:

INGEGNERIA NUCLEARE E SICUREZZA INDUSTRIALE

Tesi di Dottorato

(SSD: ING/IND 25)

DEVELOPMENT OF VULNERABILITY MODELS FOR INDUSTRIAL EQUIPMENT EXPOSED TO NATURAL PHENOMENA

PhD Student:

Giuseppa ANCIONE

Tutors:

Prof.ssa Maria Francesca MILAZZO

Prof. Giuseppe MASCHIO

Cycle XXVII ---- Years: 2012 - 2014

“La logica ti porta da A a B.
L'immaginazione ti porta ovunque.”
Albert Einstein

ABSTRACT

Natural events can be the indirect cause of technological accidents with severe consequences for human beings and the environment. In the literature, these events are also known as Na-Techs (i.e. technological events triggered by natural causes). Na-Techs may damage structures, infrastructures, chemical industries, utility distribution networks (lifelines), etc. The overall magnitude could be much greater than that of the natural event. A great concern is also related to other aspects, such as the potential overloading of the emergency response and/or the unavailability of essential utilities (water, electricity, etc.).

This thesis aimed at the investigation of volcanic Na-Tech scenario and the definition of vulnerability models, which allow implementing the Quantitative Risk Assessment procedure to include volcanic Na-Tech and identifying malfunctions in wastewater treatment. The main focus was on a particular volcanic hazard, i.e. volcanic ash fallout, whose impact covers large areas, in same case a continental dimension.

The results of this study permitted also the definition of semi-automatic procedures for the production of the vulnerability maps by using a GIS (Geographical Information System) software.

After the development of vulnerability models of some industrial equipment, it was possible to investigate a case-study, which was the surrounding of Mt. Etna (Italy).

Contents

1 INTRODUCTION 1

1.1 NATURAL TECHNOLOGICAL ACCIDENTS 1

1.2 FACTORS AFFECTING DYNAMICS OF NA-TECHS 2

1.3 EUROPEAN AND GLOBAL FRAMEWORK IN NA-TECH RISK 3

1.4 STATE OF THE ART OF NA-TECHS 4

1.4.1 VOLCANIC NA-TECHS 5

1.5 DISSERTATION OBJECTIVES AND OUTLINE 6

2 VOLCANIC HAZARDS 7

2.1 VOLCANIC ERUPTIONS 7

2.1.1 EXPLOSIVE ERUPTION 9

2.1.1.1 Pyroclastic flow 9

2.1.1.2 Volcanic ash emission 9

2.1.2 EFFUSIVE ERUPTION 10

2.1.2.1 Lava flow 10

2.2 OTHER TYPES OF VOLCANIC ACTIVITY 11

2.2.1 LAHAR 11

2.2.2 TSUNAMI 11

2.2.3 EARTHQUAKE 12

3 APPROACHES FOR EQUIPMENT VULNERABILITY MODELLING 13

3.1 DETERMINISTIC APPROACH 14

3.2 PROBABILISTIC APPROACH 14

3.3 SEMI-PROBABILISTIC APPROACH 15

3.4 UNCERTAINTY 15

3.5 EQUIPMENT VULNERABILITY MODELLING TO DAMAGE DUE TO VOLCANIC ASH FALLOUT 15

3.6 RISK ASSESSMENT FRAMEWORK 16

4 EQUIPMENT VULNERABILITY MODELS 19

4.1 ATMOSPHERIC STORAGE TANKS 19

4.1.1 FIXED ROOF TANKS 20

4.1.2 FLOATING ROOF TANKS 20

4.2 AIR INTAKE FILTERS 21

4.3 WASTEWATER TREATMENTS 23

4.3.1 SCREENS 25

4.3.2 GRIT CHAMBERS 26

4.3.2.1 Horizontal flow grit chambers 27

4.4 FAILURE MODES OF FIXED ROOF TANKS 27

4.5 FAILURE MODES OF FLOATING ROOF TANKS 27

4.5.1 SINKING A FLOATING ROOF 28

4.5.2 CAPSIZING A FLOATING ROOF 28

4.6 FAILURE MODES OF AIR INTAKE FILTERS 30

4.7 FAILURE MODES IN WASTEWATER TREATMENTS 31

4.7.1 CONDITIONS FOR THE SCREEN CLOGGING 32

4.7.2 CONDITIONS FOR THE INCOMPLETE PARTICLES REMOVAL IN HORIZONTAL FLOW GRIT CHAMBERS 34

4.8 EXCEEDANCE PROBABILITY CURVES 39

5 VULNERABILITY MAPPING AND EMERGENCY MANAGEMENT PROCEDURES 40

5.1 GEOGRAPHIC INFORMATION SYSTEM 40

5.1.1 GEOPROCESSING 41

5.2 EXCEEDANCE PROBABILITY 42

5.3 APPROACHES FOR THE VULNERABILITY MAPPING 42

5.3.1 SPATIAL INTERPOLATION METHODS 42

5.3.2 SEMI-AUTOMATIC PROCEDURE FOR VULNERABILITY MAPPING 43

5.4 PROCEDURE FOR EMERGENCY MANAGEMENT 44

6 CASE STUDY 46

6.1 CHARACTERISATION OF THE NATURAL PHENOMENON 47

6.2 CENSUS OF THE VULNERABLE ELEMENTS 47

6.3 CHARACTERISTICS OF FLOATING ROOF STORAGE TANKS 50

6.4 CHARACTERISTICS OF AIR INTAKE FILTERS 50

6.5 CHARACTERISTICS OF SCREENS 51

6.6 CHARACTERISTICS OF GRIT REMOVALS 52

6.7 VOLCANIC ASH SAMPLES COLLECTION 52

7 ASH CHARACTERISATION 54

7.1 ANALYSIS OF THE SIZE DISTRIBUTION 54

7.2 DENSITY DETERMINATION 55

7.3 SPECIFIC SURFACE AREA AND VOIDAGE DETERMINATION 55

7.4 DETERMINATION OF THE PERMEABILITY 57

8 RESULTS AND DISCUSSIONS 58

8.1 ASH CHARACTERISATION RESULTS 58

8.1.1 GRAIN SIZE DISTRIBUTIONS 58

8.1.2 DENSITY 60

8.1.3 SPECIFIC SURFACE AREA AND VOIDAGE 60

8.1.4 PERMEABILITY 63

8.2 THRESHOLD LIMIT FOR ATMOSPHERIC FIXED ROOF STORAGE TANKS 63

8.3 THRESHOLD LIMIT FOR FLOATING ROOF STORAGE TANKS 64

8.4 THRESHOLD LIMITS FOR AIR INTAKE FILTERS 67

8.5 EXCEEDANCE PROBABILITY CURVES AND VULNERABILITIES 67

8.6 VULNERABILITY MAPS 69

8.7 SCREENING CLOGGING: CONDITIONS 77

8.7.1 CRITICAL ASH DEPOSIT ON FINE SCREENS 78

8.7.2 DISCUSSION 81

8.8 INCOMPLETE GRIT REMOVAL 81

8.8.1 FRACTION OF SETTLED PARTICLES 83

8.8.2 DISCUSSION 86

9 CONCLUSIONS 88

9.1 POTENTIAL FUTURE DEVELOPMENTS 90

REFERENCE 91

ANNEX 1 LIST OF PUBLICATIONS PRODUCED DURING THE DOCTORATE COURSE (2012-2014) 96

ANNEX 2 TABLES 99

ANNEX 3 FIGURES 100

ANNEX 4 SYMBOLS 103

1

Introduction

1.1 Natural Technological accidents

Natural events can be the indirect cause of technological accidents with severe consequences for human beings and the environment, particularly in areas that are not prepared to cope with this type of emergency. In the literature, these events are also known as Na-Tech accidents or simply Na-Techs (i.e. technological events triggered by natural causes). Na-Techs may damage structures, infrastructures, industries, utility distribution networks (lifelines), etc. The overall magnitude could be much greater than that of the natural event. A great concern is also related to other aspects, such as the potential overloading of the emergency response and/or the unavailability of many essential utilities (water, electricity, etc.). Past catastrophic events highlighted the high destructive potential of a Na-Tech, some of them are mentioned below.

The accident at the Fukushima nuclear power stations in Japan was caused by an earthquake/tsunami in 2011 and caught the worldwide attention. The main failure was due to the malfunction of the pumping system of the cooling water to the reactors [1]. The earthquake also caused a fire in the Chiba oil refinery. Another significant event occurred during the Kocaeli earthquake in 1999; according to Girgin [2], the disaster hit one of the most industrialized regions of Turkey and, amongst the numerous Na-Techs, the author reported about the massive fire at the TÜPRAŞ refinery and the acrylonitrile spill at the AKSA acrylic fibre production plant. In 2005, following to the hurricane Katrina, a huge number of releases of hazardous materials occurred from over 300 chemical facilities, moreover hundreds of miles of oil and gas pipelines were displaced or broken (inland and offshore). In the Czech Republic in 2002, a flood originated a chlorine release; during the

same year, in the Southern France another flood damaged some industrial facilities with several releases of hazardous materials [3].

In some cases, even modest natural events also caused Na-Techs: as reported by many local newspapers, during some floods, occurred in autumn and winter in 2008-2012 in Sicily (Italy), several refinery shutdowns were necessary to prevent and mitigate the damage due to the overloading of the water treatment lines, which in some cases resulted in soil and groundwater contamination.

1.2 Factors affecting dynamics of Na-Techs

There is currently a little knowledge about dynamics of Na-Techs; nevertheless the potential of damage is aggravated, in some cases, by climate changes and the increasing society's vulnerability [4].

According to EPA [5] and the American Academies [6], climate changes prior to the Industrial Revolution in the 1700s can be explained by natural causes, such as changes in solar energy, volcanic eruptions and natural changes in greenhouse gas (GHG) concentrations, whereas recent climate changes (especially the global warming) cannot be explained by natural causes alone.

The vulnerability of civil societies refers to the inability of people, organizations and societies to withstand adverse impacts from multiple stressors to which they are exposed (i.e. natural hazards and anthropogenic activities). As shown in the literature, the conceptualisation and the measurement of the vulnerability are object of intense debate. Some definitions are reported below [7]:

- Vulnerability is the threat to which people are exposed (including chemical agents and the ecological situation of the communities and their level of emergency preparedness) (Gabor and Griffith, 1980);
- Vulnerability is the degree to which a system acts adversely to the occurrence of a hazardous event. The degree and quality of the adverse reaction are conditioned by a system's resilience (a measure of the system's capacity to absorb and recover from the event) (Timmerman, 1981);
- Vulnerability is the degree of loss to a given element or set of elements at risk (UNDRO, 1982; Mitchell, 1989);
- Vulnerability is the capacity to suffer harm and react adversely (Kates, 1985);
- Vulnerability is the threat or interaction between risk and preparedness (Pijawka and Radian, 1985);

- Vulnerability is operationally defined as the inability to take effective measures to insure against losses. When applied to individuals vulnerability is a consequence of the impossibility or improbability of effective mitigation and is a function of ability to detect the hazards (Bogard, 1989);
- Vulnerability refers to exposure to contingencies and stress and difficulty in coping with them (Chambers, 1989);
- Vulnerability is defined in terms of exposure, capacity and potentiality. Accordingly, the prescriptive and normative response to vulnerability is to reduce exposure, enhance coping capacity, strengthen recovery potential and bolster damage control (Watts and Bohle, 1993);
- Vulnerability is the differential capacity of groups and individuals to deal with hazards based on their positions within physical and social worlds (Dow, 1992);
- Vulnerability is the differential susceptibility to damage due to different contributing circumstances (biophysical, demographic, economic, social and technological factors) (Dow and Downing, 1995);
- Vulnerability is conceived as both a biophysical risk as well as a social response, but within a specific geographic domain. This can be geographic space (where vulnerable people and places are located) or social space (who in those places is most vulnerable) (Cutter, 1996).

At a glance, the vulnerability of a system is usually described by combining the susceptibility (inherent propensity to damage) and the resilience (propensity to deal with the emergency and the recovery of normal activity) of the territory [8].

1.3 European and global framework in Na-Tech risk

In the European framework there is not specific legislation or any type of guideline regarding risk assessment and management of Na-Techs. Nevertheless there are several laws indirectly mentioning such aspects, through the rules governing industrial establishments handling hazardous materials, landfill sites and waste treatment plants [9]. Regulations for managing operations in lifeline systems (such as electrical power plants, gas and oil pipelines, etc.) also indirectly concern to the Na-Tech risk reduction. For instance, the Seveso Directives specifically refer to the prevention of major accidents in the chemical plant [10-13] and even if these laws do not include specific requirements for Na-Tech management, they indirectly address them. Indeed, the legislation calls for the analysis of “external events” which may lead to chemical releases, this obviously implies also the consideration of the potential threat due to natural hazards. However, these

Directives do not specify the methodologies or the actions to be taken, as a consequence the levels of response preparedness vary among European countries. A summary of how various EU countries are currently facing to Na-Tech events is given in [9].

1.4 State of the art of Na-Techs

There are few studies in the literature analysing Na-Tech events, whereas several works report about natural and technological accidents as separate events. Showalter and Myers in 1994 [14] gave the first investigation of Na-Tech events; they carried out a survey to determine the number of technological scenarios triggered by natural catastrophic events during the period 1980-1989 in the United States and found that the majority of Na-Techs were triggered by earthquakes, followed by hurricanes, floods, lightning, winds and storms. Authors also observed an increasing trend of Na-Techs during the analysed period due to different causes: (1) the increasing industrialization and urbanization of the territory, (2) climate changes, etc. Such elements also increased the awareness about these events and concurred to consider these scenarios as emerging risks. The identification of the areas that are susceptible to Na-Techs, the development of specific mitigation and emergency response plans and the implementation of existing ones were recommended.

Following the Northridge earthquake in California in 1994, Lindell and Perry [15] found that the 19% of Na-Techs gave a release of dangerous substances. Cruz et al. in 2001 [16] identified potential Na-Tech scenarios from petroleum refineries under the impact of hurricanes, flooding and lightning; they found that these phenomena could trigger multiple and simultaneous hazardous releases. Steinberg and Cruz in 2004 [17] studied Na-Techs that occurred during the 1999 Turkey earthquake; they identified more than 21 releases of hazardous materials triggered by the natural phenomenon, 8 of these resulted in major consequences and impacted outside the confines of the establishments. These required the evacuation of thousands of residents and resulted in the abandonment of search and rescue operations for earthquake victims. The authors concluded that risk management and emergency response planning is a complex issue since it is necessary to take into account that the natural phenomenon may cause the simultaneous loss of electrical power and water, the failures of mitigation systems, the impediment of emergency responses, the potential simultaneous occurrence of numerous releases of hazardous substances, etc.

Lindell and Perry [18] stated that the level of disaster preparedness is correlated with the level and completeness of vulnerability assessments. In spite of this Cruz et al. [9] reported that, many countries have natural hazards but none appear to have Na-Tech vulnerability

maps. These statements suggest improving the knowledge about the vulnerability of industrial facilities and developing vulnerability maps as a tool for decision making.

1.4.1 Volcanic Na-Techs

Amongst natural events, which trigger technological disasters, volcanic eruptions should also be mentioned, even if before the recent volcanic eruption of the Mt. Eyjafjallajökull (Iceland) in 2010, only few studies focused on the impact of such destructive phenomena. This Section provides a brief review.

Blong [19] in 1984 gave a list of volcanic hazards and related effects on human health, buildings, agriculture, anthropogenic activity, etc, whereas Spence et al. [20] assessed the vulnerability of buildings under the impact of ash fallout. Self [21] listed the following potential consequences of eruptions [22]:

- *roof collapses* – the effect extends also to distances where ash fallout is a few centimetres and it could be exacerbated if rain occurs.
- *agriculture disruption* – this effect occurs at least a growing season over most of area receiving ash fallout, it also determines long term beneficial changes due to increased soil fertility.
- *contamination of drinking water and problems in waste disposal* – potential problems associated with water supply, such as blockage of sewage, etc.
- *problems in aviation* – aircrafts could have visibility problems for landing and take-off, damages on aircraft engines and instrumentation during the flight.
- *damage of power generation* (thermal, wind and photo-voltaic installations).
- *damage of power distribution* – electric pylons and power-lines might be susceptible to ash loading and associated electrostatic effects, possibly exacerbated by wet fallout.
- *health risk* – due to climate change, dry-fog and acid aerosol air pollution and ozone depletion.

Rasà et al. [23] gave a qualitative description of some consequences of ash fallout, such the damage due to the load on the roof of buildings, the clogging of gutters and the abrasion of moving parts of machines and electric motors. Baxter et al. [24] and Scandone et al. [25] analysed malfunctions of water treatments (industrial or civil installations) and accidents during the transportation of hazardous materials due to the slippery roads. Wilson et al. [26] discussed about the impact of volcanic ash on critical infrastructure, such as the electrical distribution networks and the civil aviation system. Zais [27] reported about the catastrophic impact on the wastewater treatment plants of the Mt. St. Helens eruption

(1980). In 2010, Milazzo and co-author's [22] began studying Na-Techs triggered by ash fallout and to analyse their impact on atmospheric storage tanks.

Potential volcanic Na-Techs could also be triggered by workers affected by the impact of the volcanic event while executing their works in the establishment close to the volcano.

1.5 Dissertation objectives and outline

This research aimed at the:

- extention of Na-Tech Risk analysis with particular attention to volcanic Na-Tech and the definition of vulnerability models;
- implementation of the standard QRA (Quantitative Risk Assessment) procedure to include volcanic Na-Tech;
- Definition of methods for the identification of malfunctions in wastewater treatment under the impact of volcanic phenomena;
- definition of semi-automatic procedures for the production of the vulnerability maps using a GIS software.

The performed activities can be summarised in the following. First the vulnerability was modelled according to two tiers:

- a deterministic approach based on threshold value of physical parameters;
- a semi-probabilistic approach founded on exceedance probability of threshold limit of physical parameters.

The following step was the selection of some vulnerable elements: storage tanks, filters and lifeline (screens and grit removals of wastewater treatment plants). These were analysed in details The ash fallout was the natural phenomenon investigated in this thesis, this natural phenomenon was characterised.

Finally, after the development of vulnerability models and their application, it was possible:

- the risk analysis of facilities at major risk;
- the analysis of the condition causing the damage/malfunction for lifelines;
- the development of procedures for emergencies' management;

All the developed procedures were implemented and properly automated into a GIS (Geographical Information System). To this scope, the ArcGIS software of ESRI was used.

2

Volcanic Hazards

After an eruption, several volcanic phenomena can occur, whose impact on the territory is a potential hazard as it negatively affect human health and cause damage for structures and infrastructure. This Section gives a brief overview on volcanic hazards, amongst them one was selected to be analysed as potential initial cause of Na-Techs.

2.1 Volcanic eruptions

A volcano (Figure 2.1) is a rupture on the Earth's crust that allows lava, volcanic ash and gases escaping from the magma chamber below the surface (eruption).

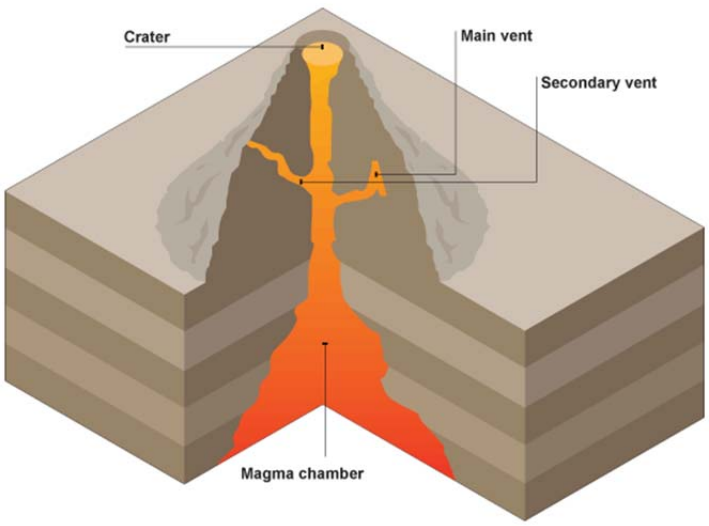

Figure 2.1. Representation of a volcano [28]

The eruption occurs when the pressure in the magma chamber forces magma up to the crater. Some magma will also be forced out from the secondary vents which can be at the side of the volcano [28].

Two main types of volcanic activity exist (Figure 2.2): explosive, causing the emission of fragmented material (pyroclastic flow or ash cloud) and effusive, which produces lava flows.

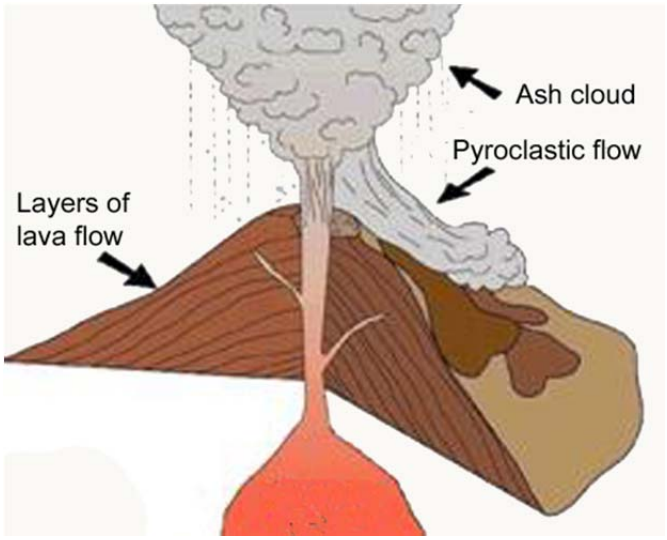

Figure 2.2. Volcanic activity types [29].

In general, eruptive scenarios are classified according to the *Volcanic Explosivity Index* (VEI) [30], which is a common used criterion to describe the severity of volcanic eruptions. The VEI takes into account the volume of ejected material, the column height and the duration of the phenomenon [31]. Figure 2.3 illustrates the VEI classification, each eruption may be assigned a VEI between 0 and 8. Eruptions with VEI ≤ 3 usually involve lava flows and/or minor explosive activity and their effects are generally localised. Events with VEI 4 or 5 often disrupt regional economies, while eruptions of VEI over 6 may impact on the global climate.

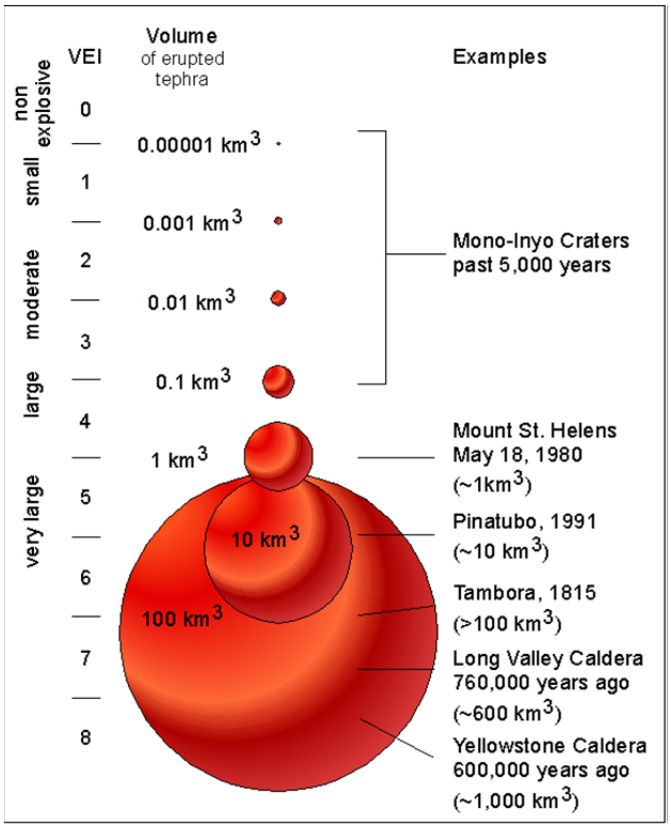

Figure 2.3. Volcanic Explosivity Index (VEI) scheme [32].

2.1.1 Explosive eruption

Explosive eruptions occur when a cooler and more viscous magma reaches the surface. Dissolved gases cannot easily escape, thus pressure may build up until gas explosions blast rock and lava fragments into the air.

2.1.1.1 *Pyroclastic flow*

The most powerful volcanic eruption gives a pyroclastic flow. It is a fast-moving current of hot gas and rock, which reaches speeds up to 700 km/h, the gas can reach temperatures of about 1000°C. Pyroclastic flows normally travel downhill or spread laterally under gravity. Their speed depends upon the density of the current, the volcanic output rate and the slope. This type of eruption took place at Vesuvius in Italy in 79 a.d.

2.1.1.2 *Volcanic ash emission*

Volcanic ash emission is produced by explosive eruptions. The diameter of particles is smaller than 2 mm (<0.063 mm for fine ash and between 0.063 and 2 mm for coarse). Depending on the velocity of formation, the ash is made of various proportions of glassy (non-crystalline), crystalline and lithic particles. The density may vary within the following

ranges: 700 ÷ 1,200 kg/m^3 for pumice, 2,350 ÷ 2,450 kg/m^3 for glass shards, 2,700 ÷ 3,300 kg/m^3 for crystals, and 2,600 ÷ 3,200 kg/m^3 for lithic particles [33]. Denser particles are deposited close to the crater, fine glassy material and pumice shards fall at distal locations.

The abrasiveness of the volcanic ash is a function of the material's hardness and the shape of particles. Small voids are typically contained in glassy particles, these are known as vesicles and are formed by the expansion of magmatic gas before the magma solidification. Ash particles have a varying degree of voids, which gives them an extremely high surface area to volume ratios.

Volcanic particles naturally tend to bind giving aggregates. As reported by volcanologists [34], the information on the aggregation processes are still either lacking or very incomplete. It seems that for dry particles electrostatic or van der Waals forces lead to successful coalescence, although such dry clusters are weakly bound and quickly collapse landing on the ground. In presence of water (such as the rain) much stronger particle bonds result from short-range surface tension forces. The presence of dissolved salts establishes more durable aggregations, when evaporation leads to enhanced concentrations, crystal bridges greatly increase the strength of the inter-particle bonds.

2.1.2 Effusive eruption

Effusive eruptions occur when magma goes upward the magma chamber, reaches the surface and dissolved gases easily escapes. The consequence of an effusive eruption is a lava flow.

2.1.2.1 *Lava flow*

Lava flow is the moving of the molten rock expelled by a volcano during an eruption with a low VEI, simply named effusive eruption. How far a lava flow travels depends on the flows temperature, silica content, extrusion rate and land slope. A cold lava flow will not travel far, neither that one having high silica content; such a flow would have a high viscosity (a high resistance to flow). A basalt flow (like those originated from eruptions in Hawaii) has low silica contents and low viscosities, thus it can flow for long distances and have a thickness of 10 m. Whereas, more silica-rich flows can move at rates of a few to hundreds meters per hour and have thicknesses of several tens of meters. If a lava flow is channelised or travels underground in a lava tube then the distance it travels is greatly extended [35].

Hence lava flows appear less dangerous for human life than other volcanic hazards; the impact on structures, traffic and communication are also even more manageable because the slow movement of the flows allows mitigation strategies to be employed (i.e. diversion

measures, cool advancing front with water or disruption of source or advancing front of lava flow by explosives may be taken in principle).

2.2 Other types of volcanic activity

There are other types of volcanic activity which could also be more dangerous than volcanic eruptions, these are lahars, tsunami, earthquakes.

2.2.1 Lahar

Lahar is an Indonesian term that describes a hot or cold mixture of water and rock fragments flowing down the slopes of a volcano. When moving, a lahar looks like a mass of wet concrete that carries rock debris ranging in size from clay to boulders more than 10 m in diameter. Lahars vary in size and speed. Small lahars are less than a few meters wide and several centimeters deep, they may flow a few meters per second. Large lahars are hundreds of meters wide and tens of meters deep, these can flow several tens of meters per second (too fast for people to outrun).

As a lahar rushes downstream from a volcano, its size, speed and amount of water and rock debris it carries constantly change. The surge of materials often erodes rocks and vegetation from the side of the volcano and along the river valley it enters. By eroding rock debris and incorporating additional water, lahars can easily grow to more than 10 times their initial size. But as a lahar moves farther away from a volcano, it will eventually begin to lose its heavy load of sediment and decrease in size.

Eruptions may trigger one or more lahars directly by quickly melting snow and ice on the volcano or ejecting water from a crater lake. Sometimes lahars are formed by intense rainfall during or after an eruption; rainwater can easily erode loose volcanic rock and soil on hillsides and in river valleys. Some of the largest lahars begin as landslides of saturated and hydrothermally altered rock on the flank of a volcano or adjacent hillslopes. Landslides are triggered by eruptions, earthquakes, precipitation or the unceasing pull of gravity on the volcano [36] .

2.2.2 Tsunami

A tsunami is a huge sea wave or is also known as a seismic sea-wave. It is very height and has extreme power. A tsunami is usually formed when there is quick ground displacement. After, the water column is pushed up above the average sea level. A volcanic tsunami (Figure 2.4) can result from violent submarine explosions, but it can also be caused by caldera collapses, tectonic movement from volcanic activity, flank failure into a water source

or pyroclastic flow discharge into the sea. As the wave is formed, it moves in a vertical direction and gains great speeds in deeper waters and can reach speeds as fast as 1000 km/h. In shallow water it can still be as fast as 320 km/h. The waves travel over the continental shelf and crash into the land. Anyway, this power does not decrease when they hit land, there is an extreme amount of energy when the water travels back towards its source. Approximately 5 % of tsunamis are formed from volcanoes and approximately 16.9 % of volcanic fatalities occur from tsunamis [37]. In December 2002 a tsunami was triggered by a flank collapse of Mt. Stromboli (Aeolian Islands, Italy).

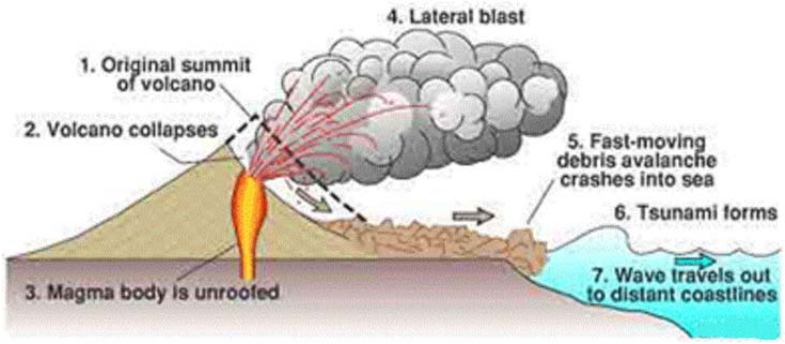

Figure 2.4 Example of how a volcanic eruption can generate a tsunami.[38]

2.2.3 Earthquake

Some earthquakes are related to volcanic activities. Most earthquakes generated by such activities are caused by the movement of magma. The magma exerts pressure on the rocks until it cracks. Then the magma squirts into the crack and starts building pressure again. Every time the rock cracks, it makes a small earthquake. These earthquakes are usually weak. Once the magma is flowing through the system, constant earthquake waves are recorded, they are called harmonic tremor. Earthquakes exhibiting volcanic tremor warn of an impending eruption so that people can be evacuated to safety areas. The volcanic tremor signal was successfully used to predict the 1980 eruptions Mount St. Helens and the 1991 eruption of Pinatubo [38].

Other earthquakes are produced by stress changes in solid rock due to the injection or withdrawal of magma and are called volcano-tectonic earthquakes. These can cause land to subside and can produce large ground cracks. These phenomena can occur as rock is moving to fill in spaces where magma is no longer present. Volcano-tectonic earthquakes do not indicate that the volcano will be erupting but can occur at any time. Volcano-tectonic earthquakes can cause damage to manmade structures and landsliding [35].

3

Approaches for Equipment Vulnerability Modelling

As described in Section 1.2, the vulnerability of a system can be determined based on its exposure, accessibility, susceptibility to be damaged under the impact of a natural hazard, a technological incident as well as a wilful intrusion or a terrorist action and resilience [39]. In the context of natural-technological events, vulnerability models allow estimating the probability of equipment damage under the impact of a natural phenomenon. These mathematical models can also be used to support decision making.

Vulnerability models, which will be developed in this thesis, assess the susceptibility of industrial equipment to be damaged due to volcanic ash fallouts. The focus is on two equipment typologies: those processing or storing hazardous substances and other industrial equipment used for air intake and wastewater treatment. The implementation of vulnerability models for the first equipment type aims achieving the goal of the integration of Na-Tech scenarios in the standard procedure for risk analysis; the conditions leading to malfunctions and efficiency losses will be defined for the second type. The choice of investigating volcanic ash fallout as initial cause of Na-Techs is due to the huge impact of ash dispersions, whose extent could also, in some cases, reach a continental dimension. This apparently rare phenomenon is actually very likely to occur in Europe, in particular in Italy and in Iceland. Significant ash fallout occurred in 2010, during the eruption of the Eyjafjallajökull volcano (Iceland); it dramatically extended at European level.

From a generic point of view, approaches for the vulnerability modelling can be divided into:

1. Determinist approaches
2. Semi-probabilistic approaches
3. Probabilistic (stochastic) approaches

The vulnerability modelling usually begins by applying a deterministic approach. It uses simple models and certain values, thus it permits estimating a threshold value of a physical parameter, which causes the equipment damage. A probabilistic assessment uses more complicated modelling approaches that depend on distributions of data for input key parameters. The output of a probabilistic assessment is a distribution of potential values, this results in a greater ability to characterise variability and uncertainty [40]. Probabilistic approaches are generally used only for higher-tier assessments, whereas the use of semi-probabilistic methods is often more diffused. A brief description of deterministic, semi-probabilistic and stochastic approaches is given below; then, the proposed approach for the estimation of equipment vulnerability under the impact of volcanic ash fallout is described.

3.1 Deterministic approach

A deterministic approach represents a mathematical model in which outcomes are precisely determined through known relationships between states and events without any random variation. By using such models, a given input will always produce the same output. Thus a deterministic model assumes certainty in all aspects [41].

A deterministic model mathematically is a representation $y = f(x)$ that allows making predictions of y based on x. This type of model is *deterministic* because y is completely determined if x is known. In real life, it is extremely rare to completely determine a y using an x because unexpected conditions often determine variability. In such cases probabilistic (stochastic) models must be used. It must be pointed that a deterministic assessment is relatively economical.

In the physical and engineering sciences, a common think is that relationships are more often deterministic, but this is not true. An example where the function is clearly not deterministic is the following: the maximum stress that a dam can bear cannot perfectly be predicted from the thickness of the concrete; it depends on the type and preparation of concrete, the dam shape and its environment and the specific physical and structural make-up of the given concrete. This means that it is not possible to characterise this information to achieve a deterministic prediction of the maximum stress level that the dam can bear [42].

3.2 Probabilistic approach

A probabilistic model incorporates aspects of the random variation and is represented as $Y = p(y)$, this notation specifically means that Y is generated at random from a probability distribution whose mathematical form is $p(y)$. This means that each time the model runs, it

likely gets different results, even with the same initial conditions. Probabilistic models allow predicting aggregate outcomes, if a large number of y values are observed.

3.3 Semi-probabilistic approach

A semi-probabilistic approach has both deterministic and probabilistic components. This model is represented by $Y = p(y|x)$, which states that, for a given x, Y is generated at random from a probability distribution whose mathematical form is $p(y|x)$.

3.4 Uncertainty

In vulnerability modelling, the uncertainty analysis is an important step. It provides a quantitative estimate of the value ranges for an outcome. These ranges are attributable to the variability and uncertainty in the input data and the uncertainties in the structure of any models used to define the relationship between exposure and effects [43].

An important issue in the uncertainty analysis is how to distinguish between the relative contribution of variability (i.e. heterogeneity) and uncertainty. Variability refers to quantities that are distributed within a defined population and cannot be represented by a single value, therefore it is only possible to determine with precision mean, variance, etc. In contrast, uncertainty or model-specification error (e.g., statistical estimation error) refers to a parameter that has a single value, which cannot be known with precision due to measurement or estimation error. Variability and uncertainty may be formally classified as follows: (i) type A uncertainty that is due to stochastic variability with respect to the reference unit of the assessment question, and (ii) type B uncertainty that is due to lack of knowledge about items that are invariant with respect to the reference unit of the assessment question.

3.5 Equipment vulnerability modelling to damage due to volcanic ash fallout

Figure 3.1 shows a simple flow-chart of the procedure developed in this thesis, which allows estimating and representing the equipment vulnerability to the given natural phenomenon [8].

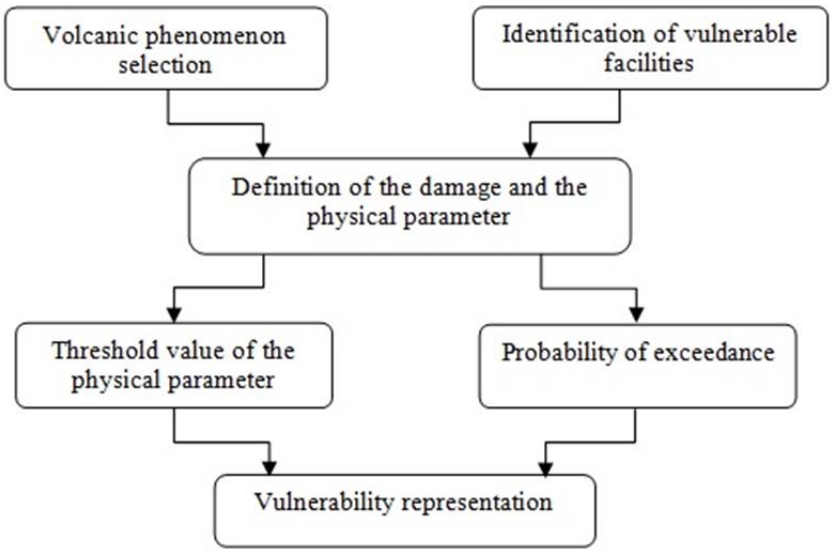

Figure 3.1. Flow-sheet for vulnerability representation

According to this approach, the first step is the selection of the volcanic phenomenon, which has to be proper characterised. In this thesis the volcanic ash fallout was analysed as potential natural phenomenon. Then given the presence of vulnerable equipment at a certain location around the volcanic crater, the failure mode and a physical parameter, (intensity variable) related to the natural phenomenon, causing the damage, must be identified. Afterwards, either the threshold limit of the physical parameter and the probability of exceeding this limit must be quantified. The vulnerability mapping is possible by combining threshold limits and exceedance probabilities, through a GIS (Geographical Information System) software.

The application of the developed approach could be deterministic, semi-probabilistic or probabilistic, further details related to its application to the study of Na-Techs triggered by volcanic ash fallout will be given in the following chapters.

3.6 Risk assessment framework

As introduced above, the implementation of vulnerability models for equipment, which processes or stores hazardous substances, aims achieving the goal of the integration of Na-Tech scenarios in the standard procedure for risk analysis (QRA, Quantitative Risk Assessment) shown in Figure 3.2.

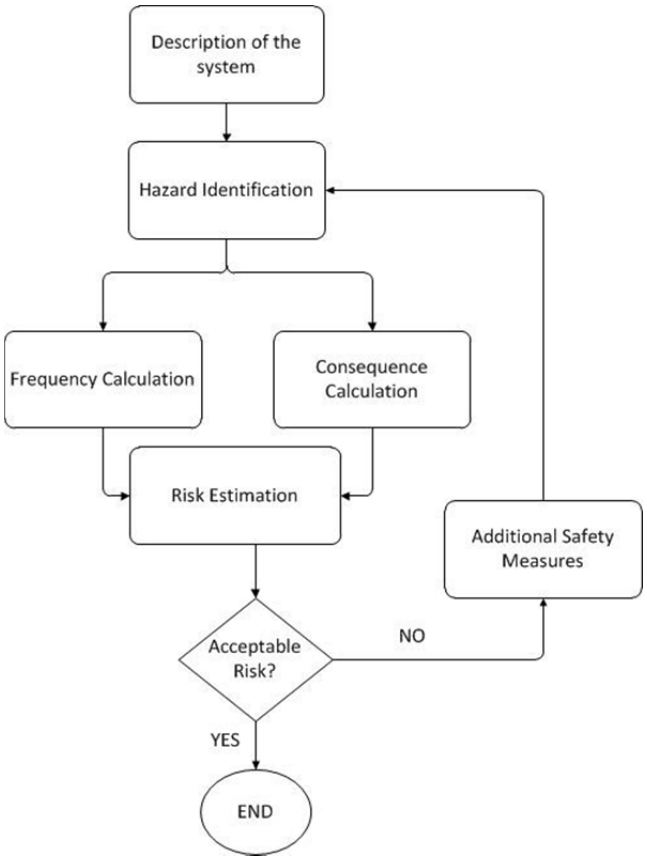

Figure 3.2. Quantitative Risk Assessment

An attempt to extent the standard procedure of Figure 3.2, to account for Na-Techs, was made by Antonioni et al. [44], it is schematised in Figure 3.3. Some steps were added to the standard procedure, such as step 1, 3, 4 and 5. These additional steps start with the characterisation of the natural phenomenon, then the type of equipment damage, caused by the natural phenomenon and leading to the release of hazardous substances, has to be identifies. Finally it is necessary to estimate the frequency and the consequences of the subsequent scenarios.

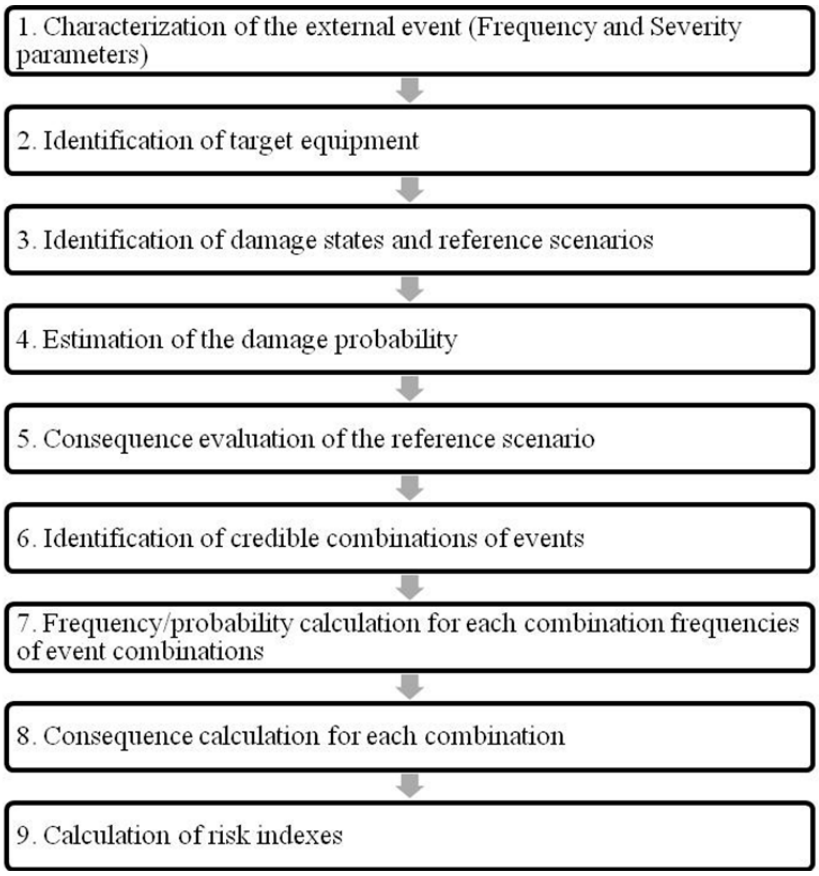

Figure 3.3. Flow-chart of the extended QRA procedure

4

Equipment Vulnerability Models

Vulnerability models were developed for equipment processing and storing hazardous substances and those used for air intake and wastewater treatment. Some facilities were selected with the aim to estimate the potential effects of volcanic ash accumulation, these are the following:

- atmospheric storage tanks (fixed and floating roof tanks);
- air intake filters;
- fine screens and grit removal systems included in primary wastewater treatment.

After a short description of the main equipment characteristics, their failure modes under the impact of the natural phenomenon and vulnerability models (which were implemented according to the approach given in Section 3.5) are illustrated.

4.1 Atmospheric storage tanks

Atmospheric storage tanks can be classified in fixed and floating roof tanks. They have size ranging from 2 to 60 m diameter or more. They are generally installed inside containment basins in order to contain spills in case of tank ruptures. Fixed roof tanks can be used for many products, such as crude oil, gasoline, fuel oil, water, etc. Floating roof tanks are used to minimize product loss by evaporation and to increase safety by minimizing the vapour space between the roof and liquid. A reliable drainage system is used to prevent the accumulation of rainwater in floating roof tanks.

The potential damage for atmospheric storage tanks, with respect to volcanic ash fallout, is correlated to the load on the roof, the abrasiveness and corrosiveness of the ash (mainly due to adsorbed acid gas). The abrasiveness can damage the rubber seals, while storage tanks and their roofs are usually coated with protective paint in order to prevent corrosion.

The only potential damage, which has been analysed in this thesis, is associated with the accumulation of material.

4.1.1 Fixed roof tanks

Fixed roof tanks have a cylindrical shape with the axis oriented perpendicular to the foundation, anyway, different type (shape) of fixed roof exist. A typical fixed roof tank consists of a cylindrical steel shell with a cone or dome shaped roof that is permanently fixed to the tank shell, Figure 4.1 shows some examples. Vapour emissions from these tanks vary with respect to the vessel capacity, vapour pressure of the stored liquid, utilization rate of the tank and atmospheric conditions at the tank location. To facilitate sliding of rain, fixed roofs have a very light slope.

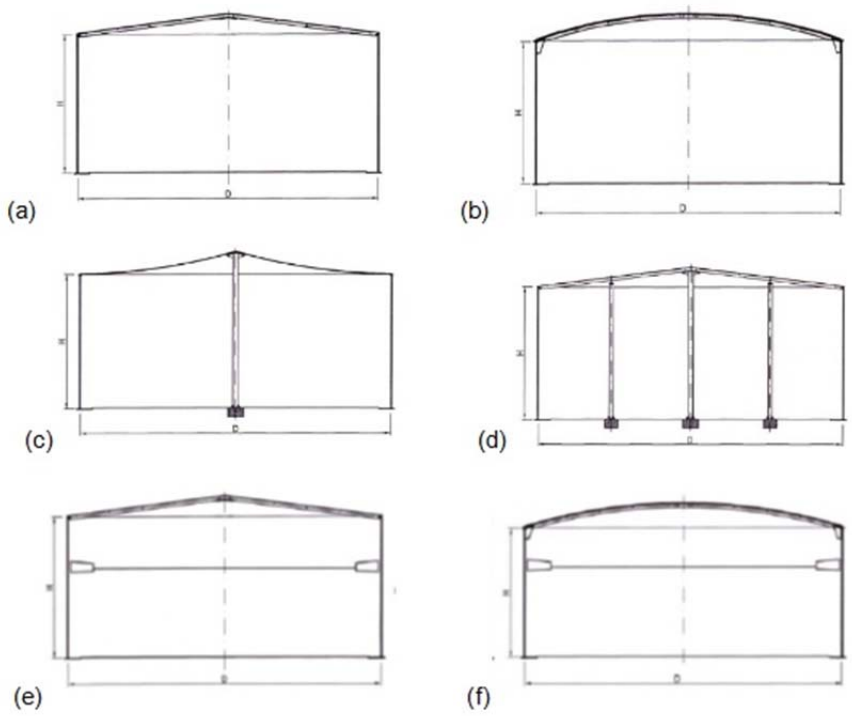

Figure 4.1. (a) Cone Roof, (b) Dome Roof, (c) Hanging Roofs, (d) Umbrella Roof, (e,f) Fixed Roofs (Dome Or Cone) With Internal Floating Roof.

The ash accumulation could cause structural damage to fixed roof; a strong similitude can be seen considering the effects of the snow load.

4.1.2 Floating roof tanks

Floating roof tanks (Figure 4.2) are classified as *single deck* or *double deck*. As given in [45], single deck floating roofs have an annular ring of pontoons providing buoyancy and a

single membrane of plates in the centre. These roofs are suitable for most applications except for the largest diameter tanks. Double deck floating roofs consist of two separate steel membranes with an air space between them. The air space is divided into different compartments guaranteeing buoyancy even if the lower membrane is ruptured. They are suitable for all sizes of tanks, especially in areas of frequent high wind speed or high temperature.

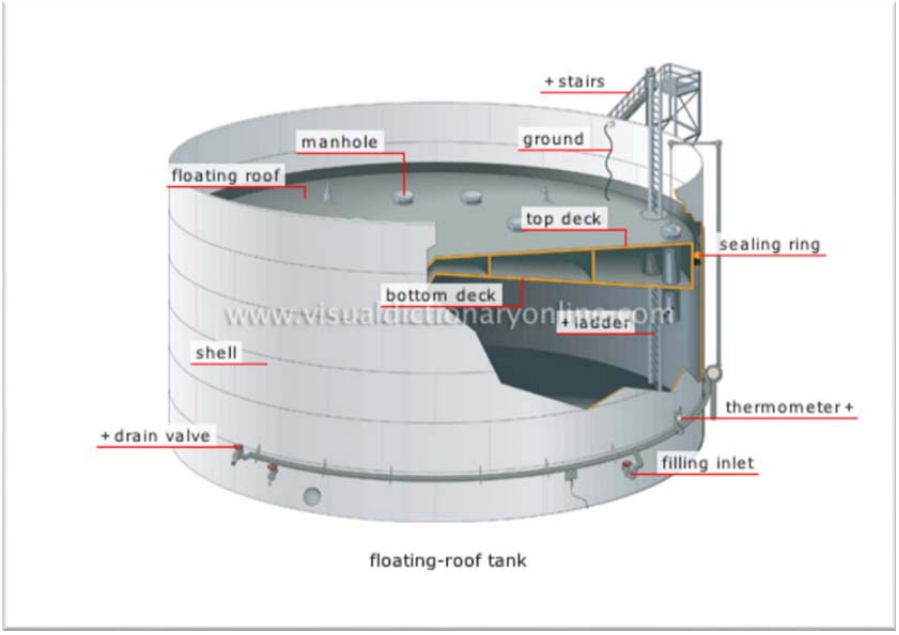

Figure 4.2. Section of a generic floating roof tanks.

This work is mainly focused on *double-deck* floating roof storage tanks because this type is the most used for flammable materials. The ash load on floating roof could cause its sinking or capsizing.

4.2 Air intake filters

In 2002, the European Committee for Standardization, Technical Committee 195, Work Group 1 (CEN/TC195-WG1) established a new standard for general ventilation filters (EN 779:2002). Member countries of CEN (*Comité Européen de Normalisation*) are obliged to issue their own national version of this standard within the existing framework of their own national standards organisations. Filters (Figure 4.3) are classified according to their efficiency or arrestance (Em or Am) under the following test conditions: the air flow shall be 0.944 m^3/s (3400 m^3/h) if the manufacturer does not specify any rated air flow rate. In the Table 4.1, the classification EN779 for air intake filters is reported (see EN779:2012).

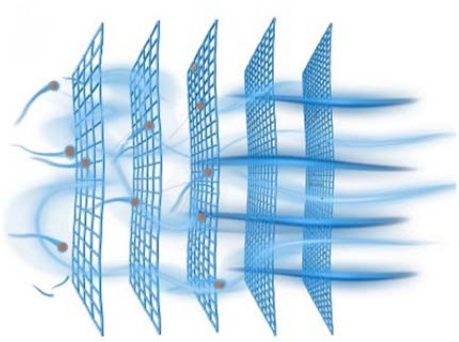

Figure 4.3. Air filter system

Table 4.1. Air filter classification (EN779:2012)

Class	Final Pressure Drop (Pa)	Average arrestance (Am) of synthetic dust (%)	Average efficiency (Em) of 0.4 μm particles (%)	Minimum Efficiency for 0.4 μm particles (%)
G1	250	$50 \leq Am \leq 65$	-	-
G2	250	$65 \leq Am < 80$	-	-
G3	250	$80 \leq Am < 90$	-	-
G4	250	$90 \leq Am$	-	-
M5	450	-	$40 \leq Em < 60$	-
M6	450	-	$60 \leq Em < 80$	-
F7	450	-	$80 \leq Em < 90$	35
F8	450	-	$90 \leq Em < 95$	55
F9	450	-	$95 \leq Em$	70

Another filter type is at High-Efficiency Particulate Arrestance (EN1822:2009) or simply named HEPA (Table 4.2). These filters must satisfy certain standards of efficiency, such as those set by the United States Department of Energy (DOE). To be qualified as HEPA, air filters must remove (from the air that passes through them) 99.97% of particles having size of 0.3 μm or larger. Filters are classified, according to results of tests, in the following ranges: E10 - E12 for EPA (Efficiency Particulate Air Filters), H13 - H14 for HEPA (High Efficiency Particulate Air Filters) and U15 - U17 for ULPA (Ultra Low Penetration Air Filters) [46]. As shown in Table 4.2, HEPA filters are classified based on the MPPS, which is the Most Penetrating Particle Size; MPPs are determined according EN1822:2009.

Filters are extensively used in buildings to remove particles from incoming outdoor air and from recirculated indoor air. Filters were historically installed to reduce the accumulation of deposited particles on heating, ventilating and air conditioning equipment which diminished

airflow rates and impeded heat transfer. Within the last two decades, the potential benefits to health have been increasingly recognised as a primary purpose of filtration [47].

Table 4.2. Classifications of high-efficiency filters.

Filter Classification	Efficiency (%) at the MPPS		Penetration (%) at the MPPS	
	Overall Value	Local Value	Overall Value	Local Value
E10	≥ 85	-	15	-
E11	≥ 95	-	5	-
E12	≥ 99.5	-	0.5	-
H13	≥ 99.95	99.75	0.05	0.25
H14	≥ 99.995	99.975	0.005	0.025
U15	≥ 99.9995	99.9975	0.0005	0.0025
U16	≥ 99.99995	99.99975	0.00005	0.00025
U17	≥ 99.999995	99.9999	0.000005	0.0001

Volcanic ash dispersions can determine accumulation of material on the filter surface, which clearly can lead to its partial clogging or to the extreme damage, i.e. its rupture.

4.3 Wastewater treatments

Water is a very valuable commodity, for this reason water supplies must be preserved and protected. After its use, it must be purified and reused. The water purification is made through a wastewater treatment plant. The general principle is to remove/reduce the following pollutants from the sewage:

- *Suspended solids* – physical particles that can clog channels as they settle under gravity;
- *Biodegradable organics* – materials that can serve as food for microorganisms;
- *Pathogenic bacteria and other disease* – these are most relevant if water is used for drinking or people would be in close contact with it;
- *Nutrients, including nitrates and phosphates* – these can lead to high concentrations of unwanted algae, which can themselves become heavy biodegradable organic loads.

A widely used terminology refers to three levels of wastewater treatment (WWT), as shown in Figure 4.4, these are primary, secondary and tertiary (or advanced).

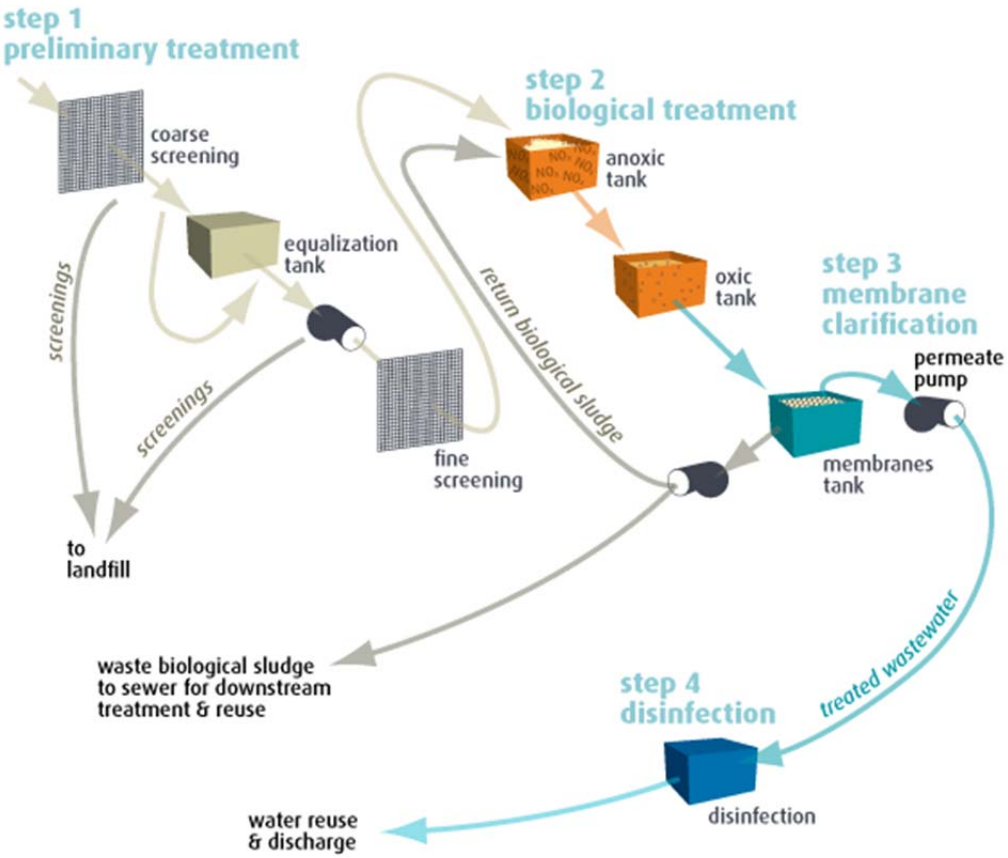

Figure 4.4. Wastewater Treatment plant (adapted from [48]).

Each level of treatment is briefly described below:

- *Primary (mechanical) treatment* deals with the removal of gross, suspended and floating solids from raw sewage. It includes screening to trap solid objects and sedimentation by gravity to remove suspended solids. This level is also referred to as *mechanical treatment*, although chemicals are often used to accelerate the sedimentation process.
- *Secondary (biological) treatment* removes the dissolved organic matter that escapes *primary treatment*, by means of microbes consuming the organic matter as food and converting it to carbon dioxide, water and energy for their own growth and reproduction. The biological treatment is followed by additional settling tanks (*secondary sedimentation*) to remove more of the suspended solids.
- *Tertiary treatment* is simply an additional treatment, which can remove more than 99% of all the impurities from sewage, producing an effluent of almost drinking-water quality. The related technology is very expensive, requiring a high level of technical know-how and well trained plant operators, a steady energy supply, chemicals and specific equipment.

This thesis focuses on the identification of the conditions leading to failures in *primary treatments*. The main equipment in a typical *primary treatment* includes screens, comminutors/grinders and grit removal. Solids in the wastewater can interfere with the downstream processes (biological and chemical treatments) or may also cause mechanical wear and increase maintenance on the equipment. The main failure modes, associated with the presence of volcanic ash in the raw sewage, were identified by an extensive literature analysis [49]; with reference to the *primary treatments* the most relevant failure modes were identified in screens and grit removal system.

4.3.1 Screens

Screening (Figure 4.5) is the first operation in wastewater treatment. This process essentially removes large non-biodegradable and floating solids (rags, papers, plastics, tins, containers and wood), which frequently enter in the treatment system. An efficient removal of these constituents will protect the downstream facilities from possible damages, unnecessary wear and tear, pipe blockages and the accumulation of unwanted material that will interfere with the subsequent processes.

Screens may be manually or mechanically cleaned; older and smaller treatment plants use manually cleaned screens. Coarse screens remove large solids and debris and typically have openings of 6 mm or larger. Fine screens are used to remove material that may cause operation and maintenance problems in downstream processes, their typical opening sizes are 1.5 to 6 mm. Very fine screens with openings of 0.2 to 1.5 mm placed after coarse or fine screens can reduce suspended solids to levels near those achieved by primary clarification. Modern plants sometimes use both coarse screens and fine screens.

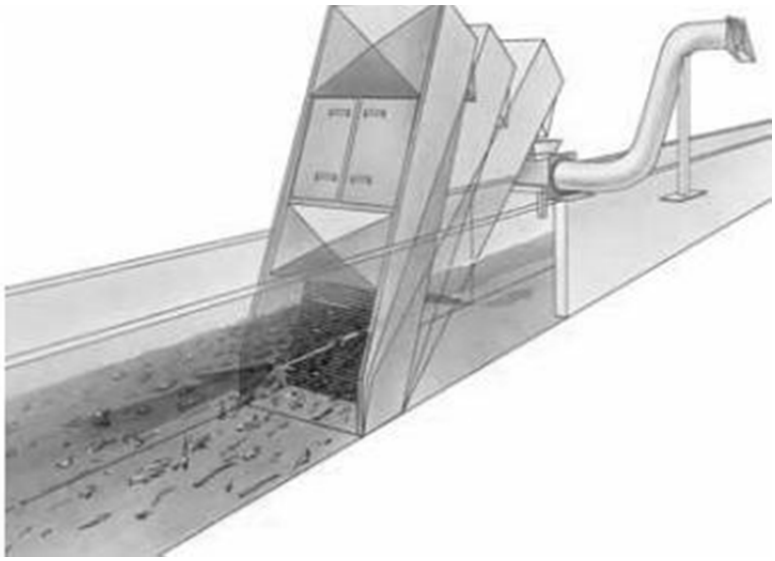

Figure 4.5. Coarse screen.

After volcanic ash fallouts, screens could clog due to ash deposit formation, this may occur when the particles' size in raw stream is greater than their openings. The malfunction is underlined by flow-rate variability (reduction).

4.3.2 Grit chambers

Fine screens are not always included in wastewater treatments, thus the removal of small particles is often provided by grit chambers. With respect to grit removal systems, *grit* is traditionally defined as particles larger than 0.21 mm and with a specific gravity (ratio of the material density to the density of water) greater than 2.65 [50]. Equipment design was traditionally based on removal of 95 % of these particles but, after the recent recognition that smaller particles must be removed to avoid damaging downstream processes, many modern systems are capable of removing up to 75 % of 0.15 mm material [51]. Grit removal facilities typically precede primary clarification and follow screening and comminuting/grinding (reducing the size of coarse solids).

The main types of grit removal include aerated grit chambers, vortex-type grit removal systems, horizontal flow grit chambers (velocity-controlled channel) and cyclones (cyclonic inertial separation).

In some cases, due to the characteristics of the volcanic ash, grit removals cannot give a complete deposition of particles, during the stream's passing in the channels. This causes abrasion and wear of mechanical equipment, grit deposition in pipelines and accumulation in anaerobic digesters and aeration basins.

4.3.2.1 *Horizontal flow grit chambers*

In this thesis only horizontal flow grit chambers have been studied (Figure 4.6), these are the oldest type of grit removal. Grit is removed by maintaining a constant upstream velocity of 0.3 m/s. In this system, heavier grit particles settle to the bottom of the channel, while lighter particles remain suspended and are transported out of the channel. Grit that does not require further classification may be removed with an effective flow control [52]. Proportional weirs or rectangular control sections are used to vary the depth of flow and keep the velocity of the flow stream at a constant 0.3 m/s. The length of the grit chamber is governed by the settling velocity of the target grit particles and the flow control section-depth relationship. An allowance for inlet and outlet turbulence is added. The cross sectional area of the channel is determined by the rate of flow and the number of channels.

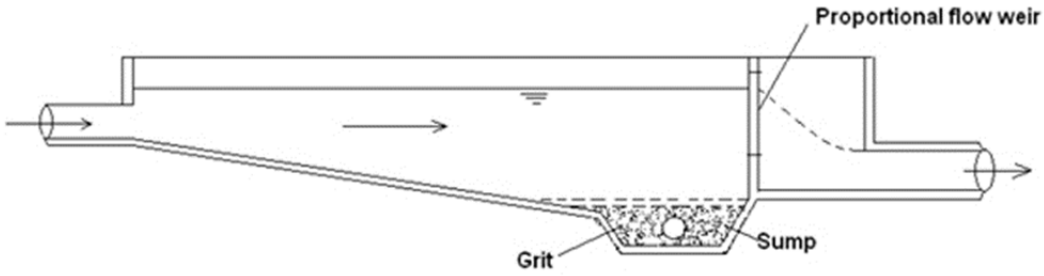

Figure 4.6. Horizontal flow grit chambers.

4.4 Failure modes of fixed roof tanks

The modelling of vulnerability of fixed roof tanks was deterministically made by Salzano and Basco [53], based on an analogy with the current studies of structural damages due to snow loads. Thus the following threshold limits are adopted:

- 1200N/m^2 (122 kg/m^2) for light damage (API 650 [54]; BS 2654 [55]);
- 3500 N/m^2 (357 kg/m^2) for structural damage (API 650 [54]);
- 7000 N/m^2 (714 kg/m^2) for collapse [53].

According to the API guideline, a load of 1205 N/m^2 is allowed on a roof with a slope less than 30°, for more highly inclined roofs a maximum load of 720 N/m^2 is possible.

4.5 Failure modes of floating roof tanks

The study of the problem of floating bodies and their stability has a history dating back to the work of Archimedes [56, 57].

Due to ash accumulation on floating roof, its sinking or capsizing could occur. These failure modes were studied by Milazzo et al. [58].

4.5.1 Sinking a floating roof

In order to sink a floating roof (double deck), Archimedes Principle requires that the combined weight of the floating roof (M_{roof}) and the ash deposit (M_{ash}) displaces a volume of liquid (V_{disp}) greater than that of the roof, or in the limiting case:

$$V_{disp} = \pi R^2 \delta \tag{1}$$

where: δ = depth of the roof (m); R = radius of the roof (m).

The weight of displaced liquid must be equal to the combined weights of the roof and the ash deposit:

$$M_{roof} + M_{ash} = \rho_{liquid} \pi R^2 \delta \tag{2}$$

where: ρ_{liquid} = density of the liquid (kg/m^3).

Assuming the ash deposit to have a density ρ_{ash} and to be a cylinder with radius R and height h:

$$M_{ash} = \rho_{ash} \pi R^2 h \tag{3}$$

$$M_{roof} = \rho_{liquid} \pi R^2 \delta_{roof} \tag{4}$$

where: δ_{roof} = immersion depth of the roof in the absence of ash (m).

Equation (2) may be rewritten as:

$$h = \frac{\rho_{liquid}}{\rho_{ash}} (\delta - \delta_{roof}) \tag{5}$$

4.5.2 Capsizing a floating roof

Euler gave a general criterion for floating body stability based on the couple produced by the weight acting vertically down through the centre of gravity and the buoyancy force acting vertically upwards through the centre of buoyancy (B) [56]. In this Section, Euler's method has been applied to calculate the minimum weight that must be added to the floating roof in order to capsize it. The floating body initially has the gravity and buoyancy forces acting along a vertical line which passes through the point located at the centre of the bottom of the floating roof Figure 4.7(a). The point M of Figure 4.7(b) is the metacentre, which is defined as the intersection point between the direction of the initial buoyancy force and the direction of the same after the perturbation of the initial conditions.

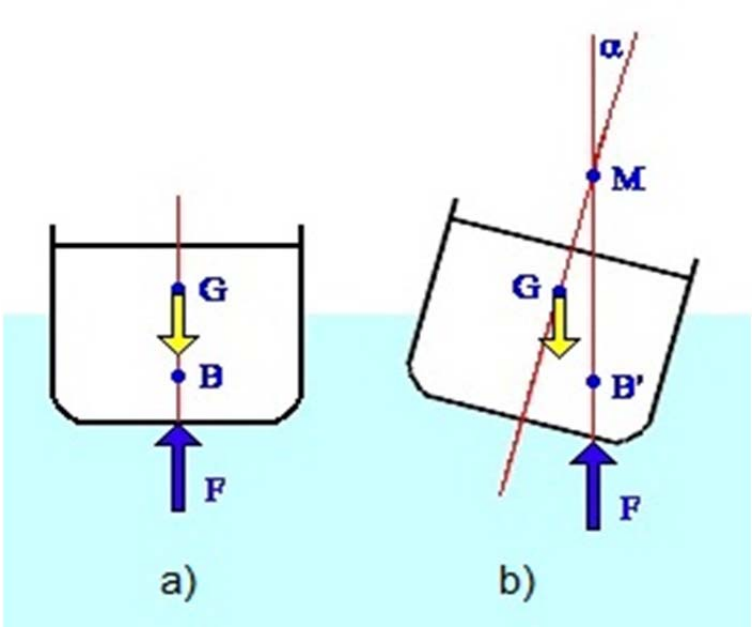

Figure 4.7. The floating body

The metacentre height (z_M) is the vertical distance between the metacentre and the centre of gravity (G) and is defined as:

$$z_M = \frac{I}{V_{imm}} \tag{6}$$

where: I = moment of inertia of the body in the flotation plane (m^4); V_{imm} = immersed volume (m^3).

For a cylinder:

$$I = \frac{\pi R^4}{4} \tag{7}$$

and

$$V_{imm} = \pi R^2 \delta_{imm} \tag{8}$$

where: δ_{imm} = depth of immersion (m).

Thus

$$z_M = \frac{R^2}{4\delta_{imm}} \tag{9}$$

The buoyancy centre is located at δ_{imm}/2 and

$$z_M - z_B = \frac{R^2}{4\delta_{imm}} - \frac{\delta_{imm}}{2} \tag{10}$$

where: (z_B) = buoyancy centre height (m).

The floating body is stable if the metacentre lies above the buoyancy centre ($z_M > z_B$).

According to these concepts, it is possible to define the conditions when the roof capsizes. It is necessary to know the weight which must be applied to a point on the edge of the roof (minimum weight) and, then, given a certain distribution of the ash on it, the weight causing the capsizing can be calculated. The calculation procedure is described elsewhere [58], in this paper it has only been applied.

4.6 Failure modes of air intake filters

Ash fallout on filter surface can clearly lead to its partial clogging or to the extreme damage, i.e. its total blockage (rupture). The clogging of a filter is caused by the formation of a deposit on its filtering surface. It depends on the characteristics of the system (material, diameter of the fibres and weaving, density, etc.) and on the characteristics of the ash (size distribution and concentration in the air). Unfortunately, to define the conditions for the clogging is not simple because the dispersion of ash is a complex phenomenon and is closely related to the local weather conditions, which vary considerably during the eruption.

Each filter has an operating limit which is identified through a threshold value for the pressure drop across its surface. The pressure drop is due to the resistance of the filtering surface to the air flow; when the filter is clean it depends exclusively on its characteristics and, while operating, it will increase due to the accumulation of ash. The operating limit is also expressed as a weight of the formed deposit, as given by the manufacturer.

In order to calculate the pressure drop due to the gas-solid (named *dusty gas*) flow in the system, an analogy with packed columns has been used. As shown by Bird et al. [59] the correlation of Ergun [60] can be applied:

$$\frac{P_o - P_L}{L} = \left(\frac{150\mu}{d_f^2 \cdot \rho} \cdot \frac{(1-\varepsilon)^2}{\varepsilon^3} \right) G_o + \left(\frac{1.75}{d_f \cdot \rho} \cdot \frac{(1-\varepsilon)}{\varepsilon^3} \right) G_o^2 \qquad (11)$$

where: (P_o – P_L) = pressure drop (Pa); ε = void fraction (e.g. the fraction of space in the filter not occupied by the material) (dimensionless); d_f = average equivalent diameter of the filter which is considered to consist of smooth rigid spheres (m); L = length of the filtering surface (m); μ= average viscosity (kg·m^{-1}·s^{-1}); ρ = density of the *dusty-gas* (kg/m^3) (arithmetic mean of the property of the fluid between the inlet and outlet of the filter); $G_o = \rho \cdot v_o$ is the mass flow rate of the *dusty-gas* through the system (v_o is the velocity of the *dusty-gas* at the inlet) (kg/m^{2}s).

The model of Ergun gives a direct analytical correlation to calculate the pressure drop but it is valid only for relatively small pressure losses, because the mass flow rate G_o is constant through the column (whereas the velocity changes through the column for a compressible fluid). In order to reduce the number of variables involved in the study and generalise the results, Equation (11) has been re-arranged in a dimensionless correlation:

$$y = \frac{150}{x} + \frac{7}{4} \tag{12}$$

where the dimensionless variables, y and x, are defined as:

$$x = \frac{D_p G_o}{\mu} \frac{1}{1-\varepsilon} \tag{13}$$

$$y = \frac{\rho \Delta P}{G_o^2} \left(\frac{D_p}{L} \right) \left(\frac{\varepsilon^3}{1-\varepsilon} \right) \tag{14}$$

Equation (12) allows determining the pressure drop at the filter outlet when the air contains volcanic ash. In order to verify the deviation from the operating conditions of the filter, it is then necessary to compare the value of pressure drop calculated with the critical pressure drop given by the manufacturer.

As mentioned above, the deposition of the threshold amount of ash on the filtering surface depends on the ash concentration in the atmosphere and the residence time of the cloud. The prediction of the amount of the deposit on the filter surface is however very complex because the meteorological conditions may vary during the day. In order to achieve the estimation of the threshold limit for the clogging, the conservative assumption that the emission is a stationary phenomenon has been made.

The use of such assumption allows calculating the time of clogging (t) for the filter, given the presence of a concentrations c of ash. The following equation has been used:

$$t = \frac{m_{ash}}{Q \cdot c} \tag{15}$$

where: m_{ash} = threshold deposit causing the filter clogging (kg); Q = volumetric flow rate of the *dusty-gas* (m^3/s).

4.7 Failure modes in wastewater treatments

As previous mentioned, the most relevant identified failure modes with respect to *primary treatments* are the following:

- *Screens' clogging* when the particles' size in raw stream is greater than their openings. The malfunction is underlined by a variability (reduction) of flow-rate [19];
- *Incomplete grit removal* when ash deposition is not complete during the stream's passing in the channels.

4.7.1 Conditions for the screen clogging

The flow-rate variability due to the ash accumulation is correlated to the screen's pressure drop (ΔP); thus the ΔP is the main indicator to underline malfunctions. Given the dimension of ash particles, the effects of accumulation should be study for fine and very fine screens, anyway it is worth noting that this equipment type is not always included in wastewater treatment plants. The ΔP in fine screens can be calculated as suggested by the literature [61], then the length of deposit causing the critical pressure drop can be quantified by means of the methodology given below.

The pressure drop in fine screen is given by the following equation [61]:

$$\Delta P = \frac{\rho}{2 \cdot C_{disch}} \cdot \left(\frac{Q}{A_s} \right)^2 \tag{16}$$

where: ΔP = pressure drop (Pa); C_{disch} = coefficient of discharge for the fine screen (typically this value for clean screens is 0.60, for dirty screens is 0.4 and for very dirty screens is 0.25); A_s = effective open area of submerged screen (m^2); ρ = fluid (sewage) density (kg/m^3); Q = volumetric flow rate of the sewage (m^3/s).

The methodology for the estimation of the ash deposit threshold on a fine screen causing malfunctions is based on the assumption that the accumulation is a granular bed and the sewage represents the fluid passing through it. The literature [62] suggests estimating the bed dimension by means of the Darcy's equation in case of streamline flows and the Carman's equation for transition and turbulent flows. In the fluid dynamic the parameter, which permits to determine the flow's regime, is the Reynolds number (Re):

$$\mathrm{Re} = \frac{D_{eq} \cdot \rho \cdot u_l}{\mu} \tag{17}$$

where: D_{eq} = equivalent diameter of the pore space (m); μ = fluid viscosity ($kg \cdot m^{-1} \cdot s^{-1}$); ρ = fluid density (kg/m^3); u_l = average velocity through the pore channels (m/s).

The equivalent diameter and the average velocity through the pore channels depend on the characteristics of granular bed, i.e. the specific surface area (S) and the voidage (e):

$$D_{eq} = \frac{e}{S \cdot (1-e)} \tag{18}$$

$$u_l = \frac{u}{e} \tag{19}$$

Hence:

$$\mathrm{Re} = \frac{u \cdot \rho}{S \cdot \mu \cdot (1-e)} \tag{20}$$

where: e = voidage or porosity, it represents the fraction of the volume of the bed which is not occupied by solid material (dimensionless); S = specific surface area of the particles, it is the surface area of the particles divided by their volume (m^{-1}); u = average velocity of the flow (m/s).

The following rules are given by Coulson et al. [63] to define the regime flows in granular beds:

$\mathrm{Re} < 10$ laminar (or streamline) flow

$\mathrm{Re} > 2000$ turbulent flow

According to the Darcy law, the average velocity is directly proportional to the driving pressure and inversely proportional to the thickness of the bed:

$$Q = \frac{K}{\rho \cdot g} \cdot A_{tot} \cdot \frac{\Delta P}{l} \tag{21}$$

where: Q = volumetric flow rate (m^3/s); A_{tot} = cross-sectional area (m^2), in this case it is effective open area of submerged screen (A_s); l = thickness of the porous medium (m); g = gravity acceleration (m/s^2); K = constant, it depends on the characteristics of the porous medium (intrinsic permeability, k_i) and the fluid characteristics (viscosity and density) (m/s).

The Carman's equation is:

$$\frac{R'}{\rho u_l^2} = \frac{e^3}{S \cdot (1-e)} \cdot \frac{(-\Delta P)}{l} \cdot \frac{1}{\rho \cdot u^2} \tag{22}$$

where: R' = component of the drag force per unit area of particle surface in the direction of motion ($kg \cdot m^{-1} \cdot s^{-2}$).

The $(R'/\rho \cdot u_l^2)$ of the Carman's equation represents the friction coefficient, which is dimensionless and is correlated to the Reynolds number as follows:

$$\frac{R'}{\rho u_l^2} = 5\,\mathrm{Re}^{-1} + 0.4\,\mathrm{Re}^{-0,1} \tag{23}$$

4.7.2 Conditions for the incomplete particles removal in horizontal flow grit chambers

The theoretical base of the solid removal from a liquid in grit chambers is the derivation of the *terminal settling velocity* (u_t). Assuming a low concentrated dispersion of particles, each particle settles discretely as if it is alone (unhindered by the presence of other particles). Starting from the rest, the settling velocity (u_s) in the fluid of the particle under gravity increases with the particle density; moreover it is accelerated until the resistance to the flow from the fluid equals the weight of the particle, then the settling velocity remains constant and this is named terminal settling velocity [62].

Given a fluid at constant temperature and a particle with constant settling velocity, the terminal settling velocity depends on various factors related to the particle and the fluid and is derived by balancing the forces acting on the particle (drag, buoyant and gravitational forces):

$$V_p \cdot g\left(\rho_s - \rho\right) = \frac{C_D \cdot u_{t,p}^2 \cdot \rho \cdot A_D}{2} \tag{24}$$

where: $u_{t,p}$ = terminal settling velocity of a particle with a diameter d_p (m/s); V_p = effective volume of the particle (m^3); g = gravitational constant (m/s^2); ρ_s = particle density (kg/m^3); ρ = fluid density (kg/m^3); C_D = drag coefficient (dimensionless); A_D = projected area of the particle in the flow direction (m^2).

Then the terminal settling velocity is given by the following equation:

$$u_{t,p} = \sqrt{\frac{2 \cdot g\left(\rho_s - \rho\right) \cdot V_p}{C_D \cdot \rho \cdot A_D}} \tag{25}$$

in case of a solid and spherical particle:

$$u_{t,p} = \sqrt{\frac{4 \cdot g\left(\rho_s - \rho\right) \cdot d_p}{3 \cdot C_D \cdot \rho}} \tag{26}$$

The terminal settling velocity is not depended on the horizontal and vertical movement of the fluid, although in real situation velocity gradients and other factor could affect the process [62], whereas the drag coefficient depends on the flow regime surrounding the particle. In the fluid dynamics the Reynolds number (Re) is used to identify the flow characteristics, thus by assuming the conditions previous described:

$$\mathrm{Re} = \frac{d_p \cdot \rho \cdot u_{t,p}}{\mu} \tag{27}$$

where: μ = fluid viscosity (kg/m·s).

An extensive review of equations for C_D calculation is given by Brown and Lawler [64]. The drag coefficient was seen that decreases as the Reynolds number increases, sometimes a shape factor is also determined and incorporated in C_D to take into account the real particle contour. In case of spherical particles, the main equations for C_D and $u_{t,p}$ are given in Table 4.3 (extracted from Coulson et al. [62]). In the laminar regime (region *a*) the equation for the calculation of $u_{t,p}$ is the Stokes' law and, in the turbulent regime (region *c*), it becomes the Newton's law.

Table 4.3. Drag and terminal settling velocity equations [20].

Regime	**Re**	C_D	$u_{t,p}$
Laminar (region *a*)	$\mathrm{Re} < 1$	24/Re	$u_{t,p} = \frac{g \cdot d_p^2 (\rho_s - \rho)}{18 \cdot \mu}$ (Stokes)
Intermediate (region *b*)	$1 < \mathrm{Re} < 1000$	24/Re + 0.44	$u_{t,p} = \sqrt{\frac{4 \cdot g (\rho_s - \rho) \cdot d_p}{3 \cdot C_D \cdot \rho}}$
Turbulent (region *c*)	$1000 < \mathrm{Re} < 2 \cdot 10^5$	0.44	$u_{t,p} = 1.75 \cdot \sqrt{\frac{g \cdot d_p (\rho_s - \rho)}{\rho}}$ (Newton)
Turbulent (region *d*)	$\mathrm{Re} > 2 \cdot 10^5$	0.10	$u_{t,p} = \sqrt{\frac{4 \cdot g (\rho_s - \rho) \cdot d_p}{3 \cdot C_D \cdot \rho}}$

If the settling velocity term is not known, to identify the range in which the motion of the particle lies, it must be eliminated from the Reynolds number. To this scope a criterion based on the K parameter (dimensionless) is introduced [65], which is defined as:

$$K = d_p \left[\frac{g \cdot \rho \cdot (\rho_s - \rho)}{\mu^2} \right]^{1/3} \tag{28}$$

The Stokes' law is to apply if $\mathrm{Re} < 1$, thus by substituting the proper $u_{t,p}$ in Equation (27)

$$\mathrm{Re} = \frac{d_p^3 \cdot g \cdot \rho \cdot (\rho_s - \rho)}{18 \cdot \mu^2} \tag{29}$$

$$\mathrm{Re} = \frac{K^3}{18} \tag{30}$$

By solving Equation (30), K = 2.6; this means that if K is less than 2.6 the Stokes' law applies. Setting Re = 1,000 and Re = 200,000, after substituting the $u_{t,p}$ from the Newton's law:

$$\mathrm{Re} = 1.75 \cdot K^{1.5} \tag{31}$$

By solving Equation (31), K is respectively equal to 68.9 and 2,360.

The criterion to choose the proper equation for the calculation of the terminal settling velocity is summarised in Table 4.4. Figure 4.8 shows the trend of the terminal settling velocity as a function of the particle's diameter (assuming the ash density equal to 2000 kg/m^3). In the same graph the range of applicability, in term of K, is highlighted by means of the lines K = 2.6, K = 68.9 and K = 2360.

Table 4.4. K parameter and regime flow regions.

Regime	**Re**	***K***
Laminar (region *a*)	$\mathrm{Re} < 1$	$K < 2.6$
Intermediate (region *b*)	$1 < \mathrm{Re} < 1000$	$2.6 < K < 68.9$
Turbulent (region *c*)	$1000 < Re < 2 \cdot 10^5$	$68.9 < K < 2{,}360$
Turbulent (region *d*)	$\mathrm{Re} > 2 \cdot 10^5$	$K > 2{,}360$

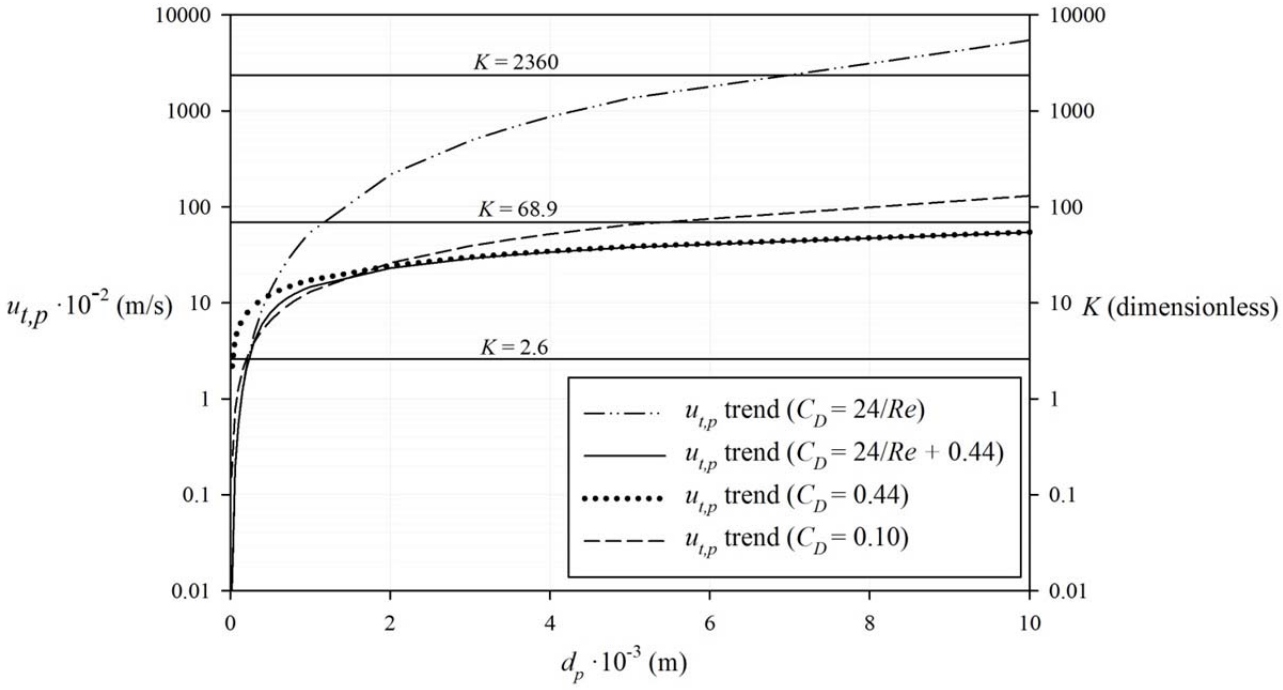

Figure 4.8. Terminal settling velocity as a function of the particle's diameter

Within the approach mentioned above, drag coefficients and terminal settling velocities of Table 4.3 are based on the following assumptions:

a) the settling is not affected by the presence of other particles in the fluid (*free settling*);

b) the walls of the vessel do not exert an appreciable retarding effect;

c) the effects of particle shape and orientation on drag are not accounted for.

As discussed in the following, several studies were made to overcome such assumptions.

When the interference of other particles is appreciable, the process is known as *hindered settling*. Richardson and Zaki [66] stated that in concentrated suspension the drag force on a particle will be influenced by the concentration of particles and the terminal settling velocity will be a function of the voidage of the suspension as given below:

$$\frac{u_{t,p|C}}{u_{t,p}} = \left(1 - c_p\right)^n = e^n \tag{32}$$

where: c_p = suspension concentration expressed as volumetric fraction (dimensionless); $u_{t,p|cp}$ = terminal settling velocity in hindered condition; e = suspension's voidage (dimensionless); n = empirical exponent dependent on Re.

Other subsequent studies were related to the quantification of the wall effects, these were taken into account by introducing some modifications in the n-value [67]; finally also the modelling of the sedimentation process of multi-sized particles was faced [68].

To take into account the effect of particle shape and its orientation on drag, two difficulties were remarked: the first is that infinite non-spherical shapes exist and the second is that each of these shapes is associated with an infinite number of orientations. Then, drag coefficients for generic non-spherical particles were defined in [69].

Assume a rectangular settling vessel (Figure 4.9), where the sewage is fed (Q = sewage flow rate (kg/s); L_v = vessel length (m); W_v = vessel width (m); H_v = vessel height (m)). During the flow of the fluid, two zones can be distinguished, the suspension zone and the sludge deposit. The following assumptions are imposed:

a) a homogenous stream, uniformly distributed over the tank cross-sectional area, is fed;

b) the liquid in the feeding zone moves at constant velocity and as a plug flow;

c) when particles enter the sludge zone (assumed at constant thickness), they exit the suspension.

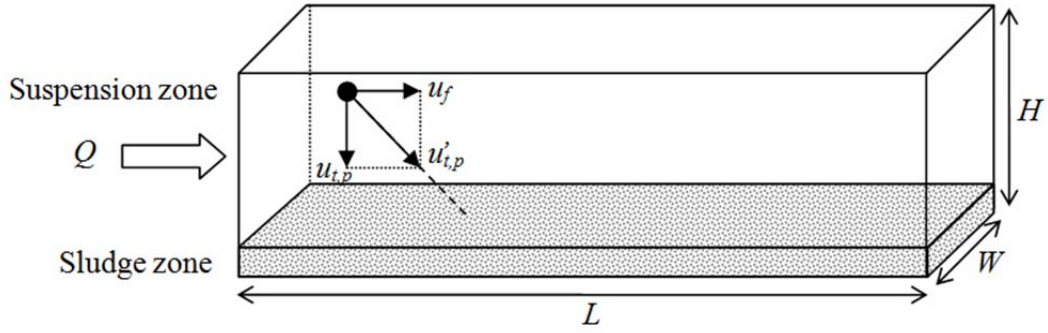

Figure 4.9. Rectangular settling vessel.

The final settling velocity of the particle ($u'_{t,p}$) is the vectorial sum of the terminal setting velocity ($u_{t,p}$) and the sewage velocity (u_f). In these conditions it is possible to define a *retention time* (t_o) and a *critical velocity of settling* for the particles (u_o). From a theoretical point of view, particles with a settling velocity equal or lower than the critical velocity will settle out from the vessel at a time equal or greater than the retention time:

$$t_o = \frac{V}{Q} = \frac{L_v}{u_f} \tag{33}$$

where: V = vessel's volume (m^3).

$$u_o = \frac{H_v}{t_o} \tag{34}$$

It must be pointed that the design factors, mentioned above, must be adjusted to account for the effects of inlet and outlet turbulence, short circuiting, sludge storage and velocity gradient. Then, assuming that particles are uniformly distributed over the entire depth (H_v) of the vessel at the inlet, a fraction of particles (X_r) with a terminal settling velocity less than u_o or equal to u_o will be removed:

$$X_r = \frac{u_{t,p}}{u_o} \tag{35}$$

In a typical suspension a large gradation of particle sizes occurs, thus to determine the removal efficiency it is necessary to consider the entire range of $u_{t,p}$ present in the system. This can be accomplished by using the results of a sieving analysis to construct a terminal settling velocity curve versus X (fraction of particles with less than the stated velocity). The total fraction of removed particles is given by:

$$x_{r,total} = (1 - X_o) + \int_o^{X_o} \frac{u_{t,p}}{u_o} dX \tag{36}$$

where: X_o = fraction of particles with $u_{t,p} \leq u_o$ (dimensionless).

The term $(1 - X_o)$ is the fraction particles with a velocity greater than u_o, whereas $\int_o^{X_o} \frac{u_{t,p}}{u_o} dX$ is the fraction of particles removed with $u_{t,p} \leq u_o$.

4.8 Exceedance probability curves

After the estimation of the threshold value of the physical parameter (ash load or concentration), the *exceedance probability* must be determined, which is given by the probability that, given the occurrence of an explosive eruption with a certain magnitude, the physical parameter will exceed the threshold limit.

5

Vulnerability Mapping and Emergency Management Procedures

A literature review showed that, beyond the improvement of the knowledge on the modes of failure of industrial facilities under the impact of natural phenomena, the development of vulnerability maps as tools for decision making is actually necessary. A useful tool for the Na-Tech risk mapping and management is a Geographical Information System (GIS). Its use allows performing the calculation of the vulnerability of facilities related to each point of the territory and the easier management of geographical data (georeferenced data). Further it also allows the development of semi-automatic procedures for the vulnerability mapping.

Using a GIS software it was possible to obtain vulnerability mapping by means interpolations of the exceedance probabilities, when these are available for a limited number of points related to the territory. Semi-automatic procedures were also developed in order to support users in vulnerability mapping and decision making. Emergency management procedures for wastewater treatments were also developed.

5.1 Geographic Information System

A Geographic Information System (GIS) allows visualising, questioning, analysing and interpreting data, to understand relationships, patterns and trends [70]. GIS is a broad term, which refers to a number of different technologies, processes and methods. It has many applications related to engineering, planning, management, transport/logistics, insurance, telecommunications and business.

In this work, the use of such technology is fundamental to apply the approaches developed (discussed in Chapter 4) to the whole studied area and to produce the vulnerability maps. Furthermore, GIS could be useful to share the results with potential stakeholders (i.e. civil protection, facilities managers, etc.). Vulnerability maps can be produced by a semi-automatic *geoprocessing* procedure, created using the ModelBuilder tool of the GIS software.

5.1.1 Geoprocessing

The *geoprocessing* is a GIS operation used to manipulate spatial data. A typical *geoprocessing operation* takes an input dataset (such as a feature class, raster or table), performs an operation on that dataset and returns back the result of the operation as an output dataset.

The *geoprocessing* is a basic function of the GIS software for the processing of geographical data, the ModelBuilder is the application which allows creating, editing and managing sequences of *geoprocessing* (models). It also allows feeding the output of one model into another one as input. Operations and datasets are the components or elements of the model interface and are represented in a flowchart by using different symbols. Some examples of *geoprocessing* tools are shown in Figure 5.1.

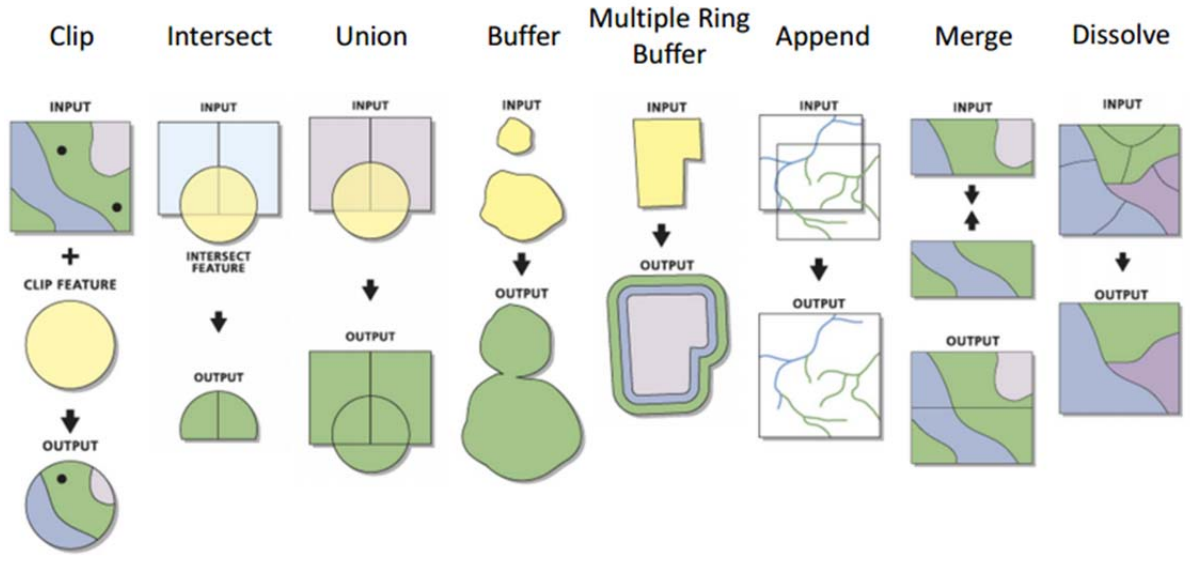

Figure 5.1. Geoprocessing tools [71].

5.2 Exceedance probability

The exceedance probability of the threshold limits of the physical parameters is the vulnerability related to a given damage. As reported by Woo [72], volcanologists are unable to forecast with certainty the characteristics of eruptive event. Thus in order to take into account uncertainties, an approach derived from the mathematic of natural catastrophes must be used. More specifically, Woo suggested performing Monte Carlo simulations of the event of interest to model the ash dispersion, assigning different input conditions which vary within pre-defined ranges. A detailed mathematical description is not the scope of this thesis, however it can be found elsewhere [72].

5.3 Approaches for the vulnerability mapping

The main difficulty in elaborating vulnerability maps for industrial facilities, in area prone to ash fallouts, is that input data is limited because the *exceedance probabilities* of ash load or concentration are usually known for few locations. This means that to achieve the mapping, a spatial interpolation method must be used to estimate the probabilities also for the locations where these are not known. The choice of the interpolation method is crucial because it approximates the spatial representation of the physical phenomenon (in this case of the volcanic ash fallout/dispersion) [73]; anyway the quality of the input data is also essential to give a reliable estimate. Non-optimal estimates usually are due to:

- few available points;
- limited spatial coverage;
- uncertainty about the location and the value of the measured physical quantity.

There are several interpolation procedures, each of them characterised by different data elaboration, accuracy, sensitivity to parameters variation and degree of smoothness of the interpolated surface. These are grouped in two main classes: deterministic methods, based on a correlation among neighbouring points whose parameters have an explicit physical meaning, and stochastic methods, which relate neighbouring points through a statistical correlation [74]. In this study two spatial interpolation methods have been chosen, these are the IDW (deterministic) and the Kriging (stochastic) methods. Then, the GIS software (developed by Esri, named ArcGIS) has been used to perform the elaborations.

5.3.1 Spatial Interpolation Methods

The IDW method assumes that each measurement has a local influence, which decreases with the distance; it is based on the following equation:

$$z_{(So)} = \frac{\sum_{i=1}^{N} w_i \cdot z_{(Si)}}{\sum_{i=1}^{N} w_i} \tag{37}$$

where: $z_{(So)}$ = value to be predicted associated with the location S_o (prediction point); N = number of locations used for the estimation (identification number for the points around the prediction point); i = 1, 2, 3, ...; $z_{(Si)}$ = measured value of the variable at the i-th location; $w_i = 1/d_i^2$ = weight coefficient for the measured value at the i-th location (d_i is the distance between the i-th point and S_o).

The Kriging method is a geostatistical procedure for data interpolation [75, 76]. The model takes into account the value of the variable in the other locations and a weight coefficient based not only on the distance between the measured points (as the IDW approach), but also on the overall spatial arrangement of the measured points. This means that it is based on a probabilistic elaboration in order to develop more complex predictive models. The use of the Kriging allows including the estimation of the error and the uncertainty associated with each prediction [74]. The correlation is:

$$z_{(So)} = \sum_{i=1}^{N} \lambda_i \cdot z_{(Si)} \tag{38}$$

where: λ_i = weight assigned to each measured value at the i-th location, it is based not only on the distance between the measured points and the prediction location but also on the overall spatial arrangement of the measured points.

5.3.2 Semi-automatic procedure for vulnerability mapping

By means of the ModelBuilder tool, a simple model to elaborate the vulnerability of atmospheric storage tanks to volcanic ash deposits and air intake filters to volcanic ash dispersion in the atmosphere has been created. It allows a quick vulnerability mapping, based on the use of both the interpolation procedures described above in Section 5.2.1.

Figure 5.2 shows the flowchart of the whole procedure. The model runs in a semi-automatic mode and, finally, the *geoprocessing* model provides the vulnerability maps. The operations and the datasets are represented in the flowchart by using different symbols: dark coloured rectangles are inputs (locations related to the sample points and exceedance probabilities); the other rectangles are outputs (exceedance probabilities mapping); ovals give operations to be performed on the input data; the connecting arrows indicate the direction of the processing sequence.

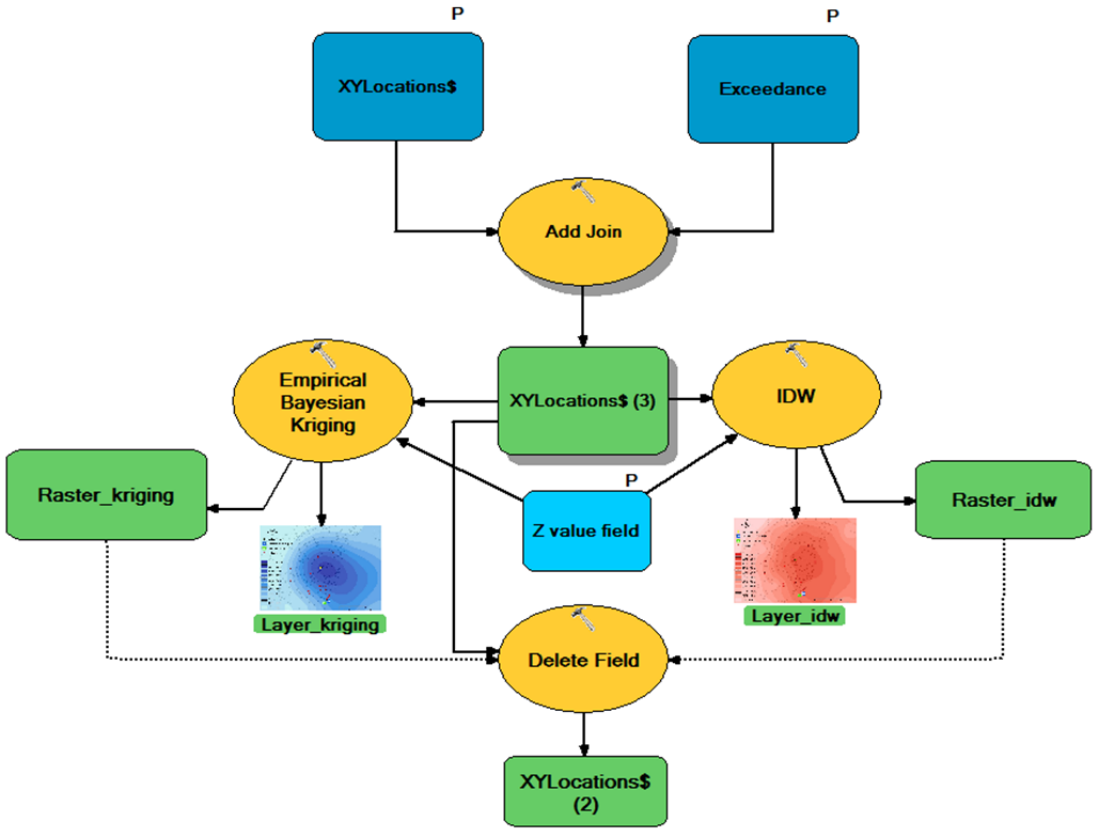

Figure 5.2. Flowchart of the developed semi-automatic procedure.

5.4 Procedure for emergency management

A procedure for the management of wastewater treatment equipment has been implemented within the GIS. Figure 5.3 shows a simply scheme of the proposed methodology for the management of Na-Techs triggered by volcanic ash fallouts.

Firstly two databases must be constructed: the first database collects the volcanic eruptive scenarios and second one stores data about the plants located in the territory. Furthermore the GIS could be used to include other information related to the distribution of urban centres, the use of the territory, the electric network, the water supply network, etc.

In order to identify the impact areas for each eruptive scenario, a threshold value of thickness for the ash deposit must be defined. To achieve this scope, data from different sources have been taken into account:

- Day & Fisher [77] discussed that serious problems occur with deposit >10 mm (although these are rare events);
- Blong [78] reported about the eruption of Mt. Spurr in Alaska, where 3 mm of volcanic ash (~ 5000 g/m^2) fell on Anchorage in 1992 and caused many pipe blockages;

- in 2002, during the eruption of Mt. Etna (Italy), small amounts of ash caused the blockages of the rainwater drainage systems in the city of Catania [79], due mainly to the formation of not easily pumped material.

To make this analysis conservative, in this study, a threshold limit of deposit of 1000 g/m^2 has been considered.

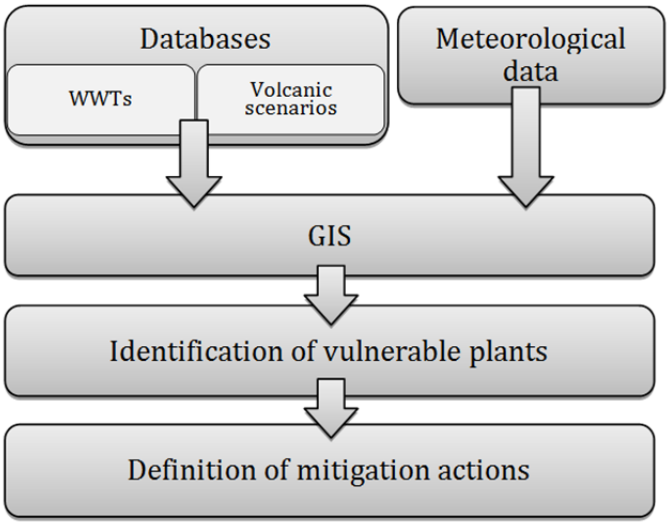

Figure 5.3. Scheme of the proposed methodology for the emergency management.

The use of real-time meteorological information (i.e. wind direction and velocity) and the characteristics of the eruption (emission rate) allow selecting the scenario. The impact of the volcanic ash on the territory is then easily evidenced because a map quickly identifies the impact regions and the potential WWTs, which are involved at different time from the starting of the eruption. Their identification allows focusing on the mitigation actions for the plants.

The last step of the approach regards the definition of the measures that could be implemented to protect some parts of the wastewater treatment. These can be:

- the timely cleaning of roads;
- putting in place all protective measures for each equipment (i.e. the coverage of settling tanks);
- the extraordinary maintenance of the WWT.

The use of the available resources must be rational, especially when this requires the use of public funding.

6

Case study

The approaches and procedure described in the previous Sections were applied to a case-study, which is the surrounding of Mt. Etna (Sicily – Italy). Etna is a volcano ~ 3300 m high and is characterised by both basaltic explosive behaviour and effusive activity. As shown in Figure 6.1, it has five craters: North-East Crater (NEC), Voragine (VOR), Bocca Nuova (BN), South-East Crater (SEC) and New South-East Crater (NSEC). This last crater emerged very recent, i.e. during an eruption occurred in 2014. The surrounding the volcano is characterised by the presence of the city of Catania (300 thousand inhabitants), by many small urban centres and agricultural and industrial areas. In the Southern area there is one of the most complex industrial sites in Europe (Priolo-Augusta-Melilli), which could be involved during specific weather conditions.

Two reasons oriented towards the choice of this case-study [80]: (i) an increased trend to give explosive eruptions with ash emission has recently been observed [81]; and (ii) the expected damage due to ash fallout is expected to be larger because of the increased urbanization and number of industrial infrastructures installed in the recent years.

In the following, the characterisation of the natural phenomenon (volcanic ash fallout) is described; a census of establishments at major risk, power plants and wastewater treatment plants is given, followed by the description of the main characteristics of investigated equipment in this thesis. Finally, given that the application of most models (see Chapter 4) requires the characteristics of volcanic ash, some samples were collected in order to make an ash characterisation.

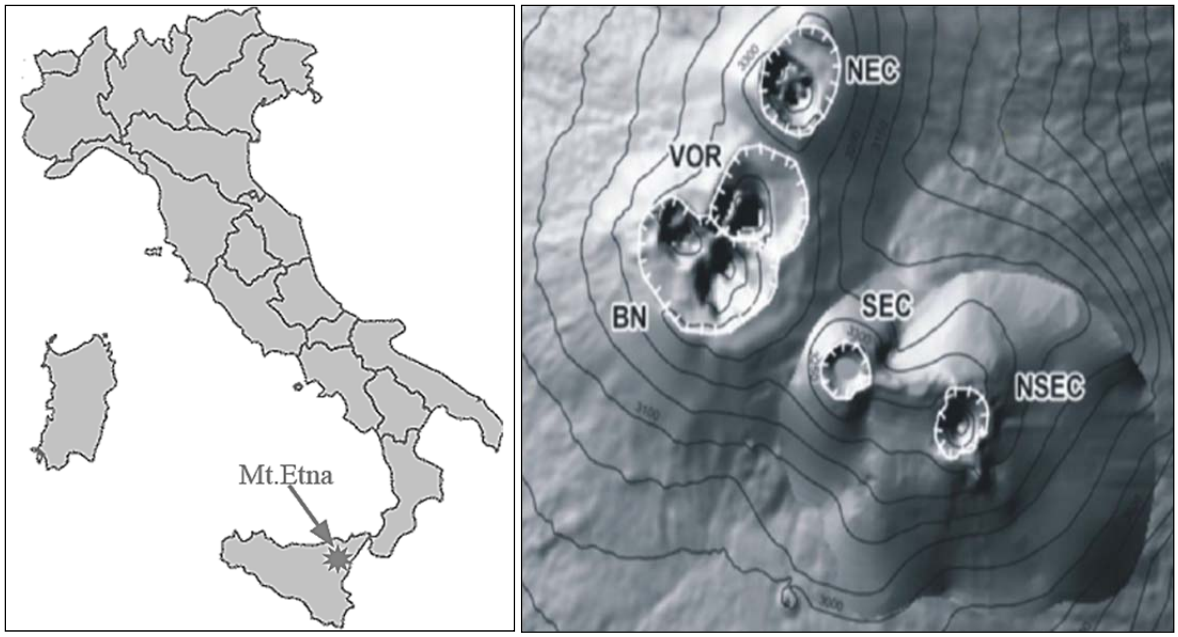

Figure 6.1 Location of Mt. Etna (Italy) and main craters

6.1 Characterisation of the natural phenomenon

Palumbo [82] analysed the eruptions of Mt. Etna for to the period 1790 – 1993 and showed that no eruptions with VEI > 4 occurred. According to this work, the average number of eruptions with VEI = 1 over a time interval of 20 years is 3.1, with VEI = 2 it is 4.6 and with VEI = 3 it is 1. Branca and Del Carlo [81] showed that from ~ 1950, the volcano has changed its eruptive characteristics and more violent explosive eruptions occurred. More recent details about the eruptive activity of Mt. Etna are reported by the National Museum of Natural History and published in the related web-site [83]. Furthermore, based on the current state of knowledge, it is not possible to forecast the characteristics of next eruptive events. For this reasons, two representative scenarios for the volcano were considered in this study (characterised by different emission rate Q_e). As suggested by Scollo et al. [84], the representative events (both characterised by VEI = 3) are:

- *Scenario 1*: the event occurred during the period 21st – 24th July 2001 (Q_e = 5·10^3 kg/s), which represents the most frequent explosive event;
- *Scenario 2*: the event occurred during the period 27th October – 30th December 2002 (Q_e = 10^5 kg/s), which is the worst observed explosive event.

6.2 Census of the vulnerable elements

Figure 6.2 and Figure 6.3, respectively, give the census of establishments at major risk and power plants and of wastewater treatment plants for the case-study.

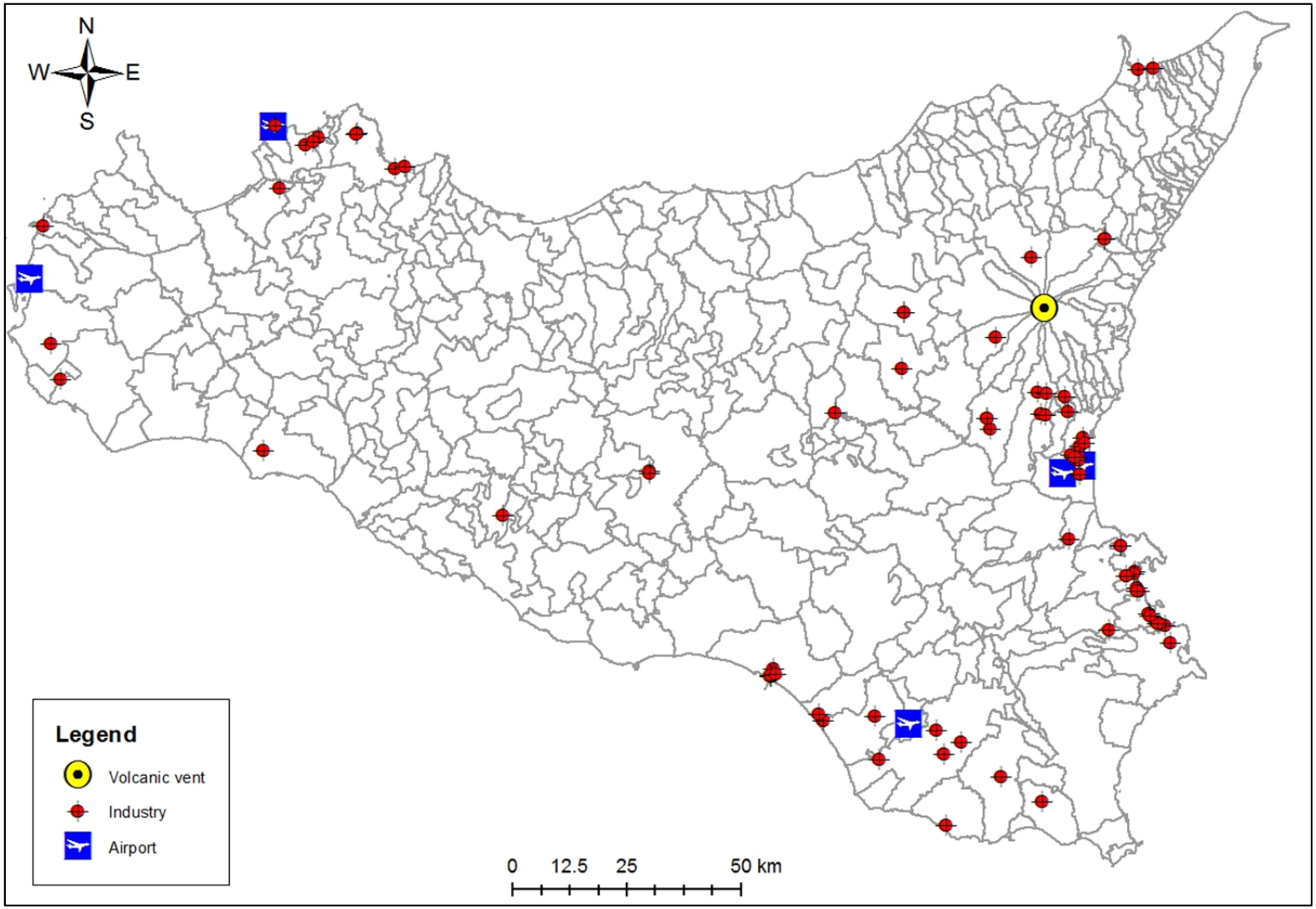

Figure 6.2. Census of industries at major risk and power plants.

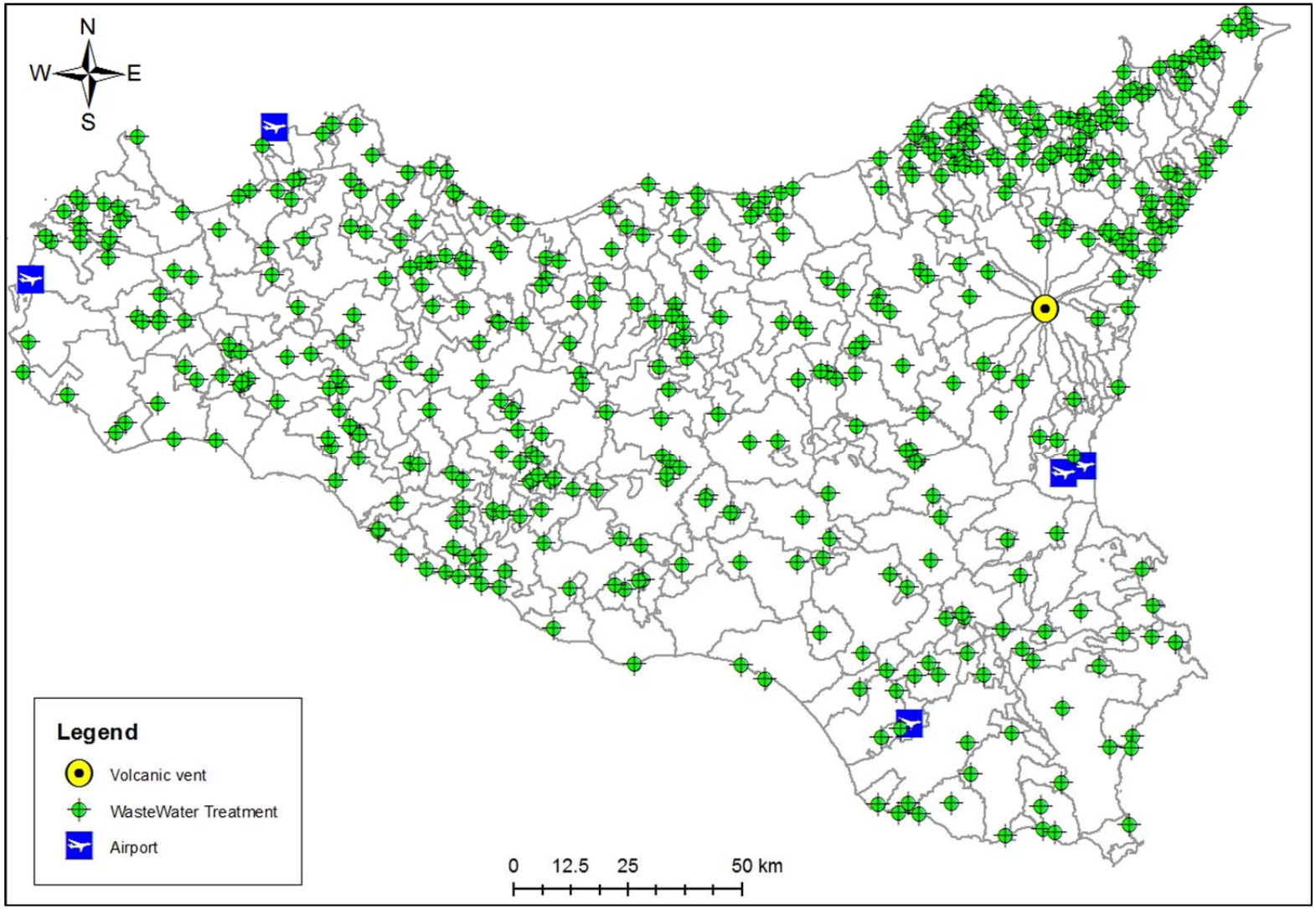

Figure 6.3. Census of WasteWater Treatment plants.

6.3 Characteristics of floating roof storage tanks

A model of floating roof was chosen. The roof was assumed a cylinder with radius of 20 m, depth 1 m and weight $1.5 \cdot 10^5$ kg, which may be considered to be a reasonable approximation to a double deck floating roof.

6.4 Characteristics of air intake filters

To identify the conditions leading to malfunctions of filters through the Ergun equation, the density and viscosity of the *dusty gas* were calculated. Density was determined by using the ash particle size distribution [85] and is a function of the ash concentration c. The viscosity was estimated through the Einstein correlation, which assumes that the *dusty gas* is a dilute suspension of spheres in the air. Figure 6.4 shows the trend of μ (black line) and ρ (red line) with respect to c for both the eruptive scenarios.

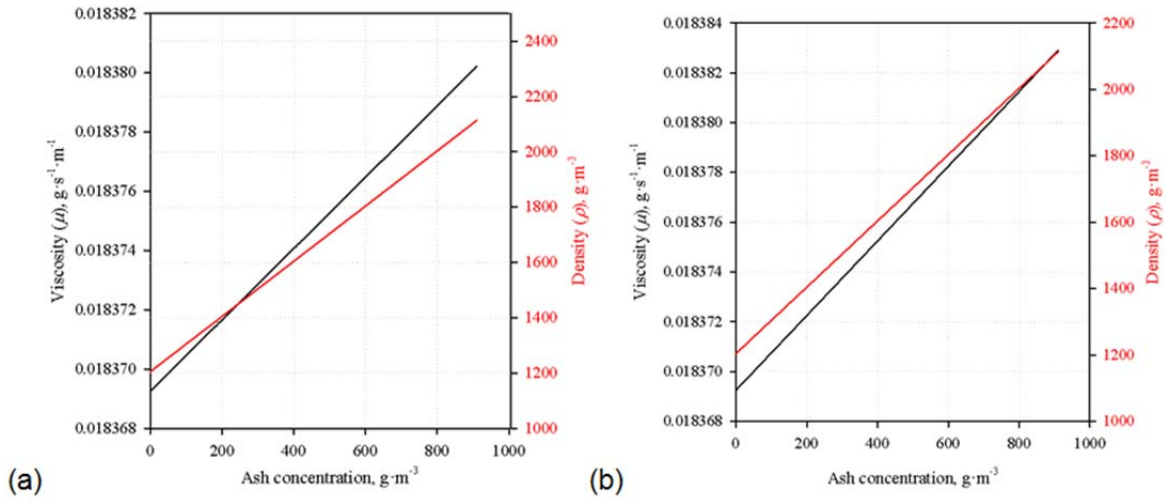

Figure 6.4. Viscosity (black line) and density (red line) of the dusty gas vs. ash concentration (a) scenario 1 and (b) scenario 2.

Given the presence of pharmaceutical and microelectronic industries in the area surrounding Mt. Etna, numerical calculations were made for a filter F7 (according to the European classification [86]). The system is at high-efficiency of filtration and/or for fine dust and has the following characteristics:

- flow rate Q = 0.9444 m^3/s,
- filtering surface A_f = 6.60 m^2.

6.5 Characteristics of screens

The characteristics of the square opening fine screen (Figure 6.5), chosen for this study, are given in Table 6.1.

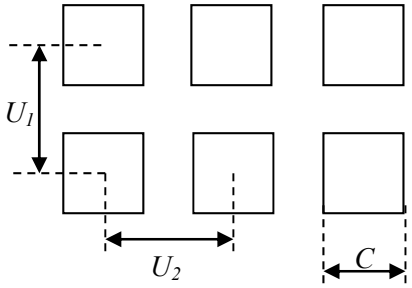

Figure 6.5. Square opening fine screen.

Table 6.1. Fine screen characteristics

Parameter	Symbol	Unit	Value
Wastewater flow rate	Q	m^3/s	0.8
Wastewater velocity	uf	m/s	0.7
Area of submerged screen	A	m^2	1.14
Effective open area of submerged screen	A_s	m^2	0.285
Opening size	C	m	$0.5 \cdot 10^{-4}$
Vertical opening distance	U_1	m	10^{-3}
Horizontal opening distance	U_2	m	10^{-3}
Bar spacing	b_1	m	$0.5 \cdot 10^{-3}$
Bar thickness	b_2	m	$0.5 \cdot 10^{-3}$

The first step of the methodology of Section 4.7.1 was the calculation of the Reynolds number for the wastewater stream, which flows in the granular bed (ash deposit). Thus the characterisation of some ash samples was necessary to obtain the main parameters for the particles (dimension, ρ, S, e and k) needed to calculate the Reynolds number of the wastewater stream and to make possible the choice of the approach for the computation of the thicknesses of the deposit.

6.6 Characteristics of Grit Removals

The characteristics of the equipment, chosen for this study, are given in

Table 6.2. Also in this case, to apply the methodology described in Section 4.7.2, it was necessary to know the ash characteristics; thus the characterisation of some ash samples was necessary. Then, the K parameter for the wastewater stream was calculated to make possible the choice of the approach for the computation of the terminal settling velocities.

Table 6.2. Horizontal grit removal chamber characteristics [87].

Parameter	**Symbol**	**Unit**	**Value**
Wastewater flow rate	Q	m^3/s	1.215
Wastewater velocity	u_f	m/s	0.3
Vessel length	L_v	m	18.00
Vessel width	W_v	m	3.00
Vessel height	H_v	m	1.35
Cross section	A_{gr}	m^2	4.05
Retention time	t_o	s	60
Critical velocity of settling	u_o	m/s	0.0225

6.7 Volcanic ash samples collection

Volcanic ash samples, produced by eruptions of Mt. Etna, were collected at different locations (see Figure 6.6):

- Sample ID=1 – close to Cratere Silvestri (coordinates: lat. 37°41'55.73"N , long. 15°0'16.94"E; distance 5,5 km);
- Sample ID=2 – urban area of Messina during the eruption of the 23rdFebruary 2013 (coordinates: lat. 38°10'16.66"N, Long: 15°31'25.56"E; distance 65 km);
- Sample ID=3 – Giarre (coordinates: lat. 15°10'9"E, long. 37°44'5"N; distance 15.5 km).

Figure 6.6. Locations of the collected ash samples.

7

Ash Characterisation

Some experimental tests were made to characterise the volcanic ash and obtain size distribution, density, specific surface area, voidage and permeability. The results of ash characterisation were needed in order to apply the methodologies described above. The following experimental tests were performed:

- Analysis of the size distribution (sieving)
- Density determination (EN 1097-3 standard)
- Specific surface area measurement (BET method) and calculations of specific surface area and voidage
- Determination of the permeability (permeameter at constant head)

7.1 Analysis of the size distribution

The sieving is the method used to determine the size distribution of the volcanic particles. The analysis makes use of special sieves arranged in a column; each of them retains the fraction of granules having larger dimensions compared with those of the holes of the sieve. The sieves must be stacked in such a way that the top has the larger mesh and the others have a gradually smaller mesh going down to the bottom. At the base of the column, there is a plate which is used to collect the granules with smaller diameters than the holes of the sieve with the lower mesh. The column is placed on a mechanical shaker for 20 min and, after the shaking, the solid fractions retained by each sieve is weighted. The weight of each solid fraction is then compared to the weight of the total solid to obtain the percentage of solid retained by each sieve. In this study a wet sieving has also been used to determine the potential of the particles to coalesce due to the weak interaction with water.

To determine the size distribution of the dry samples, these have been weighted and dried in an oven, then each sample was placed in the top sieve and the column was shaken. The wet samples are the result of a mixing process of ash and water and a subsequent filtration. The mixing allowed simulating the effect of the rain.

The results of the size distributions of the ash samples were calculated and presented in a logarithmic graph of the retained percentage of solid versus the parameter ϕ (Krumbein parameter), which is expressed by the following correlation:

$$\phi = -\log_2 \frac{d_p}{d_0} \tag{39}$$

where: d_p = diameter of the particle (mm); d_o = reference diameter, which is equal to 1 mm to make the equation dimensionally consistent [88].

7.2 Density determination

The density determination was performed according to the EN 1097-3 standard [89]. The density is the *loose bulk density* (*bulk density*), which is defined as the mass of the dried particles (not compressed). The total volume includes particles volume, inter-particles void volume and internal pore volume [90]. According to this definition, the density determination was executed by using a container, whose volume and weight are known. It was filled with the volcanic ash and, subsequently, weighed. The weight and the volume of the ash allowed to determinate the density of samples.

7.3 Specific surface area and voidage determination

Several methods were used to estimate specific surface area and voidage:

- measurements with a Micromeritics ASAP 2020 sorption apparatus;
- comparison between sample characteristics and literature data;
- numerical elaborations.

These allowed achieving different results for the parameters to be estimated.

Specific surface area measurements were initially executed by using a Micromeritics ASAP 2020 sorption apparatus. The samples (~ 1 mg) were outgased in vacuum at 250°C at least 16 h. The S values were calculated by applying the BET model (S_{BET}).

By comparing the geometrical characteristics of collected ash with those of different granular beds given by Coulson et al. [62] (Table 7.1), some representative values of e and S were assumed (associated with particles having similar dimensions).

Table 7.1. Properties of beds of some regular-shaped materials [62].

N.	Sample	d_p (mm)	S (m^{-1})	e	B (m^2)
1	Spheres	0.794	7600	0.39	$6.2 \cdot 10^{-10}$
2	"	1.588	3759	0.41	$2.8 \cdot 10^{-9}$
3	"	3.175	1895	0.39	$9.4 \cdot 10^{-9}$
4	"	6.35	948	0.41	$4.9 \cdot 10^{-8}$
5	"	7.94	756	0.42	$9.4 \cdot 10^{-8}$
6	Cubes	3.175	1860	0.19	$4.6 \cdot 10^{-10}$
7	"	3.175	1860	0.43	$1.5 \cdot 10^{-8}$
8	"	6.35	1078	0.32	$1.4 \cdot 10^{-8}$
9	"	6.35	1078	0.46	$6.9 \cdot 10^{-8}$
10	Hexagonal prisms	4.76 x 4.76	1262	0.36	$1.3 \cdot 10^{-8}$
11	"	4.76 x 4.76	1262	0.47	$5.9 \cdot 10^{-8}$
12	Triang. pyramids	6.35 x 2.87	2410	0.36	$6.0 \cdot 10^{-9}$
13	"	6.35 x 2.87	2410	0.52	$1.9 \cdot 10^{-8}$
14	Cylinders	3.175 x 3.175	1840	0.4	$1.1 \cdot 10^{-8}$
15	"	3.175 x 3.175	1585	0.4	$1.2 \cdot 10^{-8}$
16	"	6.35 x 6.35	945	0.41	$4.6 \cdot 10^{-8}$
17	Plates x 0.794	6.35 x 6.35	3033	0.41	$5.0 \cdot 10^{-9}$
18	"	6.35 x 6.35	1984	0.41	$1.1 \cdot 10^{-8}$
19	Discs	3.175 x 1.59	2540	0.4	$6.3 \cdot 10^{-9}$
20	Porcelain Berl saddles	6	2450	0.69	$9.8 \cdot 10^{-8}$
21	"	6	2450	0.75	$1.73 \cdot 10^{-7}$
22	"	6	2450	0.79	$2.94 \cdot 10^{-7}$
23	"	6	2450	832	$3.94 \cdot 10^{-7}$
23	"	6	2450	832	$3.94 \cdot 10^{-7}$
24	Lessing rings	6	5950	0.87	$1.71 \cdot 10^{-7}$
25	"	6	5950	0.89	$2.79 \cdot 10^{-7}$

Then numerical elaborations were performed to achieve the specific surface area and voidage by means of the Equations (40) and (41) [62], which are based on the assumption that the samples are composed of spherical particles (with the same dimensions):

$$S = \frac{6}{d_p \cdot \rho \cdot 1000} \tag{40}$$

$$e = 1 - \frac{\rho_{loose\ bulk}}{\rho_{solid}} \tag{41}$$

where: $\rho_{loose\ bulk}$ = density of not compressed dried particles (kg/m^3) and ρ_{solid} = density of particles without inter-particles void (kg/m^3).

In Equation (40) the diameter of the particle (d_p) is expressed in m, thus the calculated specific surface area (S) has the unit m^2/g.

7.4 Determination of the permeability

Permeability (or hydraulic conductivity, k) refers to the ease with which water can flow through a granular solid. It is determined by using the constant head (load) test (according to the standard ASTM D 2434 [91]), which is used only for permeable materials (k > 10^{-4} cm/s). A homemade permeameter at constant head was made for such experiments (see scheme in Figure 7.1). The sample was subjected to a fixed piezometric load (Δh); then, the volume of water, passing through it during a certain time (t), was measured. The value of k is given by the equation:

$$k = \frac{L}{\Delta h \cdot A} \cdot \frac{V}{t} \tag{42}$$

where: L_{pm} = length of the porous medium (sample) (m); A_{pm} = cross section of the porous medium (sample) (m^2); V_{water} = volume of water collected during the time t (m^3); Δh = piezometric load (m).

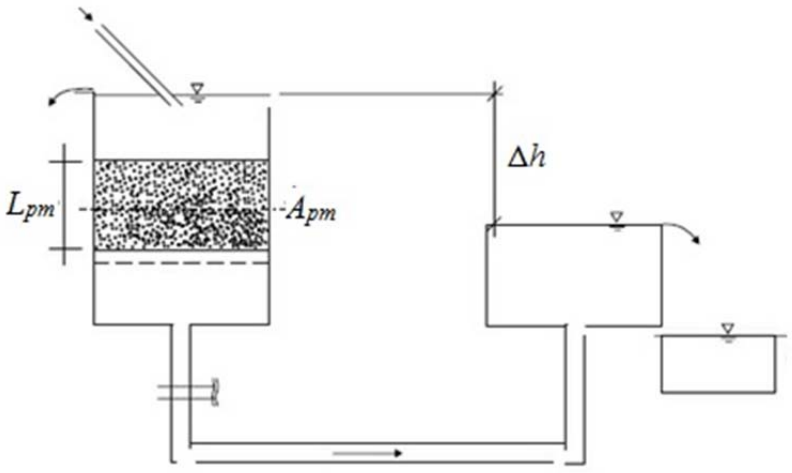

Figure 7.1. Permeameter at constant head.

8

Results and Discussions

This Chapter is composed of two parts: the first one gives the ash characterisation results and the other one illustrates those of the estimation of the equipment vulnerability.

8.1 Ash characterisation results

In this Section, the results of the ash characterisation are presented.

8.1.1 Grain size distributions

Figure 8.1, Figure 8.2 and Figure 8.3 give the grain size distributions of the volcanic ash samples.

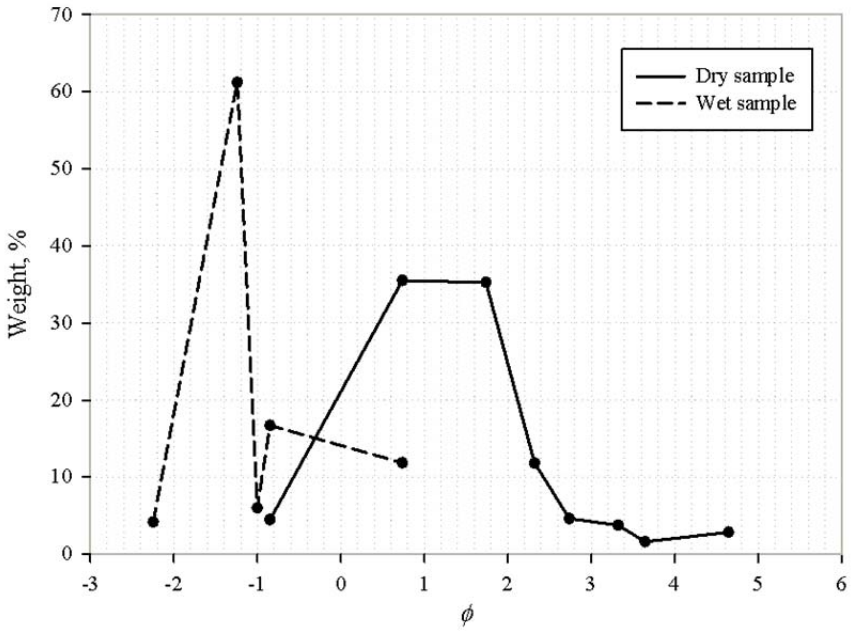

Figure 8.1. Size distribution for Sample ID 1.

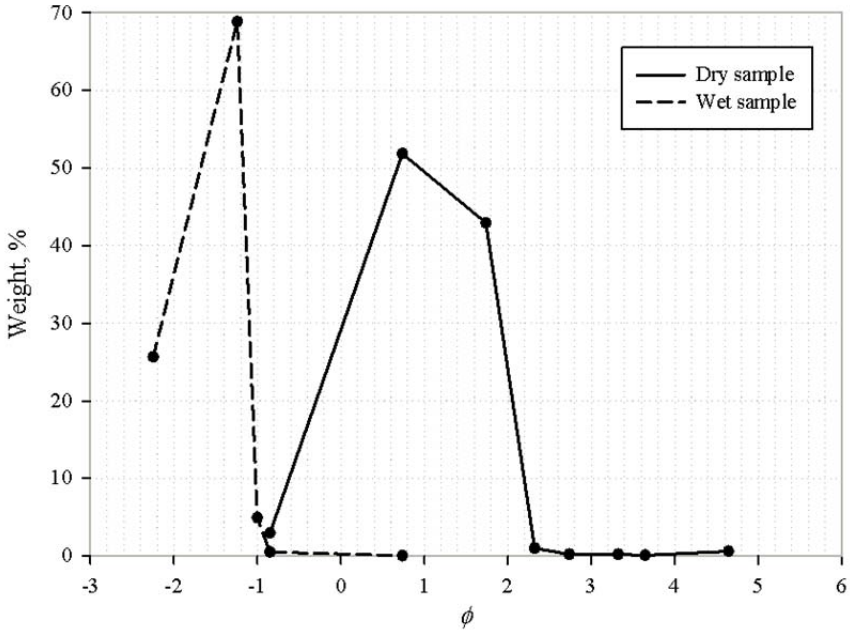

Figure 8.2. Size distribution for Sample ID 2.

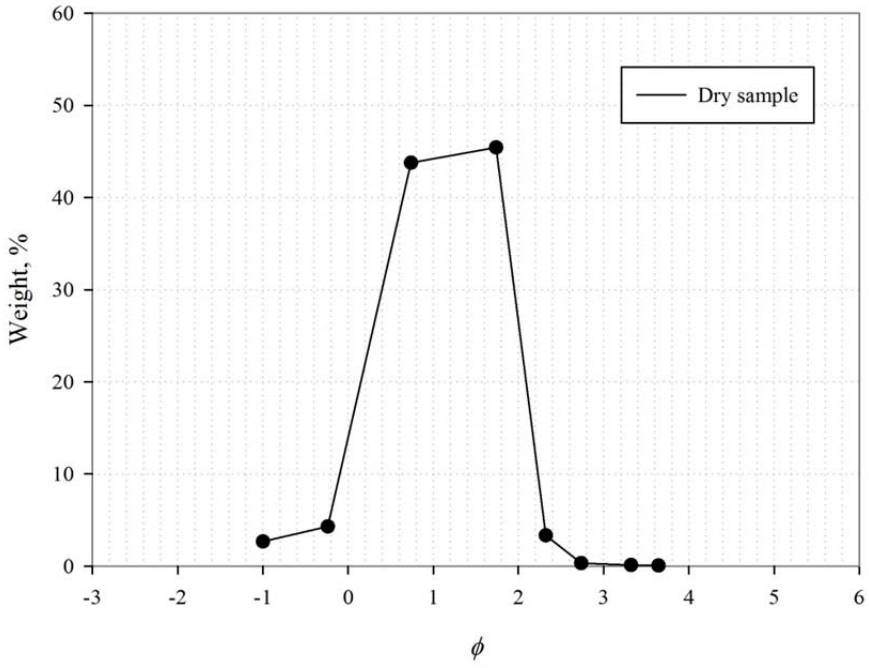

Figure 8.3. Size distribution for Sample ID 3.

Due to some technical problems, the aggregation tests of the ash in presence of water was not carried out for the Sample ID 3, thus the particle size distribution analysis of the wet particles were executed only for samples ID 1 and 2.

By analysing the results, the prevailing diameters for dry ash particles are:

- 0.1 ÷ 1,18 mm (ϕ = 3.3 ÷ -0.24) for the Sample ID 1;
- 0.15 ÷ 1.18 mm (ϕ = 2.7 ÷ -0.24) for the Sample ID 2;
- 0.15 ÷ 2 mm (ϕ = 2.7 ÷ -1) for the Sample ID 3.

After the mixing of ash with distilled water, a certain degree of aggregation is observed as indicated by Textor et al. (2006) [34]; the prevailing diameters for the aggregates are:

- 0.6 ÷ 4.75 mm (ϕ = 0.7 ÷ -2.2) for Sample ID 1;
- 2 ÷ 4.75 mm (ϕ = -1 ÷ -2.2) for the Sample ID 2.

The size distribution analysis gave the data of Table 8.1

Table 8.1. Diameter of particles (dry samples).

Sample ID	Weighted Average Diameter (m)	Maximum Diameter (m)	Minimum Diameter (m)
1	$4.09 \cdot 10^{-4}$	$1.18 \cdot 10^{-3}$	$6 \cdot 10^{-5}$
2	$4.78 \cdot 10^{-4}$	$1.18 \cdot 10^{-3}$	$6 \cdot 10^{-5}$
3	$5.1 \cdot 10^{-4}$	$2 \cdot 10^{-3}$	$7.5 \cdot 10^{-5}$

8.1.2 Density

The weighted ash densities of the samples are given in Table 8.2. It must be pointed that Sample ID 2 was collected at about 65 km away from the main crater, thus it is obvious to suppose that the light particles were transported at greater distances during the ash cloud dispersion.

Table 8.2. Ash densities.

Sample ID	Bulk density (kg/m^3)	Solid density (kg/m^3)
1	1470	2830
2	1070	2100
3	1550	3050

8.1.3 Specific surface area and voidage

The measurements of the specific surface area provided a very low S value, which was close to the sensitivity limit of the sorption apparatus. Further investigation would be needed. The measured value is higher than that indicated for sands by Jury and Horton [92]. By comparing particles having the same size, a comparable S reflects probably a high porosity.

Previously to the execution of the ash characterisation, by comparing the geometrical characteristics (weighted average diameter and shape) with those given in Table 7.1, the following preliminary values were assumed: S = 7600 m^{-1} and e = 0.393.

Then the specific surface area was calculated using the weighted average diameter of the particles, its maximum and minimum values were also determined. Results are given in Table 8.3.

Table 8.3. Specific surface area.

Sample ID	Specific surface area (m^2/g)			
	BET method	dp = weighted average diameter	dp = maximum diameter	dp = minimum diameter
	S_{BET}	S_{av}	S_{min}	S_{max}
1	--	$9.97 \cdot 10^{-3}$	$3.46 \cdot 10^{-3}$	$6.80 \cdot 10^{-2}$
2	--	$1.17 \cdot 10^{-2}$	$4.75 \cdot 10^{-3}$	$9.35 \cdot 10^{-2}$
3	--	$7.58 \cdot 10^{-3}$	$1.94 \cdot 10^{-3}$	$5.16 \cdot 10^{-2}$

The weighted specific surface area was elaborated by using the values of S of each grain class of ash (calculated by Equation (40)). Finally the weighted voidage was also determined by using both *loose bulk* and *solid* densities of each grain class and Equation (41). Results are given in Table 8.4; Figure 8.4 and Figure 8.5, respectively, show the specific surface area and the voidage with respect to the class of particles' size. Results for Sample ID 2 are not available given that its quantity was not enough to make further analysis.

Table 8.4. Weighted values for S and e for Sample ID 1 and 3.

Sample ID	Specific surface area		Voidage (dimensionless)
	(m^{-1})	(m^2/g)	
1	~ 22,500	15.19	0.48
3	~ 15,000	9.75	0.49

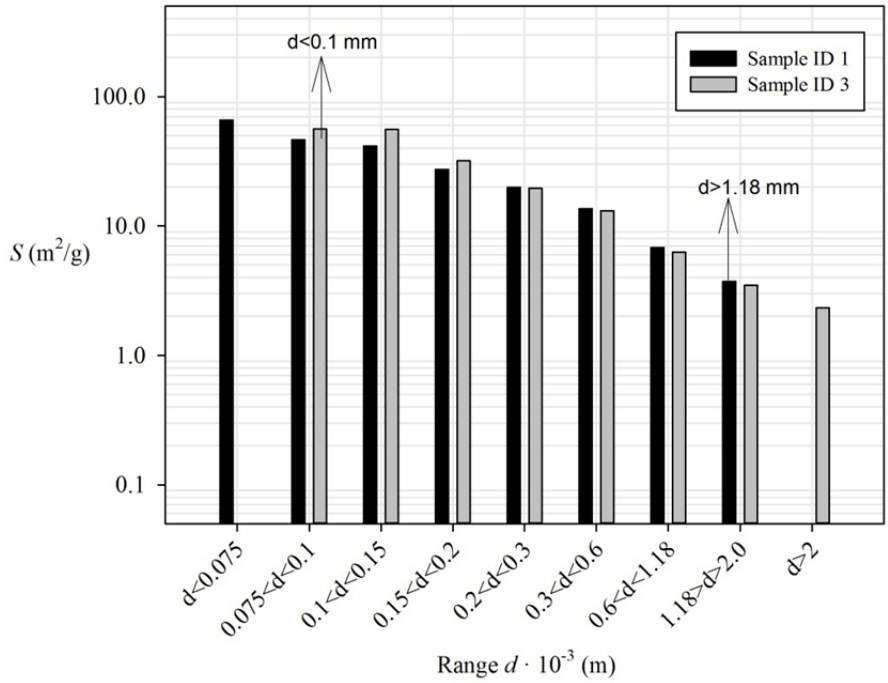

Figure 8.4. Specific surface area with respect to the class of particles' size.

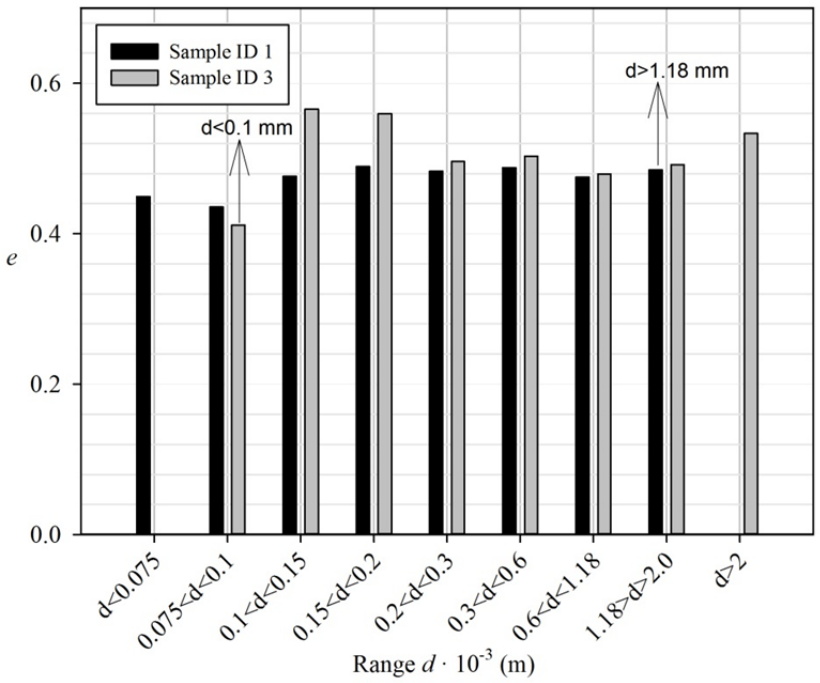

Figure 8.5. Voidage with respect to the class of particles' size.

Thus, the calculation of S was made by assuming a smooth and spherical shape and the same dimension for the particles. It was carried out assuming that the diameter of the spheres is equal to the weighted average diameter and, subsequently, equal to the maximum and minimum diameter of the particles (Table 8.3). It was found that S clearly increases as d decreases and, by assuming a constant diameter (as in the case of the maximum diameter, which is the same for Samples ID 1 and 2), S is greater for the sample having a lower density (Sample ID 2), reflecting a higher porosity. Further confirms can been found in the last case, where, by comparing the Samples ID 1 and 3, S resulted greater for Sample ID 3 only for particles with d < 0.2 mm (in this case Sample ID 3 has the lowest density, this reflects a higher porosity); whereas when d > 0.2 mm, S is almost the same for Samples 1 and 2 (S_1 is slightly higher than S_3, meaning that the porosity is comparable for both samples).

Concerning data of the voidage of the Sample ID 1, it ranges between 0.46 and 0.49 (Figure 8.5), with a prevailing contribution of the particles' class having 0.15 < d < 0.2 mm; while the Sample ID 3 shows a greater voidage variability than the Sample ID 1, in this case e is higher (~ 0.56) for the classes having 0.1 < d < 0.15 mm and 0.15 < d < 0.2 mm, but the prevailing contribution to the weighted voidage is given by the classes 0.3 < d <0.6 mm and 0.6 < d < 1.18 mm. The voidage for Sample ID 2 is not available for the reason mentioned above.

8.1.4 Permeability

The measurements, executed with the permeameter at constant head, allowed the calculation of k. The permeability is close to $2.5 \cdot 10^{-5}$ m/s; it can be stated that the ash samples from Etna has an average permeability according to the International classification of soils (because k is comprised in the range $10^{-3} \div 10^{-5}$ m/s).

8.2 Threshold limit for atmospheric fixed roof storage tanks

The threshold limits of ash load on fixed roof tanks were calculated using the analogy with the snow load. The threshold limits S1, S2 and S3 are, respectively, the load causing light damage, structural damage and the collapse of the fixed roof. The ash loads are given in Table 8.5.

Table 8.5. Threshold limits for damage to a fixed roof tank

	Light damage (S1)	**Structural damage (S2)**	**Structure collapse (S3)**
Load (kg/m^2)	122	357	714

8.3 Threshold limit for floating roof storage tanks

To apply the approach described in Section 4.5.2, Equation (10) was firstly applied to two laboratory floating beakers in water (as described in [58]), which were used to simulate by extrapolation the behaviour of floating roofs. Their characteristics and those of the floating roof are given in Table 8.6, where the results of the calculation of their flotation stability are also shown.

Table 8.6. Characteristics and floatation stability for the immersion in water of two laboratory beakers and the model floating roof.

Parameters	**Beaker A**	**Beaker B**	**Parameters**	**Floating roof**	
R (cm)	4.708	3.436	R (m)	20	
δ (cm)	5.490	9.642	δ (m)	1	
M_{beaker} (g)	92.27	96.01	$M_{roof}/10^5$ (kg)	1.5	
z_B (cm)	1.963	4.135	z_B (m)	0.5	
$\rho_{liquid}/10^3$ (kg·m^{-3})	1.0	1.0	$\rho_{liquid}/10^3$ (kg·m^{-3})	1.0	0.8
δ_{imm} (cm)	1.325	2.589	δ_{imm} (m)	0.119	0.149
z_M (cm)	4.843	2.434	z_M (m)	837.58	670.32
(z_M-z_B) (cm)	2.880	-1.701	(z_M-z_B) (m)	837.08	669.82

Figure 8.6 shows the variation of the height of the ash deposit with respect to the immersion depth for different liquid and ash densities. The right ordinate shows the ratio of the weight of ash to the weight of the roof. It can be seen that, in order to sink the roof, the weight of the ash deposit must be several times larger than the weight of the roof [93].

Generic values of ash density were considered to represent dry particles (1000 kg/m^3) and wet particles (2000 kg/m^3) of ash, whereas two liquid densities were assumed (respectively 800 and 1000 kg/m^3) to include all liquid fuels.

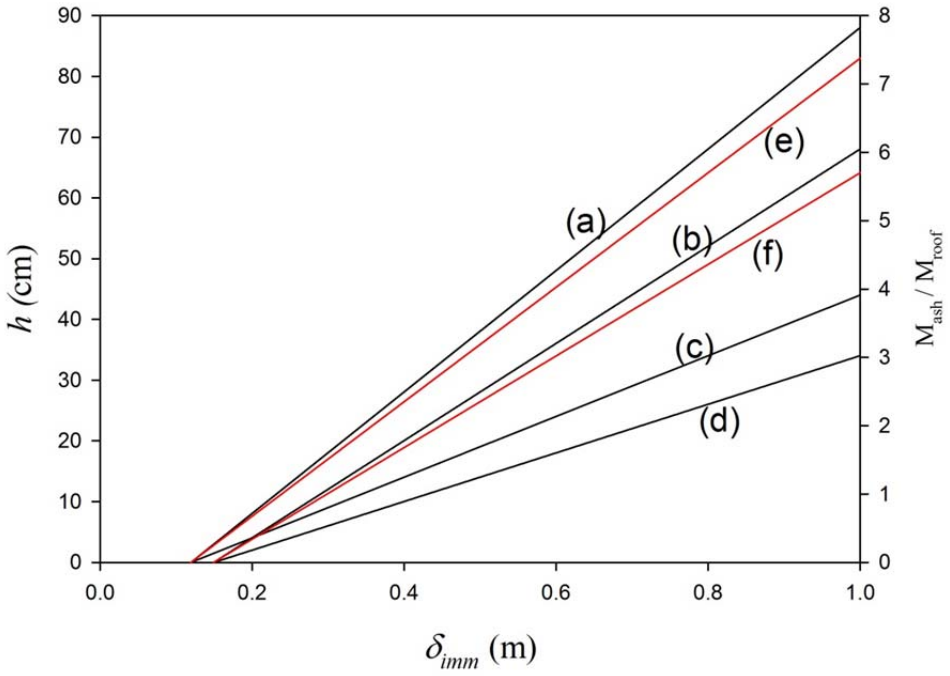

Figure 8.6. Variation of the height of the ash deposit with respect to the immersion depth for different liquid and ash densities. Depth of the ash deposit to sink the floating roof for ρ_{liq} = 1,000 kg m^{-3}: (a) ρ_{ash} = 1,000 kg m^{-3} (c) ρ_{ash} = 2,000 kg m^{-3} and ρ_{liq} = 800 kg m^{-3}: (b) ρ_{ash} = 1,000 kg m^{-3} (d) ρ_{ash} = 2,000 kg m^{-3}. The right ordinate shows the ratio M_{ash}/M_{roof} for (e) ρ_{liq} = 1,000 kg m^{-3} and (f) ρ_{liq} = 800 kg m^{-3} [93].

The potential failures are the sinking and the capsizing of the roof, related threshold limits are indicated as T1, T2 and T3 [94]. T1 is the ash load which causes a partial immersion of the roof leading to the release of a liquid quantity equal to ¼ the volume of the roof (Figure 8.7(a)). T2 is the ash load, which sinks the roof (full immersion); this failure is an extreme damage (due to the great ash amount required to sink it) and causes the release of a liquid volume equal to that of the roof plus the ash deposit (Figure 8.7(b)). To capsize the roof the deposit must become asymmetric, assuming an initial symmetric ash distribution, the asymmetry is caused by local wind. The threshold value for the roof capsizing (T3) is the mass of ash that, assuming a specific asymmetric distribution, leads to an asymmetrical immersion of the roof as shown in Figure 8.7(c). It is obvious that once T3 is known, related to this particular asymmetrical deposition, the probability of capsizing is conditioned by the occurrence of certain weather conditions. Also this mode failure is an extreme damage. Table 8.7 gives the threshold limits for sinking and capsizing for the model double deck floating roof.

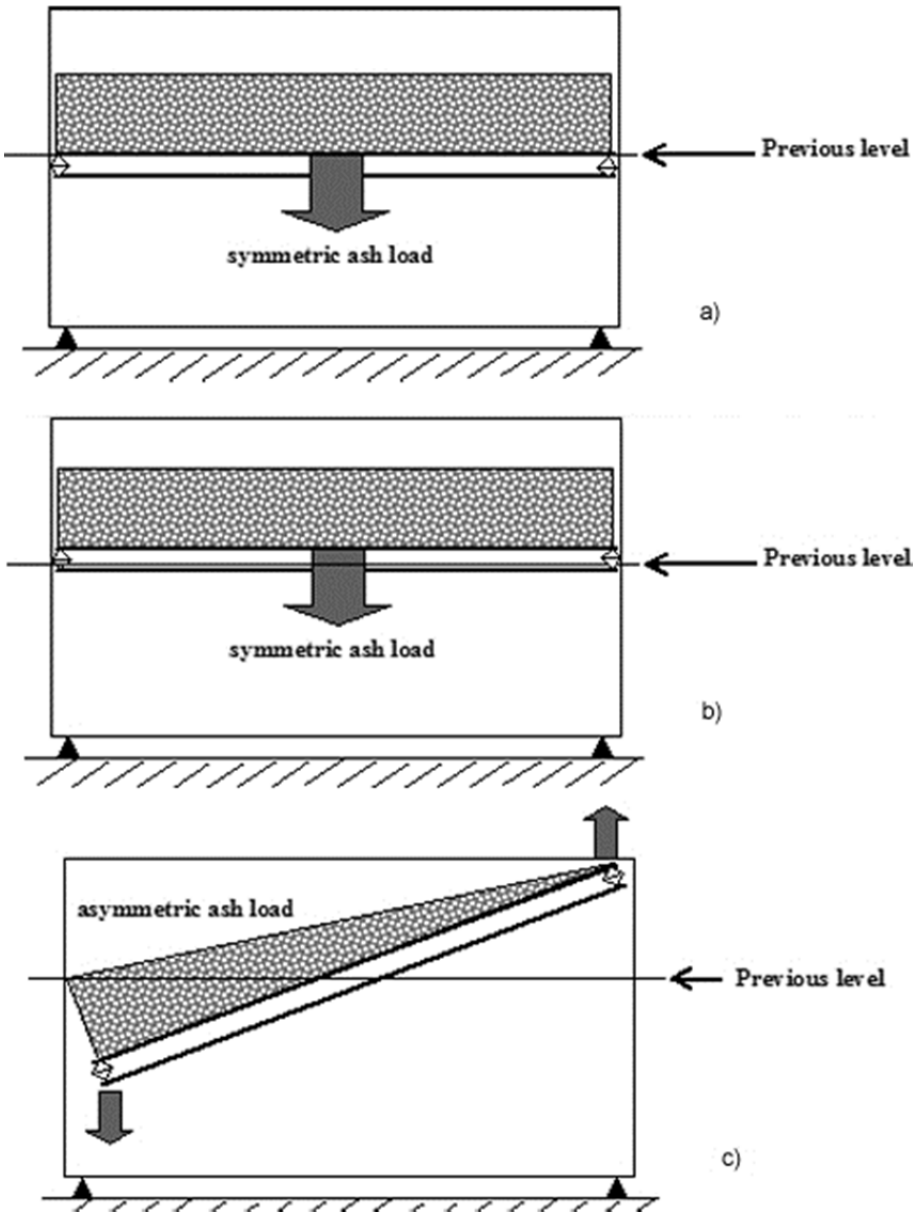

Figure 8.7. Potential failure modes for floating roof tanks: (a) partial immersion of the roof leading to a release of a liquid quantity equal to one-fourth of the volume of the roof, (b) roof sinking and (c) roof capsizing.

Table 8.7. Threshold limits for sinking and capsizing for the model double deck floating roof.

	Partial immersion of the roof (T1)	**Roof Sinking (T2)**	**Roof capsizing (T3)**
Load (kg/m^2)	170*	680	135**

*causing the release of an amount of liquid equal to ¼ the roof volume

**with an ash distribution causing an asymmetrical immersion of the roof equal to ½ its height

8.4 Threshold limits for air intake filters

The threshold limits of volcanic ash deposit on the filtering surface are indicated M1 and M2 [94]. M2 is calculated by the manufacturer using the critical value of pressure drop and represents the mass of deposit causing the rupture; whereas M1 was assumed as a threshold for partial damage and is defined as the mass accumulated on the surface equal to ½ the amount of ash causing the filter rupture (partial clogging). For the filter typology considered in this study, the numerical values are:

- M1 = 250 g
- M2 = 450 g

8.5 Exceedance probability curves and vulnerabilities

After the estimation of the threshold value of the physical parameter, the exceedance probability must be determined, which is given by the probability that, given the occurrence of an explosive eruption having a certain magnitude, the physical parameter will exceed the threshold limit. This probability is the equipment vulnerability to the ash fallout with respect to a given damage mode. Figure 8.8 and Figure 8.9 show the probability of exceedance curves of the physical parameters (ground ash load and concentration in the atmosphere) for a location of the case-study. In both the figures, the dashed line refers to the most frequent scenario and the solid one to the worst-case scenario.

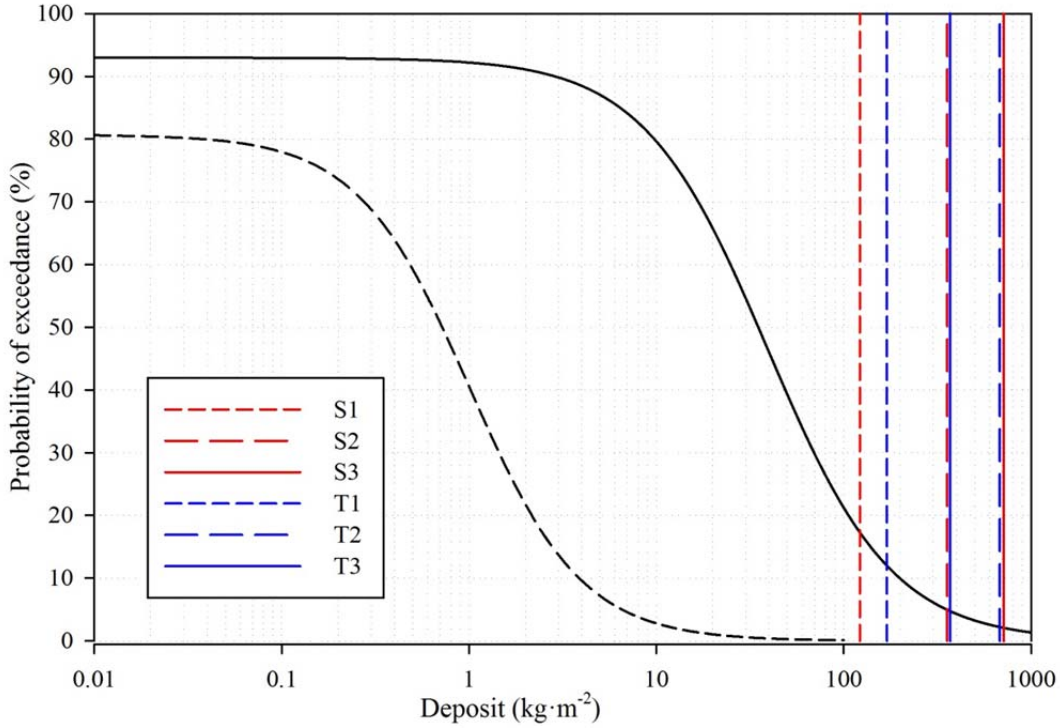

Figure 8.8. Exceedance probability as a function of ash load.

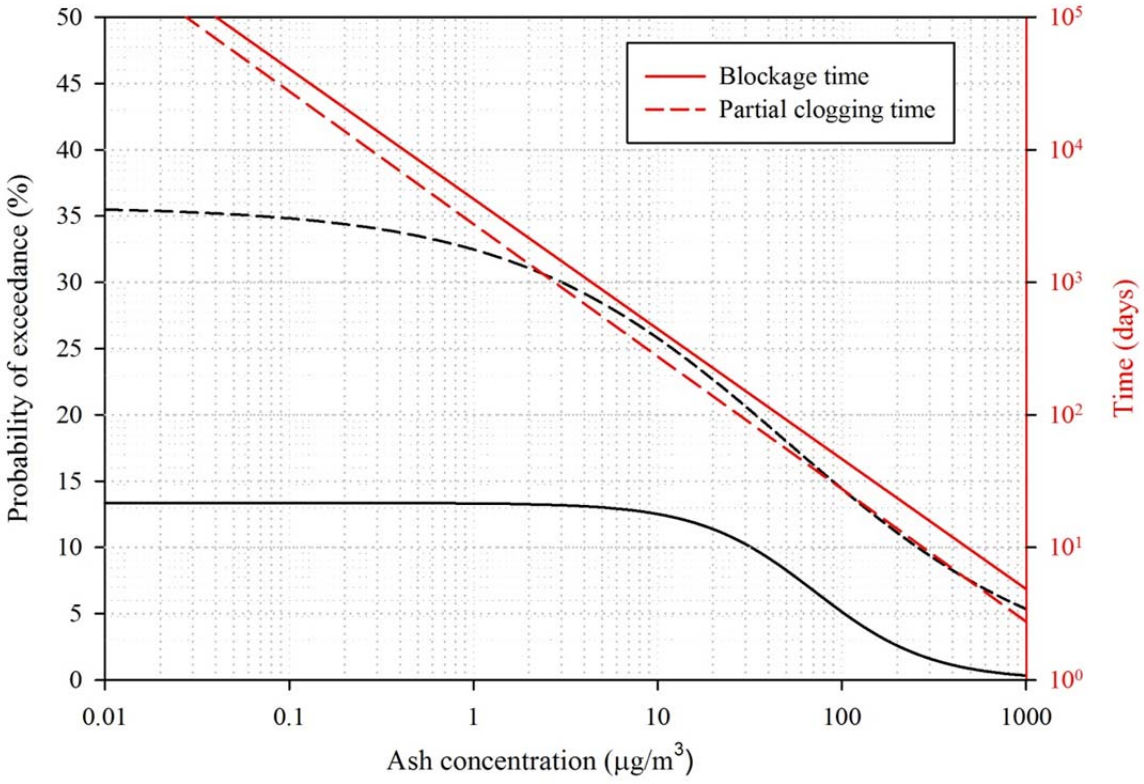

Figure 8.9. Exceedance probability and the time of clogging as a function of ash concentration.

At a given location, the vulnerability for storage tanks can be obtained from Figure 8.8. Through the use of the threshold values defined above, the exceedance probabilities can be directly read on the graph (the lines S1, S2, S3 refer to fixed roof tanks, whereas T1, T2, T3 to floating roof tanks).

In order to determine the probability of occurrence of the conditions leading to the partial clogging or the rupture of the filter, the exceedance curve of ash concentrations was overlapped to the line giving the trend of the time of clogging. Thus the graph of Figure 8.9 associates each concentration with both the exceedance probability and the time necessary to clog the filter. In this case, the failure probability has to be conditioned by the occurrence of an event with certain duration. The values M1 and M2 derive from different combinations of t and c, this means that, once the concentration is known, the probability of exceedance can be read on the left ordinate and is associated with a specific time, respectively, of clogging or blockage (right ordinate). As an example, given the occurrence of a volcanic ash emission and assuming a concentration of 200 μg/m^3 in the location related to Figure 8.9, the time for the clogging of the filter is about 5 days and for the blockage is equal to 10 days. Using the same graph the exceedance probability of the concentration of 200 μg/m^3 can be achieved, it results about 7 % for most frequent scenario and 1 % for the worst-case.

8.6 Vulnerability maps

By using the ModelBuilder, the vulnerability maps are provided through the geo-processing model of Figure 5.2, it runs in a semi-automatic mode. It is necessary to know the exceedance probabilities related to some locations in the area. In the flow chart of Figure 5.2, the inputs are geospatial data (locations) related to the sample points and the exceedance probabilities; the first operation gives the correlation between the inputs, then a spatial interpolation approach is automatically run and, finally, maps will be produced. The last operation, “delete field”, restores the input files, this permits an easy management of the dataset.

In this work, the spatial distribution of points of Figure 8.10 was used as a base for the interopolation. Then by means of the semi-automatic procedure the vulnerability maps for the case-study have been obtained (Figure 8.11, Figure 8.12, Figure 8.13, Figure 8.14). Each map represents a iso-probability curve on cartography: Figure 8.11 and, Figure 8.12 refer to light damage of fixed roof tanks, whereas Figure 8.13 and Figure 8.14 show probabilities of exceedance of threshold limit for filters’ partial clogging.

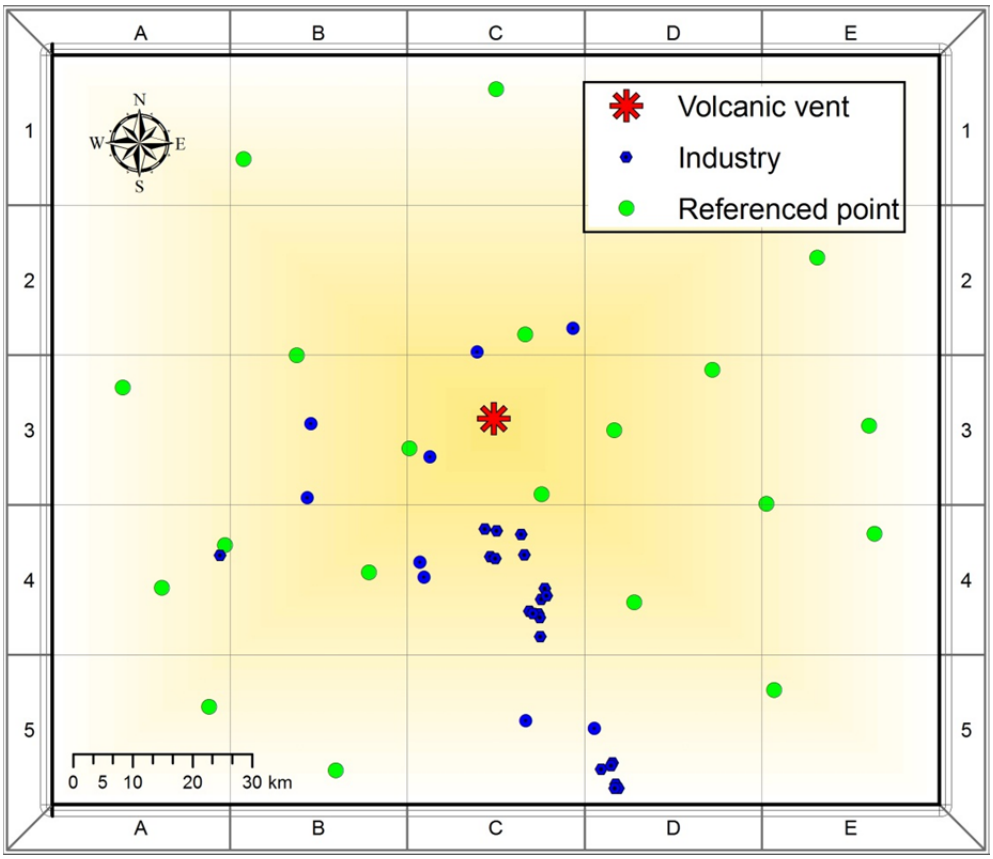

Figure 8.10. Spatial distribution of points.

Figure 8.11 and Figure 8.13 were produced by using the IDW method and Figure 8.12, Figure 8.14 show the results obtained by the Kriging interpolation procedure. A legend of colours has been defined: each colour is associated with a class of exceedance probabilities. Ten classes have been defined, each of them has amplitude of 10%; the darkest colour represents the highest probability class (ranging 91÷100 %).

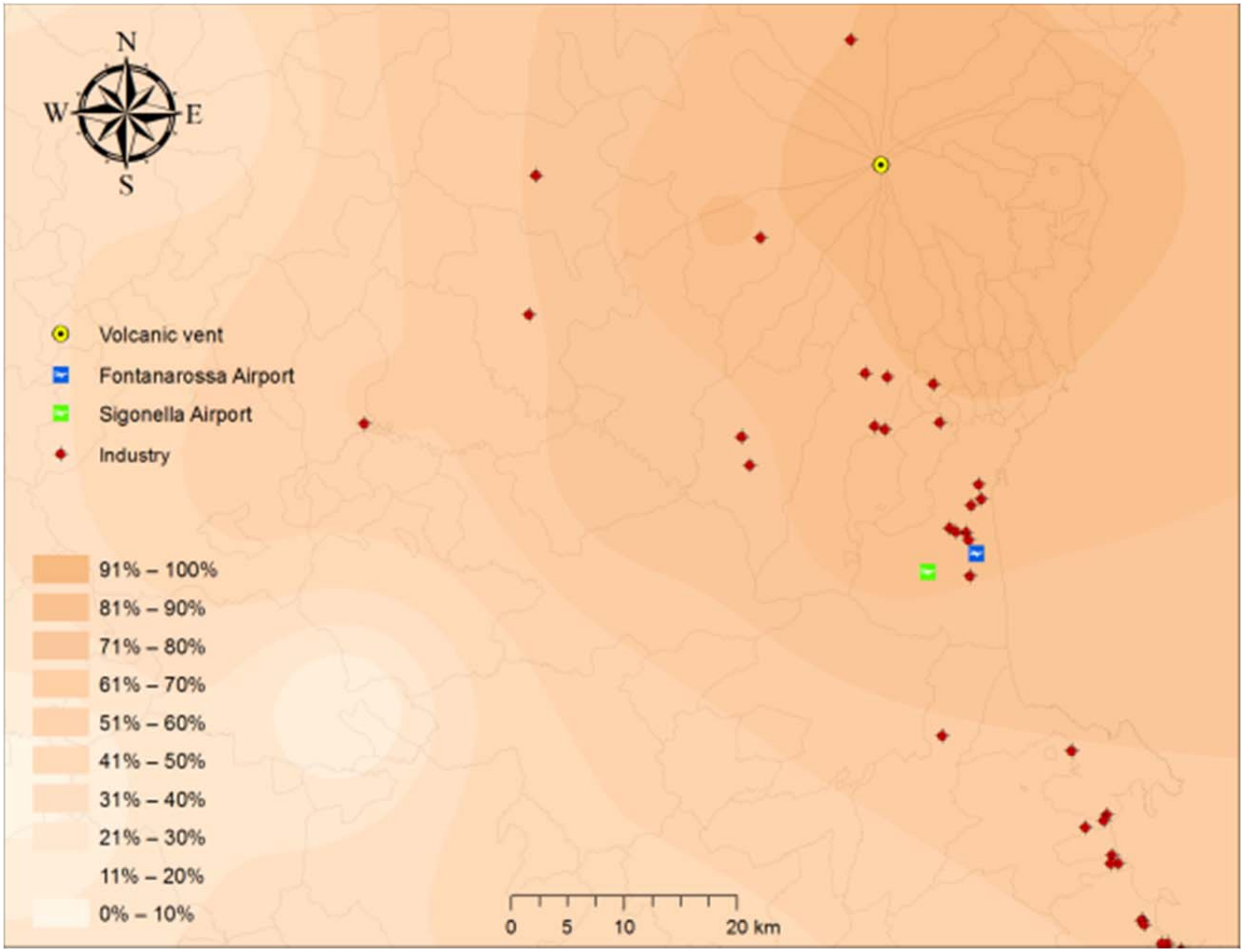

Figure 8.11. Vulnerability map for light damage of fixed roof tanks (Inverse Distance Weighting approach).

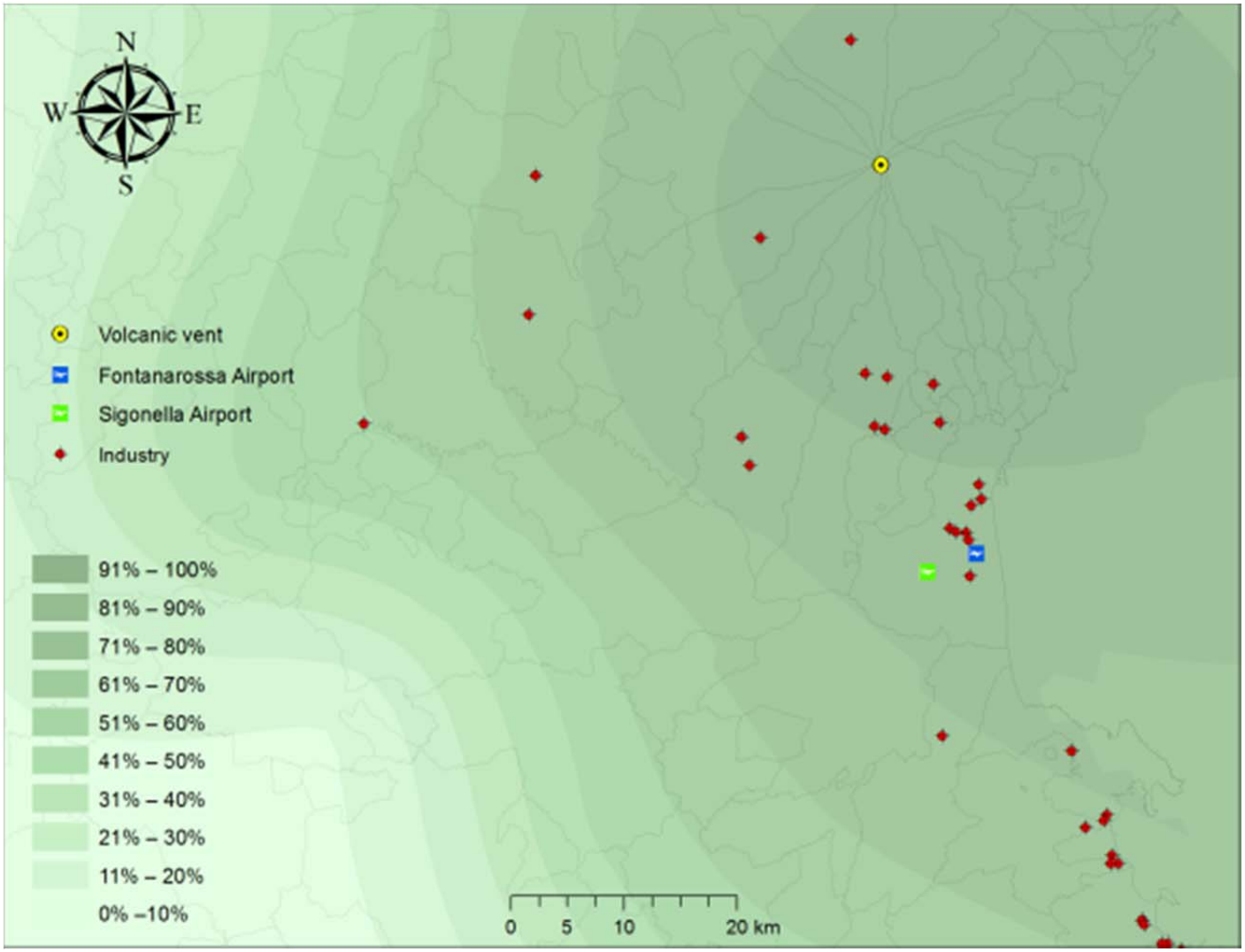

Figure 8.12. Vulnerability map for light damage of fixed roof tanks (Kriging approach).

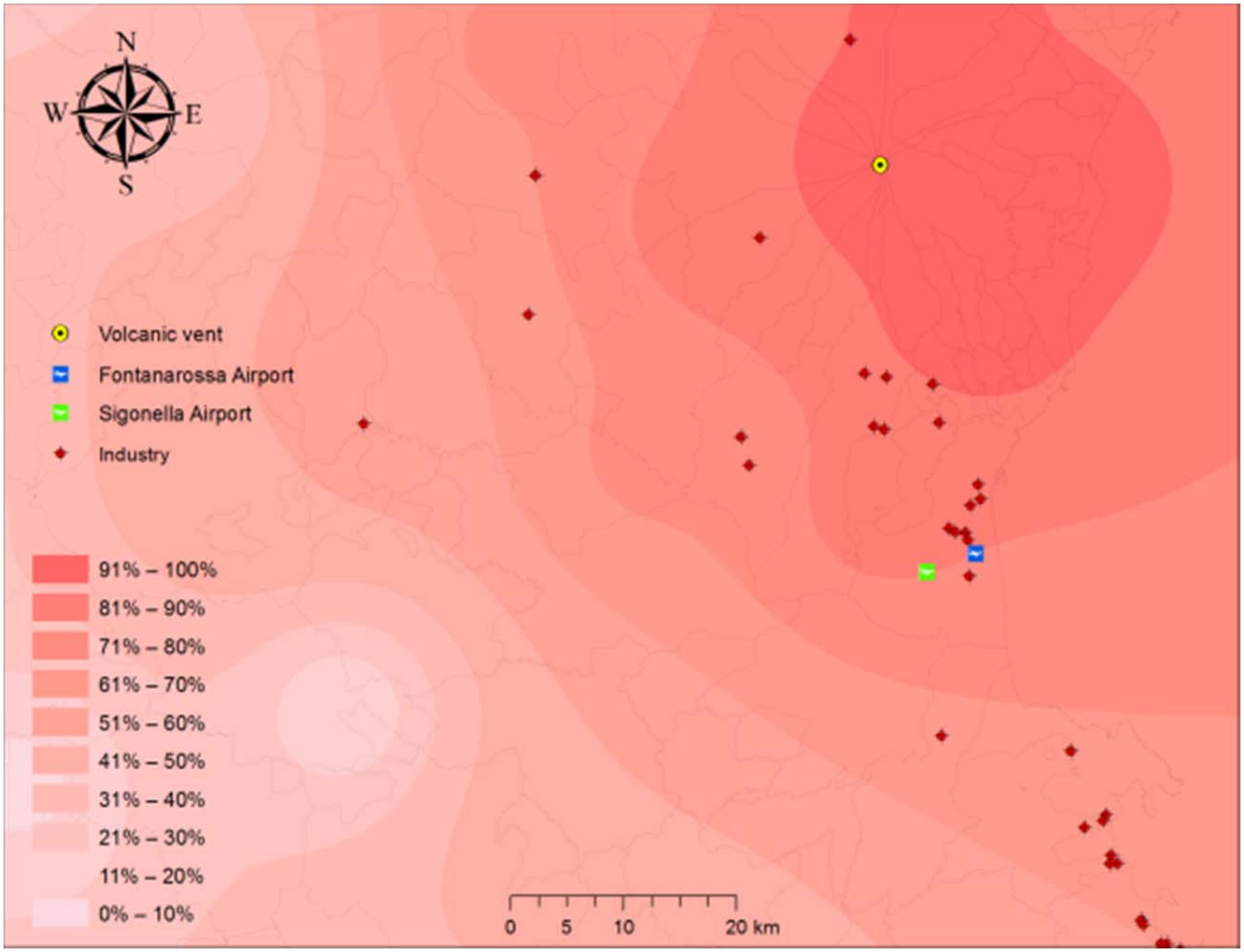

Figure 8.13. Vulnerability map for filters' partial clogging (Inverse Distance Weighting approach).

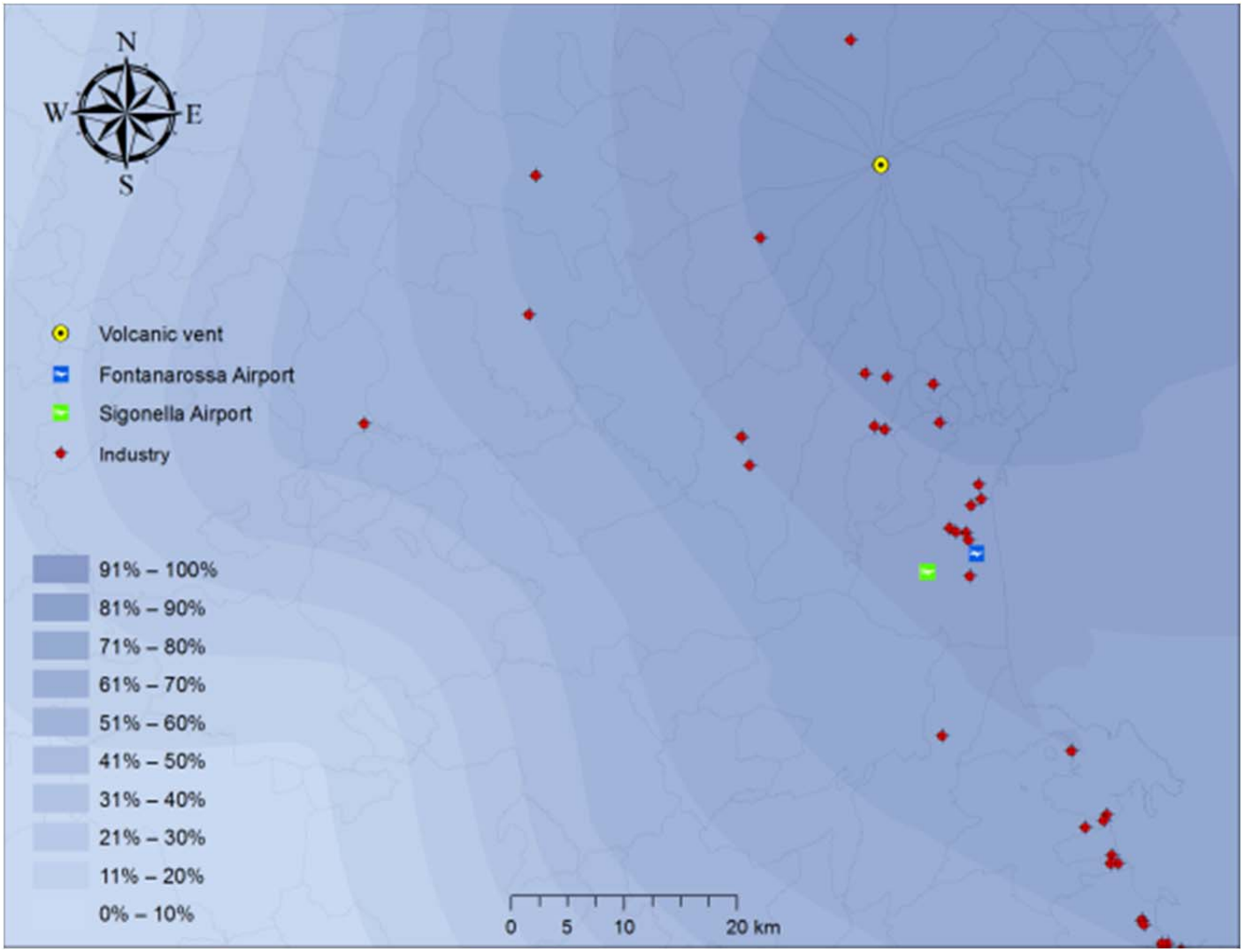

Figure 8.14. Vulnerability map for filters' partial clogging (Kriging approach).

The IDW allows a quick calculation, but the geostatistical approach gives a more accurate estimation even if the data-processing is time-consuming. After the interpolation, each prediction needs to be validated. The validation procedure used in this work is the *cross-validation*, it consists in plotting the predicted value as a function of the measured value in a Cartesian graph. The results of the validation are shown in Figure 8.15 (a,b) and Figure 8.16 (a,b). It can be observed that the predictions of Figure 8.15 (b) and Figure 8.16 (b) give a slope close to 1 demonstrating a good applicability of the Kriging method.

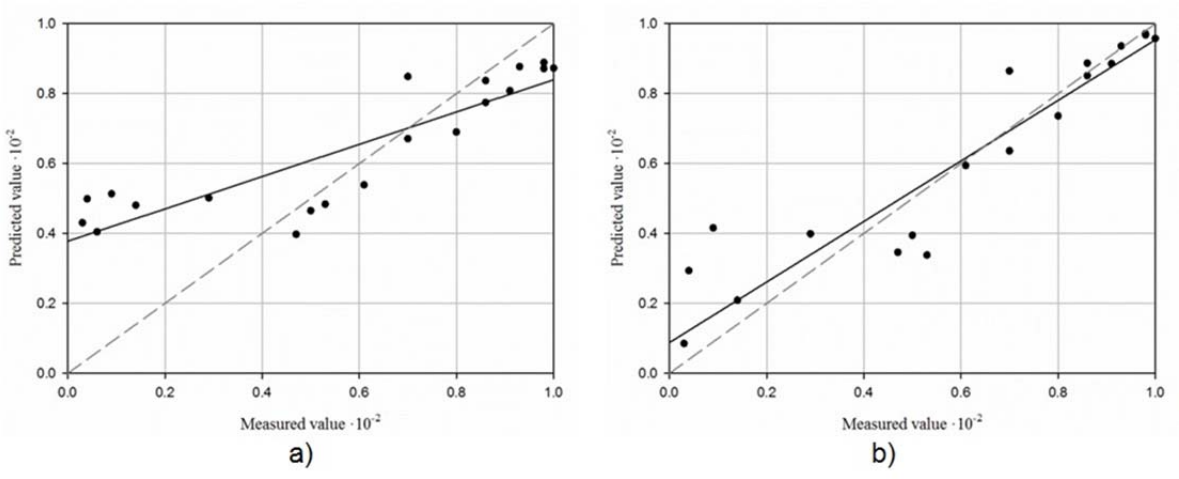

Figure 8.15. Validation of predictions for vulnerability maps related to light damage of fixed roof tanks: (a) IDW method and (b) Kriging method.

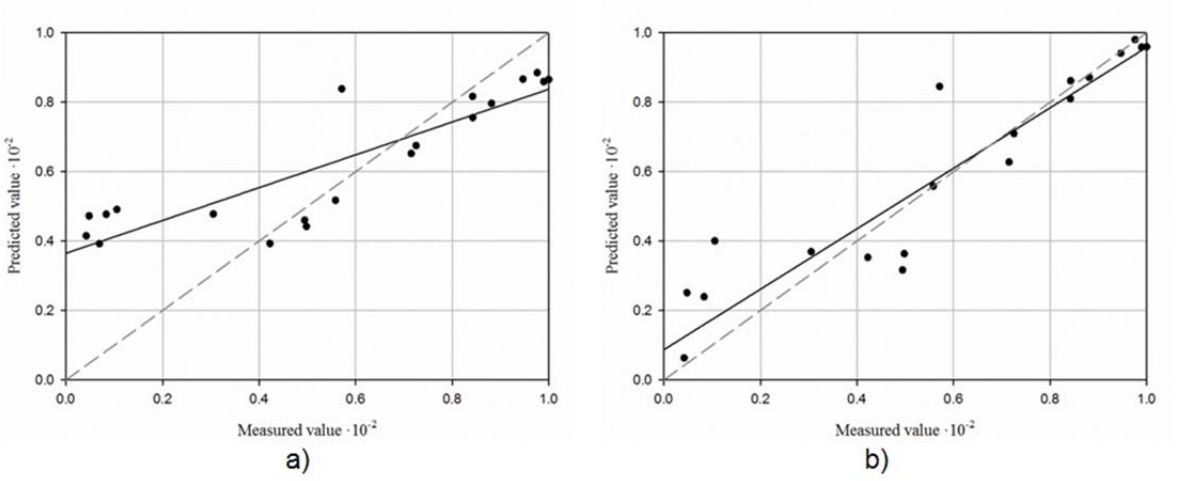

Figure 8.16. Validation of predictions for vulnerability maps related to partial clogging of filters: (a) IDW method and (b) Kriging method.

The *cross-validation* allows determining “how good” the model is, but to be applicable, the method must have a *Mean Error* (the average difference between the measured and the predicted values) close to 0.

In order to determine the applicability of the models, the spatial distribution of errors was studied in relationship to the measured values (20 samples). The error plots of Figure 8.17 (a,b) and Figure 8.18 (a,b) give both the error value per measure (measured value subtracted from the predicted value, indicated by each point) and the *Mean Error* (indicated by the fitting line) vs. the measured values. Figure 8.17 refers to fixed roof tanks, whereas Figure 8.18 is for filter. The trend of the *Mean Error* is slightly decreasing and close to 0 by using the Kriging, whereas a more decreasing trend is observed for the IDW. According to the error estimation, within the interpolation methods used, the Kriging method is the one that best estimated the vulnerability. Anyway a limit to the application of the approach could be related to the limited number of sample points.

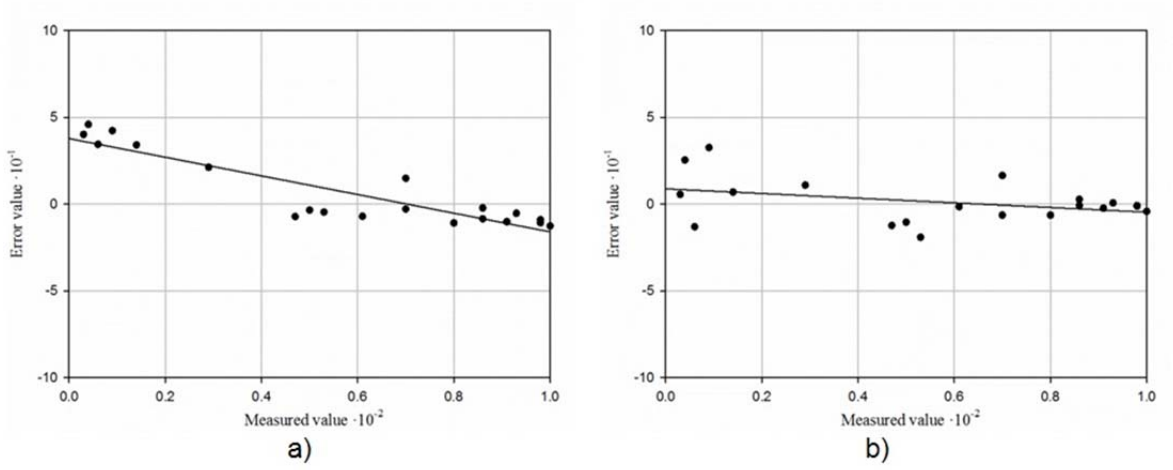

Figure 8.17. Error estimation for predictions related to light damage of fixed roof tanks: (a) IDW method and (b) Kriging method.

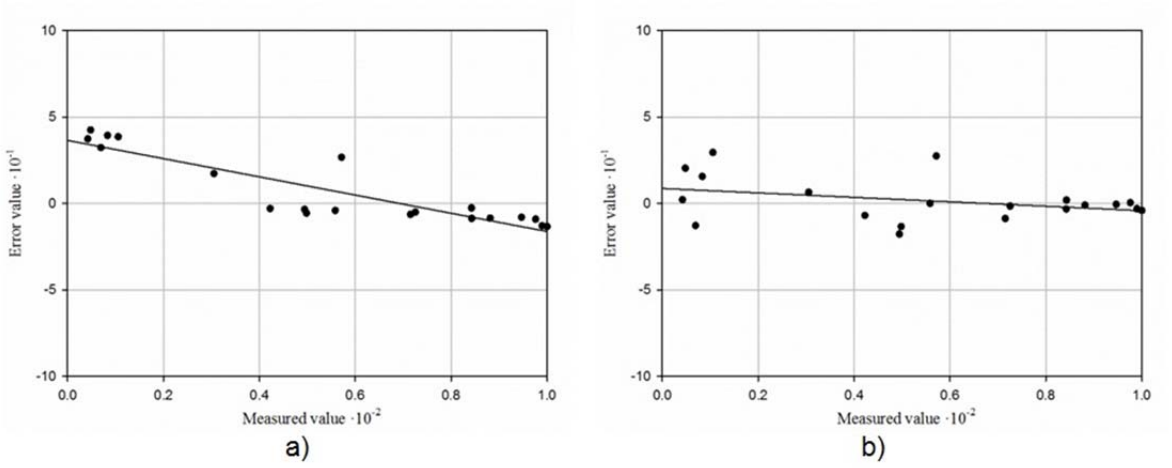

Figure 8.18. Error estimation for predictions related to partial clogging of filters: (a) IDW method and (b) Kriging method.

8.7 Screening clogging: conditions

The Reynolds number was calculated for the wastewater flow inside the pore channels using the weighted values of S and e given in Table 8.8. Results are shown in the same table with the indication of the resulting flow regime. The flow is never streamline; this means that the thickness of the deposits must be quantified with the Carman equation.

Table 8.8. Reynolds numbers and regime flow (using weighted S and e).

Sample ID	u_l (m/s)	S_w (m^2/g)	e_w (dimensionless)	Re (dimensionless)	Regime
1	1.79	15.19	0.48	91.89	Transition
3		9.75	0.49	117.52	Transition

To take into account the variability of the dimension of volcanic ash particles and the voidage, several calculations were made by referring to data of Table 8.9 and Table 8.10.

Table 8.9. Reynolds numbers and regime flow (using average, minimum and maximum S).

Sample ID	u_l (m/s)	S (m^{-1})	e (dimensionless)	Re (dimensionless)	Regime
1	1.79	$S_{avarage}$	0.392	78.57	Transition
		$Smin$		226.43	Transition
		$Smax$		11.51	Transition
2	1.79	$S_{avarage}$		91.75	Transition
		$Smin$		226.43	Transition
		$Smax$		11.51	Transition
3	1.79	$S_{avarage}$		97.94	Transition
		$Smin$		383.77	Transition
		$Smax$		14.39	Transition

Table 8.10. Reynolds numbers and regime flow (using literature data for e).

Sample	u_l (m/s)	S (m^{-1})	e (dimensionless)	Re (dimensionless)	Regime
Case 1	1.79	7600	0.393	151.7	Transition
Case 2			0.4	153.5	Transition
Case 3			0.5	184.2	Transition
Case 4			0.6	230.3	Transition
Case 5			0.7	307	Transition
Case 6			0.8	460.5	Transition
Case 7			0.9	921	Transition

8.7.1 Critical ash deposit on fine screens

Malfunctions and efficiency reductions of screens are defined by means of the pressure drop (ΔP). ΔP was calculated using Equation (16), by choosing a proper C_{disch} value. It is worth noting that the extreme event, which is the total screen clogging, was not considered in this work, since cleaning operations were assumed to be executed before the occurrence of a total blockage. The resulting pressure drops are:

- ΔP_o ~ 6570 Pa (initial screen's pressure drop)
- ΔP_1 ~ 9850 Pa (dirty screen)
- ΔP_2 = 15760 Pa (very dirty screen)

The trend of the head loss in screen ($\Delta h = \Delta P/(g \cdot \rho)$) versus the stream velocity is shown in Figure 8.19.

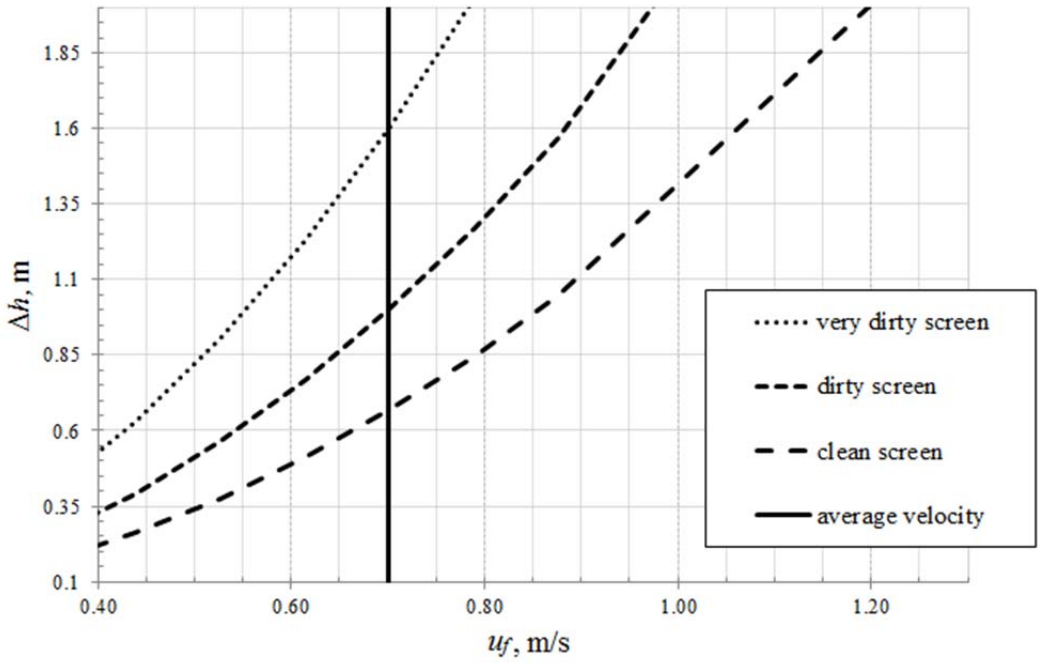

Figure 8.19. Head losses for fine screens vs. stream velocity.

Then, by using the Carman equation (22), the thicknesses of the ash deposit on the screen were calculated using data of Table 8.8. Results are given in Table 8.11 where l_1 and l_2 are respectively the thicknesses of the ash deposit causing a pressure drop equal to ΔP_1 and ΔP_2. Figure 8.20 shows the critical thickness (l_1 and l_2) as a function of d, it can be evidenced that a very small quantity of ash is enough to clog this type of screen.

Table 8.11. Weighted average critical thicknesses of ash deposit (using weighted S and e).

Sample ID	Re (dimensionless)	l_1 (mm)	l_2 (mm])
1	91.89	0.98	1.57
3	117.52	1.45	2.31

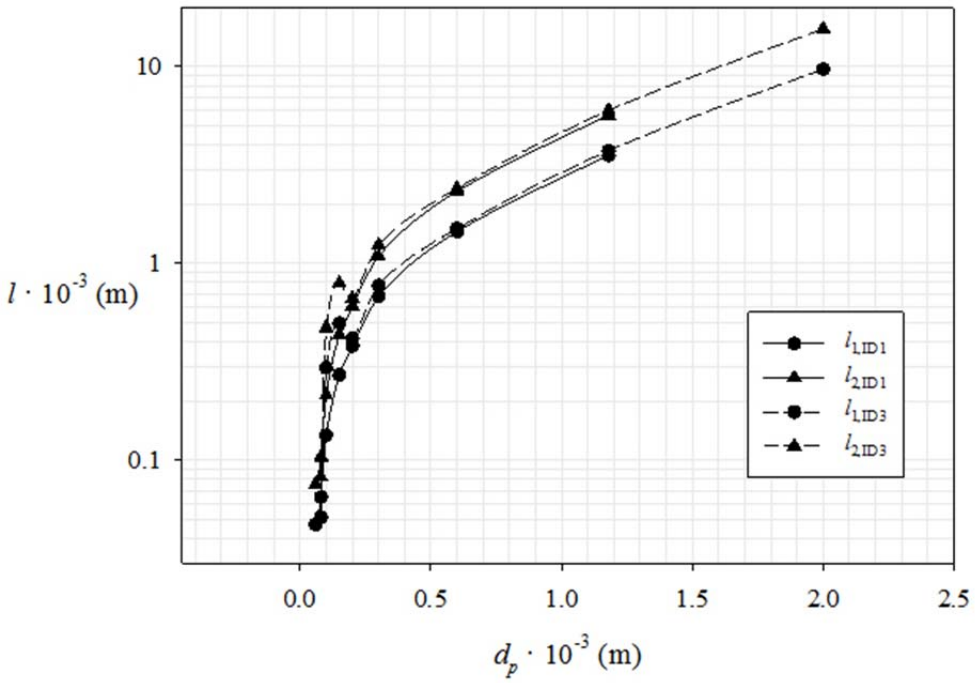

Figure 8.20. Critical thicknesses of ash deposit with respect to the particles' diameter for (using weighted S and e).

Results obtained by using data of Table 8.9 and Table 8.10 are given in Table 8.12 and Table 8.13.

Table 8.12. Thickness of ash deposit (using average, minimum and maximum S).

Sample ID	S (m^{-1})	Re (dimensionless)	l_1 (mm)	l_2 (mm)
1	S_{av}	78.57	0.42	0.67
	Smin	226.43	1.54	2.46
	Smax	11.51	0.03	0.04
2	S_{av}	91.75	0.51	0.82
	Smin	226.43	1.54	2.46
	Smax	11.51	0.03	0.04
3	S_{av}	97.94	0.56	0.89
	Smin	383.77	2.84	4.55
	Smax	14.39	0.04	0.06

Table 8.13. Thickness of ash deposit (using literature data for e).

Sample	Re (dimensionless)	l_1 (mm)	l_2 (mm)
Case 1	151.7	0.3	0.8
Case 2	153.5	0.3	0.8
Case 3	184.2	0.7	2
Case 4	230.3	1.7	4.5
Case 5	307	3.7	10
Case 6	460.5	8.9	23.7
Case 7	921.1	27.8	74

8.7.2 Discussion

At a glance, the deposit thicknesses causing the critical pressure drops are very small, in some cases these do not reach the value of 1 mm. This observation allows stating that the presence of few quantities of volcanic ash, with the characteristics similar to those emitted by Mt. Etna, causes instantly the system clogging. It should be underlined that, in this Section, the study has been focused on fine screens because the size distribution analysis showed that these are the equipment typology able to retain such particles, even if fine screens are not always installed in wastewater treatments. If such screens are not included within the plant, the particles' removal is provided by grit chambers, these are also affected by the presence of ash [95].

Results showed that the increase of the voidage for the granular bed determines an increase of the deposit thickness (Table 8.13). By applying the approaches for the calculation of the critical thicknesses, it was observed that the flow had always a transition regime; the increase of S (related to the decrease of the diameter of the particles) causes the decrease of the Reynolds number up to bring the flow close to the laminar regime. It must be recalled that S rises also as the porosity increases. Consequently, the critical thickness increases with the decrease of S and, thus, with the increase of d.

8.8 Incomplete grit removal

To calculate the terminal settling velocities of the ash particles, the assumptions discussed in Section 4.7.2 were necessary and justified as follows:

(1) given that the sewage is a dilute suspension, the *free settling* condition occurs in the chamber;

(2) the effect of the walls of the vessel is negligible as this an industrial-scale equipment;

(3) the particle shape is greatly variable to account for the infinite shapes, thus they need to be assumed spherical.

By applying the K parameter criterion, described above, the proper correlation for $u_{t,p}$ was chosen. Then the terminal settling velocity was calculated for each representative diameter of the particle size classes, identified by sieving, and for all the samples (Table 8.14, Table 8.15 and Table 8.16).

Table 8.14. Terminal settling velocity for the Sample ID 1 of volcanic ash.

$d_p \cdot 10^{-3}$ (m)	1.18	0.6	0.3	0.2	0.15	0.1	0.08	0.06
K	30.90	15.71	7.86	5.24	3.93	2.62	1.96	1.57
$u_{t,p} \cdot 10^{-2}$ (m/s)	23.13	14.08	6.59	3.53	2.12	1.00	0.56	0.36
$u'_{t,p} \cdot 10^{-2}$ (m/s)	37.88	33.14	30.71	30.21	30.07	30.02	30.01	30.00

Table 8.15. Terminal settling velocity for the Sample ID 2 of volcanic ash.

$d_p \cdot 10^{-3}$ (m)	1.18	0.6	0.3	0.2	0.15	0.1	0.08	0.06
K	26.08	13.26	6.63	4.42	3.31	2.21	1.66	1.33
$u_{t,p} \cdot 10^{-2}$ (m/s)	17.47	10.18	4.35	2.22	1.30	0.60	0.34	0.22
$u'_{t,p} \cdot 10^{-2}$ (m/s)	34.71	31.68	30.31	30.08	30.03	30.01	30.00	30.00

Table 8.16. Terminal settling velocity for the Sample ID 3 of volcanic ash

$d_p \cdot 10^{-3}$ (m)	2	1.18	0.6	0.3	0.2	0.15	0.1	0.08
K	54.39	16.32	8.16	5.44	4.08	2.72	2.04	1.63
$u_{t,p} \cdot 10^{-2}$ (m/s)	33.57	15.11	7.20	3.91	2.36	1.10	0.63	0.40
$u'_{t,p} \cdot 10^{-2}$ (m/s)	45.03	33.59	30.85	30.25	30.09	30.02	30.01	30.00

Figure 8.21 shows the trend of the settling velocity (left hand axis) as a function of particle diameter. In the right axis the K value is shown (in logarithmic scale) and allows identifying the regime flow.

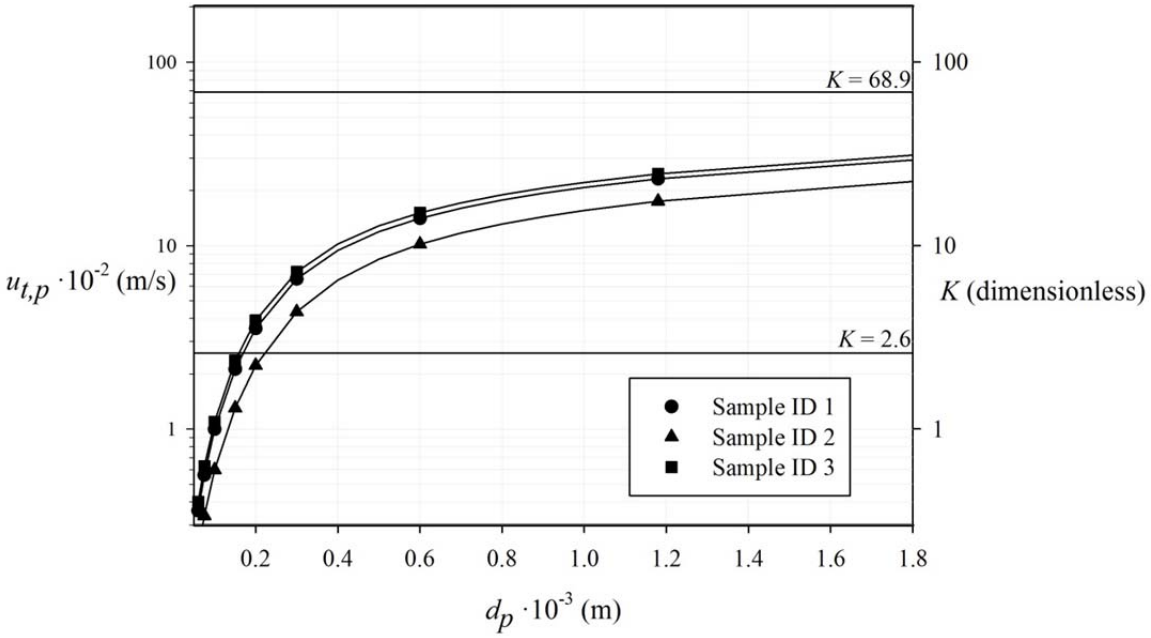

Figure 8.21 Terminal settling velocity of volcanic ash particles versus particles' diameter.

8.8.1 Fraction of settled particles

The weight fraction of each sample remaining to each sieve (X_w) was plotted against the terminal settling velocity as shown in Figure 8.22. Then, using the results of the analysis of the particle size distribution, the weight fraction having a velocity of settling less than $u_{t,p}$, which is the fraction passing each sieve (X), was calculated. Figure 8.23, Figure 8.24 and Figure 8.25 give the curves representing the weight fraction versus the terminal settling velocity, respectively, for Sample ID 1, 2 and 3; u_o is indicated in each figure.

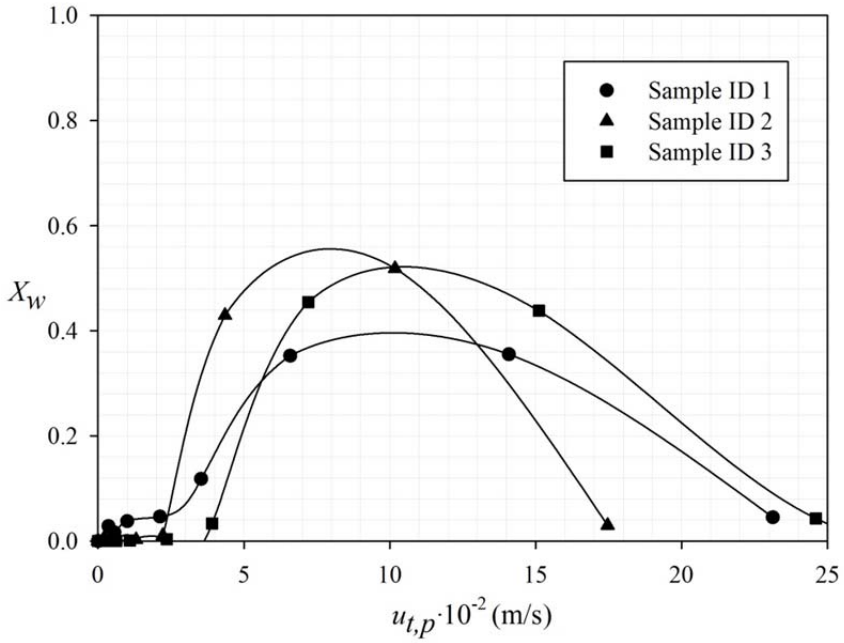

Figure 8.22. Weight fraction remaining at each sieve versus terminal settling velocity of particles.

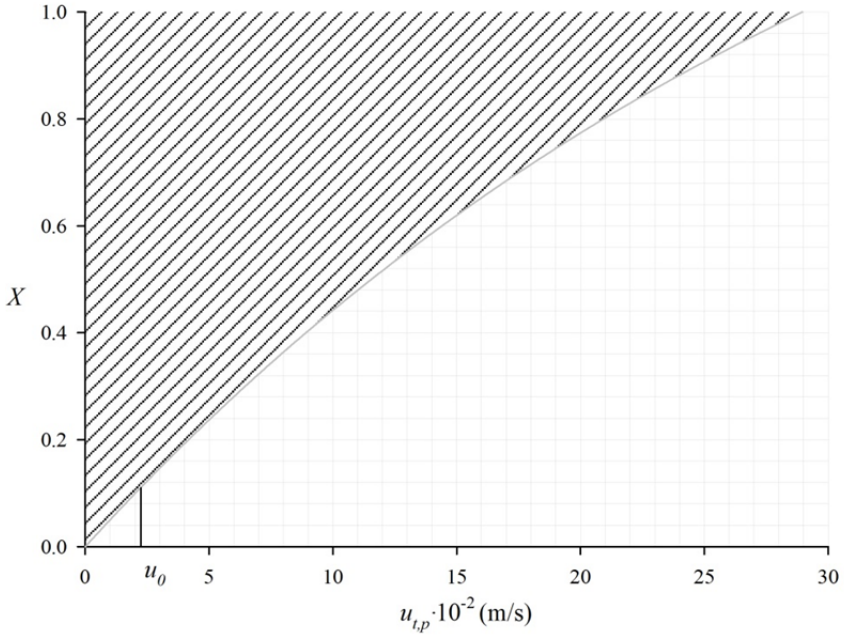

Figure 8.23 Fraction of ash with settling velocity less than $u_{t,p}$ versus settling velocity (Sample ID 1).

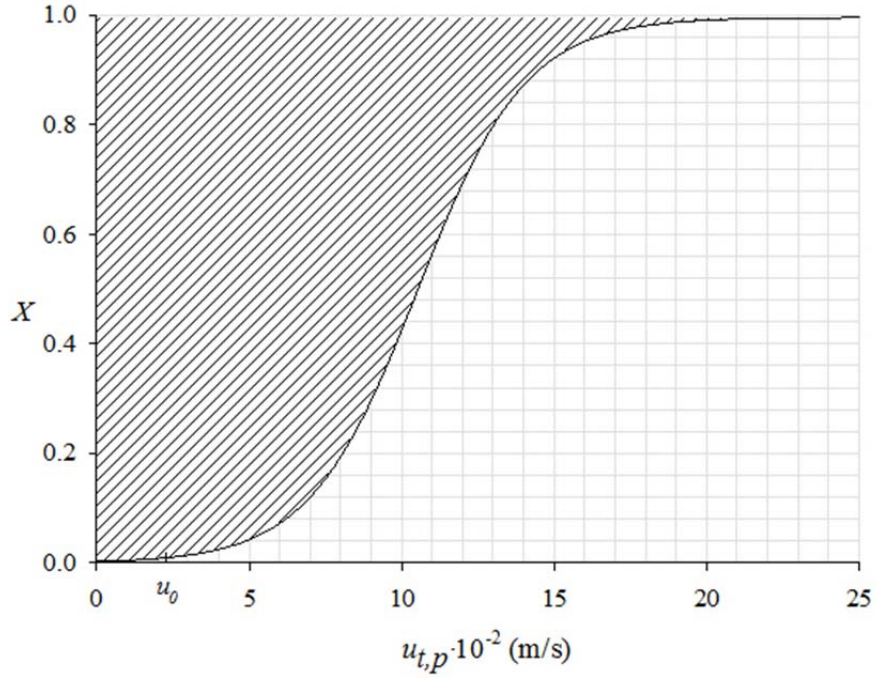

Figure 8.24. Fraction of ash with settling velocity less than $u_{t,p}$ versus settling velocity (Sample ID 2).

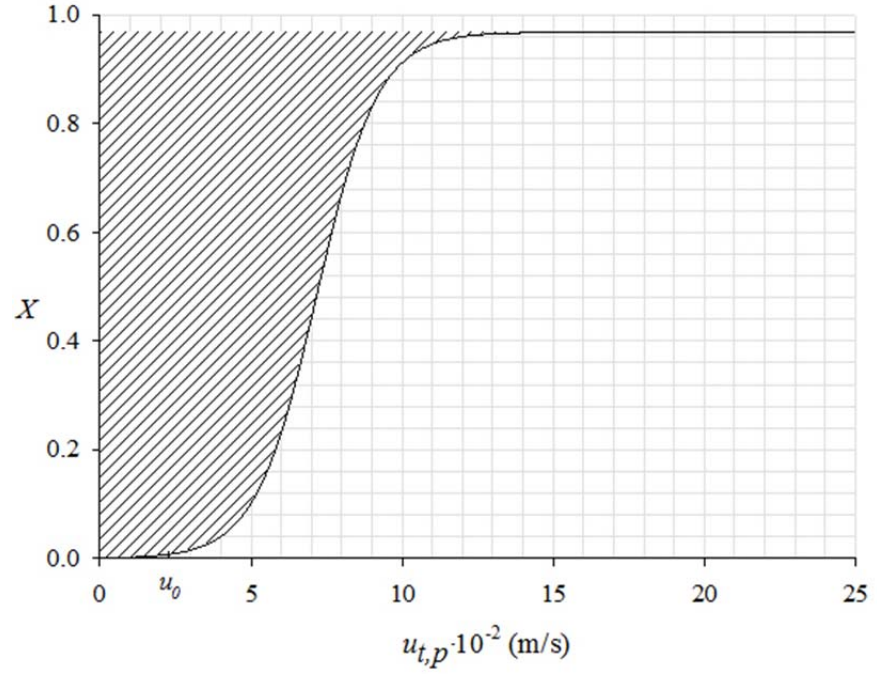

Figure 8.25. Fraction of ash with settling velocity less than $u_{t,p}$ versus settling velocity (Sample ID 3).

After derivation of the equation of the curves of Figure 8.23, Figure 8.24 and Figure 8.25, by means of a regression procedure, the total fraction of removed particles was calculated for each sample by using equation (36). The unsettled fraction is given by the area on the left

side of the curve, comprised between the x axis and the line passing through X_o divided by u_o. The results of the total fraction of removed particles are given in Table 8.17.

Table 8.17. Fraction of removed particles.

Sample ID	X_o	$1 - X_o$	$\int_o^{X_o} \frac{u_{t,p}}{u_o} dX$	$X_{r,total}$
1	0.125	0.875	0.089	0.914
2	0.011	0.989	negligible	~ 0.999
3	0.012	0.988	negligible	~ 0.988

8.8.2 Discussion

It was observed that the K parameter is always smaller than 68.9. The particle sizes do not allow the achievement of the values required to apply the Newton's law (68.9 < K < 2,360) or the correlation associated with the region *d* (K > 2,360). As shown in Section 4.7.2, the density values influence the terminal settling velocity. By comparing particles with the same diameter, Sample ID 1 has a greater sedimentation velocity than Samples ID 2 and 3. Figure 8.22 gives an instant view of the weighted fraction of particles for each value of terminal settling velocity. The results of the size distribution analysis allowed drawing the curves of the fraction of particles having less than a stated velocity $u_{t,p}$ for each samples. Then, by computing the critical velocity u_o for particles in the grit chamber, the fraction of removed particles was quantified. Results showed that ~ 94 % of particles of Sample ID 1 are removed; particles of Samples ID 2 and 3 can be considered totally removed.

Additional considerations can be made on the choice of the equipment design parameters or the formulation of potential alternatives to horizontal grit chambers. Given that wastewater plants are designed to remove about the 95 % of particles with a diameter of 0.21 mm, it can be observed that: in the case of Sample 1 the $u_{t,p}$ is $3.3 \cdot 10^{-2}$ m/s for particles with d_p = 0.2 mm, this means that there is a no-negligible fraction of particles having $u_{t,p} < u_o$; in the case of Samples ID 2 and 3, the $u_{t,p}$ of particles of the same diameter is ~ $2.03 \cdot 10^{-2}$ m/s that is greater than u_o. The critical settling velocity can be increased only by raising the depth of the chamber, since a reduction of t_o bring out from the range of the design values for u_f and L_v. Thus, in this frame the only possible alternative is the use of vortex-type grit chambers, as they remove particles up to 0.11 mm with a retention time of 30 s [61], but unfortunately their use increase costs; aerated grit chambers are not recommended because they eliminate particle up to 0.20 mm and hence, on the basis of the results of this

study, they do not introduce any significant improvement in the removal process compared to a horizontal grit chamber.

9

Conclusions

The analysis of the state of the art related to the approaches to industrial risk assessment coupled with catastrophic natural phenomena shows that few methodologies assessing Na-Tech risks exist. Given that (1) Na-Techs are increasing and (2) Na-Techs often cause releases of great amount of hazardous substances, it is strongly recommended the analysis of potential industrial accidents triggered by natural phenomena and the development/consolidation of tools to achieve this aim. In this context the main efforts have to be dedicated to the implementation of the Quantitative Risk Analysis (QRA) through different levels of complexity; then in carrying out Na-Tech risk assessment, the level of the analysis to be used depends on the scope of the study [96]. The basis for the integration of Na-Techs in QRA regards the development of specific models for the estimation of the equipment vulnerability under the impact of natural phenomena. To this scope, in this thesis, two types of equipment were studied: atmospheric storage tanks and air intake filters. Some conclusive considerations can be given:

1. The behaviour of floating roof storage tanks under the impact of volcanic ash load was studied. On the basis of some physical concepts, the ash load of 680 kg/m^2 sinks the roof of the model double deck floating roof tank (containing a liquid having a density of 1000 kg/m^{-3}). The height of the deposit to sink the roof decreases as the liquid density decreases and the ash density increases. To study the capsizing of roofs the theories of stability of floating bodies and the concept of metacentre have been applied. A metacentre height equal to ~ 840 m has been calculated, for a liquid density of 1000 kg/m^{-3}, and to 670 m, for a liquid density 800 kg/m^{-3}. These heights reflect a great stability of floating roofs. Their stability was verified also through the

application of the Euler method to calculate the minimum load to be applied for capsizing the roof; this load is greater than the weight of the roof.

The analysis of the case-study (the surrounding Mt. Etna) showed that combining the probability of exceedance and the threshold value for fixed roof and floating roof tanks it is possible to create a simple description of the vulnerability of equipment. It was found that the probability of damage is no-significant for an event having the magnitude of scenario 1 and is slightly greater for scenario 2. These results may be useful for planning land-use close to the volcano and for implementing maintenance procedures for existing facilities.

2. A procedure for the estimation of threshold values of physical parameters causing damage on filtration systems due to ash emissions was defined. In this case the exceedance probability of concentration must be associated with both the concentration and the time necessary to clog the filter. This means that the failure probability has to be conditioned by the occurrence of an event with certain duration. The method also is applicable to other filtration systems such as that of systems of air conditioning and in the filtering of operating rooms.

Another objective of this study was to provide local authorities and planners with useful procedure and tools for planning emergencies connected to volcanic Na-Tech risks. In this context, the development of vulnerability models, interfaced with a Geographic Information System (GIS) software, makes more efficient the management of data for the risk calculation and also more effective the planning and management of emergencies. It was seen that the greatest concern of Na-Techs is related to the potential overloading of the emergency response system and its ability to minimise losses to persons and property. More specifically, technological accidents may be triggered by natural events and their effects may add to or worsen the condition of people and environment struggling with the effects of the natural event. Safety and rescue operations may be impeded by the shortage of resources (water, energy, etc.) or by the reduction of accessibility due to debris and the fleeing population. In this context, the interactive GIS interface of the vulnerability maps helps to identify available refuges, escape paths, etc.

In this thesis, Na-Techs in wastewater treatments were also investigated, focusing mainly on primary treatments (screening processes and grit removals). The conditions leading to malfunctions of screens, with respect to the phenomenon of volcanic ash emission, were determined. The estimation of the threshold amounts of ash causing the reduction of

functionality of fine screens was made for the case-study by using literature data and experimental results from the ash characterisation. The study was based on two assumptions: (i) the sewage characteristics were assumed to be equal to those of water, and (ii) the particles were assumed having a smooth and spherical shape. Then the conditions leading to malfunctions of grit removal facilities, with the respect to the phenomenon of volcanic ash emission, were also determined. The work was mainly addressed to the investigation of horizontal grit chambers. Also in this case, some assumptions were necessary for the application of the methodology discussed in Section 5.2.2.

All these assumptions were proper discussed and justified. Even if they were necessary to simplify the application of the proposed approaches, the results gave a valid support in addressing alternative solutions for the ash removal (such as the use of a vortex-type grit chamber) and more efficient management planning (frequent cleaning operations in screens).

9.1 Potential future developments

The study of volcanic Na-Tech risks, which are currently considered emerging risks, and of the vulnerability of territory and people allow understanding that the knowledge about natural-technological scenarios is still beginning. Many gaps can be found in the current knowledge, which must be remedied. In this frame this thesis represents a starting point to approach to the investigation of the vulnerability of equipment to natural phenomena, in particular concerning to volcanic Na-Techs.

Future developments could be the development of further methodologies for the assessment of the vulnerability of other equipment types. This is important to build a strong base to achieve the prevention of Na-Tech accidents and also for a more efficiency management of the territory, human health and environment issues.

Concerning the case-study, a probabilistic investigation to understand the possible trend of explosive eruptions of Mt. Etna must be executed. This will allow providing a consolidated probabilistic base to the study (in particular for to broad the standard QRA), which is strongly affected by several uncertainties.

REFERENCE

[1] INPO, 2011. Special Report on the Nuclear Accident at the Fukushima Daiichi Nuclear Power Station. Report INPO 11-005

[2] Girgin, S., The natech events during the 17 August 1999 Kocaeli earthquake: aftermath and lessons learned. *Nat. Hazards Earth Syst. Sci.*, 2011. 11(4): p. 1129-1140.

[3] WebPage: http://www.mona.uwi.edu. December 2014.

[4] WebPage: https://www.ec.europa.eu/.

[5] WebPage: http://www.epa.gov/. February 2015.

[6] WebPage: http://www.nas-sites.org/. February 2015.

[7] WebPage: https://www.weadapt.org/. February 2012.

[8] Milazzo, M.F., R. Lisi, G. Ancione, D. Lister, and G. Maschio. Vulnerability maps for industrial facilities in areas with the potential volcanic ash fallout. in *11th International Probabilistic Safety Assessment and Management Conference and the Annual European Safety and Reliability Conference 2012, PSAM11 ESREL 2012*. (2012). Helsinki.

[9] Cruz, A.M., L.J. Steinberg, A.L.V. Arellano, J.-P. Nordvik, and F. Pisano, State of the art in Natech risk management. *European Commission Directorate General Joint Research Centre, EUR*, 2004. 21292.

[10] European_Commission, Council Directive 82/501/EEC of 24 June 1982 on the major-accident hazards of certain industrial activities. Government Document, 1982.

[11] European_Commission, Council Directive 96/82/EC of 9 December 1996 on the control of major-accident hazards involving dangerous substances. Government Document, 1996.

[12] European_Commission, Council Directive2003/105/EC of 16 December 2003 amending Council Directive 96/82/EC on the control of major-accident hazards involving dangerous substances. Government Document, 2003.

[13] European_Commission, Council Directive 2012/18/EU of 4 July 2012 on the control of major-accident hazards involving dangerous substances, amending and subsequently repealing Council Directive 96/82/EC. Government Document, 2012.

[14] Showalter, P.S. and M.F. Myers, Natural disasters in the United States as release agents of oil, chemicals, or radiological materials between 1980-1989: analysis and recommendations. *Risk Analysis*, 1994. 14(2): p. 169-182.

[15] Lindell, M.K. and R.W. Perry, Hazardous materials releases in the Northridge earthquake: implications for seismic risk assessment. *Risk Analysis*, 1997. 17(2): p. 147-156.

[16] Cruz, A., L. Steinberg, and R. Luna, Identifying Hurricane-Induced Hazardous Material Release Scenarios in a Petroleum Refinery. *Natural Hazards Review*, 2001. 2(4): p. 203-210.

[17] Steinberg, L.J. and A.M. Cruz, When natural and technological disasters collide: lessons from the Turkey earthquake of August 17, 1999. *Natural Hazards Review*, 2004. 5(3): p. 121-130.

[18] Lindell, M.K. and R.W. Perry, Addressing gaps in environmental emergency planning: hazardous materials releases during earthquakes. *Journal of Environmental Planning and Management*, 1996. 39(4): p. 529-543.

[19] Blong, R.J., Volcanic Hazards: A Sourcebook on the Effects of Eruptions. (1984): Academic Press.

[20] Spence, R.J.S., P.J. Baxter, and G. Zuccaro, Building vulnerability and human casualty estimation for a pyroclastic flow: a model and its application to Vesuvius. *Journal of Volcanology and Geothermal Research*, 2004. 133(1–4): p. 321-343.

[21] Self, S., The effects and consequences of very large explosive volcanic eruptions. *Philosophical Transactions of the Royal Society A: Mathematical, Physical and Engineering Sciences*, 2006. 364(1845): p. 2073-2097.
[22] Milazzo, M.F., G. Ancione, A. Basco, E. Salzano, and G. Maschio. Industrial hazards associated with the eruption of Etna. in *European Safety and Reliability Conference: Advances in Safety, Reliability and Risk Management, ESREL 2011*. (2011). Troyes.
[23] Rasà, R., A. Tripodo, S. Casella, and M.L. Szilagyi, Contributi alla valutazione della pericolosità e rischio vulcanico nell'area etnea ed alla mitigazione dei danni attesi. "Carta Tematica di Rischio Vulcanico della Regione Sicilia" Generic, 2007, Ed. C.R.P.R.: Regione Sicilia Palermo.
[24] Baxter, P.J., R.S. Bernstein, H. Falk, J. French, and R. Ing, Medical aspects of volcanic disasters: An outline of the hazards and emergency response measures. *Disasters*, 1982. 6(4): p. 268-276.
[25] Scandone, R., G. Arganese, and F. Galdi, The evaluation of volcanic risk in the Vesuvian area. *Journal of Volcanology and Geothermal Research*, 1993. 58(1–4): p. 263-271.
[26] White, J., C. Stewart, D. Wareham, and T. Wilson, Treatment of volcanic ash-contaminated surface waters through the optimisation of physical and chemical processes. (2011), Lower Hutt, N.Z.: GNS Science.
[27] Zais, D.: http://www.volcanoes.usgs.gov. 06.08.2014.
[28] WebPage: http://www.bbc.co.uk/. 21 December 2014.
[29] WebPage: http://www.geolsoc.org.uk/. 05 February 2015.
[30] Tsuya, H., Geological and Petrological Studies of Volcano, Fuji, V.: 5. On the 1707 eruption of Volcano Fuji. 1955.
[31] Newhall, C. and R. Hoblitt, Constructing event trees for volcanic crises. *Bulletin of Volcanology*, 2002. 64(1): p. 3-20.
[32] Newhall, C.G. and S. Self, The volcanic explosivity index (VEI) an estimate of explosive magnitude for historical volcanism. *Journal of Geophysical Research: Oceans*, 1982. 87(C2): p. 1231-1238.
[33] Wilson, T.M., C. Stewart, V. Sword-Daniels, G.S. Leonard, D.M. Johnston, J.W. Cole, J. Wardman, G. Wilson, and S.T. Barnard, Volcanic ash impacts on critical infrastructure. *Physics and Chemistry of the Earth, Parts A/B/C*, 2012. 45–46(0): p. 5-23.
[34] Textor, C., H.F. Graf, M. Herzog, J.M. Oberhuber, W.I. Rose, and G.G.J. Ernst, Volcanic particle aggregation in explosive eruption columns. Part I: Parameterization of the microphysics of hydrometeors and ash. *Journal of Volcanology and Geothermal Research*, 2006. 150(4): p. 359-377.
[35] WebPage: http://www.geo.mtu.edu/.
[36] WebPage: http://volcanoes.usgs.gov/.
[37] Tanguy, J.C., C. Ribière, A. Scarth, and W.S. Tjetjep, Victims from volcanic eruptions: a revised database. *Bulletin of Volcanology*, 1998. 60(2): p. 137-144.
[38] WebPage: http://volcano.oregonstate.edu/. 25 January 2015.
[39] WebPage: http://www.create.usc.edu/. 03 February 2015.
[40] WebPage: http://www.epa.gov/. 2 February 2015.
[41] WebPage: https://www.learnandteachstatistics.wordpress.com. 7 March 2015.
[42] WebPage: http://www.courses.ttu.edu/. 1 March 2015.
[43] Milazzo, M.F. and T. Aven, An extended risk assessment approach for chemical plants applied to a study related to pipe ruptures. *Reliability Engineering and System Safety*, 2012. 99: p. 183-192.
[44] Antonioni, G., S. Bonvicini, G. Spadoni, and V. Cozzani, Development of a framework for the risk assessment of Na-Tech accidental events. *Reliability Engineering & System Safety*, 2009. 94(9): p. 1442-1450.

[45] Institute, A.P. and S.f.T.s.E. Partnership, Welded Steel Tanks for Oil Storage, API Standard 650. (1998): API.
[46] WebPage: http://www.aafeurope.com/.
[47] Fisk, W.J., D. Faulkner, J. Palonen, and O. Seppanen, Performance and costs of particle air filtration technologies. *Indoor Air*, 2002. 12(4): p. 223-234.
[48] WebPage: http://www.sawater.com.au/.
[49] Ancione, G., E. Salzano, G. Maschio, and M.F. Milazzo, Vulnerability of wastewater treatment plants to volcanic Na-Tech events. *Chemical Engineering Transactions*, 2014. 36: p. 433-438.
[50] USEPA, 2003. Wastewater Technology Fact Sheet. Screening and Grit Removal. . Document no. EPA832-F-03-011
[51] Federation, W.E., Operation of Municipal Wastewater Treatment Plant. Generic, 2007. .
[52] Metcalf & Eddy, Inc. Wastewater engineering Treatment, Disposal, and Reuse, (3rd ed.) Irwin/McGraw-Hill: Boston, US 1991; pp 1-13.
[53] Salzano, E. and A. Basco. A preliminary analysis of volcanic Na-Tech risks in the Vesuvius area. (2009).
[54] Institute, A.P., API 650. Welded steel tanks for oil storage. Standard, 1988: USA.
[55] Institution, B.S., BS 2654. Specification for manufacture of vertical steel welded storage tanks with butt-welded shells for the petroleum industry. Standard, 1984: London.
[56] Mégel, J. and J. Kliava, Metacenter and ship stability. *Am. J. Phys*, 2010. 78: p. 738-771.
[57] Kliava, J. and J. Mégel, Non-uniqueness of the point of application of the buoyancy force. *Eur. J. Phys.* , 2010. 31: p. 741-762
[58] Milazzo, M.F., G. Ancione, D.G. Lister, A. Basco, E. Salzano, and G. Maschio, Analysis of the Effects due to Ash Fallout from Mt. Etna on Industrial Installations. *Chemical Engineering Transactions*, 2012. 26: p. 123-128.
[59] Bird, R.B.S.W.E.L.E.N., Transport phenomena. (2002), New York: J. Wiley.
[60] Ergun, S., Flow through packed columns. *Chem. Eng. Progress.*, 1952. 48.
[61] Metcalf, L., H.P. Eddy, and G. Tchobanoglous, Wastewater engineering : treatment, disposal, and reuse. McGraw-Hill series in water resources and environmental engineering. (2004), New York [etc.]: McGraw-Hill.
[62] Coulson, J.M.R., J. F.; Backhurst, J. R.; Harker, J. H. , Chemical engineering: Particle technology and separation processes, (5th ed., 2002). Vol. 2. (2002), Oxford, UK 191-203.
[63] Coulson, J.M., J.F. Richardson, and J.R. Backhurst, Coulson & Richardson's Chemical Engineering: Fluid flow, heat transfer, and mass transfer (6th ed., 1999). (1999): Butterworth-Heinemann.
[64] Brown, P. and D. Lawler, Sphere Drag and Settling Velocity Revisited. *Journal of Environmental Engineering*, 2003. 129(3): p. 222-231.
[65] Zhang, J., Motion of Particles through Fluids. Study Notes, Chapter 2. Electronic Book Section.
[66] Richardson, J.F. and W.N. Zaki, Sedimentation and fluidisation: part 1. *Trans Inst Chem Eng* 1954. 32: p. 35-53.
[67] Cheng, N., Effect of Concentration on Settling Velocity of Sediment Particles. *Journal of Hydraulic Engineering*, 1997. 123(8): p. 728-731.
[68] Kothari, A.C., Sedimentation of Multisized Particles. Thesis in Chemical Engineering. Thesis, 1981 Texas Tech University.
[69] Clift, R., J.R. Grace, and E. Weber, Bubbles, Drops, and Particles. (2013): Dover Publications.
[70] WebPage: http://www.esri.com/.
[71] WebPage: http://www.library.rice.edu/.

[72] Woo, G., The mathematics of natural catastrophes. (1999): Imperial College Press.
[73] Waters, N.M., Expert Systems and Systems of Experts. Ch. 12 in Geographical Systems and Systems of Geography: Essays in Honour of William Warntz. (1988). 173-187.
[74] Johnston, K. and E.S.R. Institute, ArcGIS 9: Using ArcGIS Geostatistical Analyst. (2004): Esri Press.
[75] Bailey, T.C. and A.C. Gatrell, Interactive spatial data analysis. Vol. 413. (1995): Longman Scientific & Technical Essex.
[76] Hengl, T., G. Heuvelink, and A. Stein, A generic framework for spatial prediction of soil variables based on regression-kriging. *Geoderma*, 2004. 120(1): p. 75-93.
[77] Day, T.G. and J.E. Fisher, Mt. St. Helens: How a Wastewater Plant Coped with Its Aftermath. *Journal (Water Pollution Control Federation)*, 1980. 52(8): p. 2082-2089.
[78] Blong, R., Building damage in Rabaul, Papua New Guinea, 1994. *Bulletin of Volcanology*, 2003. 65(1): p. 43-54.
[79] Barnard, S.T., Results of a reconnaissance trip to Mt. Etna, Italy: The effects of the 2002 eruption of Etna on the province of Catania. *Bulletin of the New Zealand Society for Earthquake Engineering*, 2004. 37(2): p. 47-61.
[80] Milazzo, M.F., G. Ancione, E. Salzano, and G. Maschio, Risks associated with volcanic ash fallout from Mt.Etna with reference to industrial filtration systems. *Reliability Engineering and System Safety*, 2013. 120: p. 106-110.
[81] Branca, S. and P. Del Carlo, Eruptions of Mt. Etna During the Past 3,200 Years: a Revised Compilation Integrating the Historical and Stratigraphic Records, in *Mt. Etna: Volcano Laboratory*. (2013), American Geophysical Union. p. 1-27.
[82] Palumbo, A., Long-term forecasting of the extreme eruptions of Etna. *Journal of Volcanology and Geothermal Research*, 1998. 83(1–2): p. 167-171.
[83] WebPage: http://www.volcano.si.edu/.
[84] Scollo, S., M. Prestifilippo, G. Spata, M. D'Agostino, and M. Coltelli, Monitoring and forecasting Etna volcanic plumes. *Nat. Hazards Earth Syst. Sci.*, 2009. 9(5): p. 1573-1585.
[85] Scollo, S., P. Del Carlo, and M. Coltelli, Tephra fallout of 2001 Etna flank eruption: Analysis of the deposit and plume dispersion. *Journal of Volcanology and Geothermal Research*, 2007. 160(1–2): p. 147-164.
[86] EN779, Particulate air filters for general ventilation – Determination of the filtration performance, in *European standard* Standard, 2002.
[87] Liu, D.H.F. and L.B. G., Environmental Engineers' Handbook (2nd ed.). . 1997: p. pp 658-664.
[88] Krumbein, W.C., Size frequency distributions of sediments. *J. Sediment. Petrol.* , 1934. 4: p. 65–77.
[89] 1097-3, E., Tests for mechanical and physical properties of aggregates - Part 3: Determination of loose bulk density and voids. Standard.
[90] Brisi, C., Chimica applicata (Applied Chemistry), 2nd Edition. (1981), Italy.
[91] 2434, A.D., Standard test method for permeability of granular soils (constant head). (2006), Philadelphia, Pa.: ASTM International.
[92] Jury, W.A. and R. Horton, Soil physics. (2004): John Wiley & Sons.
[93] Grillo, F., Analisi degli effetti dovuti a deposito di cenere vulcanica su serbatoi di stoccaggio in *Dipartimento di Chimica Industriale e Ingegneria dei Materiali*. Thesis, 2011, Università di Messina.
[94] Ancione, G., E. Salzano, G. Maschio, and M.F. Milazzo, A GIS-based tool for the management of industrial accidents triggered by volcanic ash fallouts. *Journal of Risk Research*, 2014.
[95] Ancione, G., Milazzo, M. F., Salzano, E. Maschio, G. , The impact of volcanic ash fallout on industrial facilities: Natural-Technological hazards in wastewater

treatments (Grit removal), in *Volcanic Ash: Chemical Composition, Environmental Impact and Health Risks*, N.P.I. Press), Editor. (2014).

[96] Milazzo, M.F., Approaches to industrial risk assessment coupled with catastrophic natural phenomena. *Journal of Polish Safety and Reliability Association*, 2013. 4(2).

ANNEX 1

LIST OF PUBLICATIONS PRODUCED DURING THE DOCTORATE COURSE (2012-2014)

1. M.F. Milazzo, **G. Ancione**, D.G. Lister, A. Basco, E. Salzano, G. Maschio. 2012 «Analysis of the effects due to ash fallout from Mt. Etna on industrial installations». *CHEMICAL ENGINEERING TRANSACTIONS*, Vol.26, pp. 123-128. ISSN: 1974-9791. DOI:10.3303/CET1226021.

2. M.F. Milazzo, D.G. Lister, **G. Ancione**, E. Salzano, A. Basco, G. Maschio. 2012. «Potential loading damage to industrial storage tanks due to volcanic ash fallout». *NATURAL HAZARDS* (2012). ISSN: 0921-030X. DOI: 10.1007/s11069-012-0518-5.

3. M.F. Milazzo, R. Lisi, **G. Ancione**, D.G. Lister, G. Maschio. 2012. «Vulnerability maps for industrial facilities in areas with the potential volcanic ash fallout». 11th International Probabilistic Safety Assessment and Management Conference and the Annual European Safety and Reliability Conference 2012, PSAM11 ESREL 2012; Helsinki, Finland (25-29 June 2012). ISBN: 978-162276436-5

4. M.F. Milazzo, **G. Ancione**, D.G. Lister, E. Salzano, G. Maschio. 2012 «Potential damage to filtration systems due to volcanic ash fallout». 11th International Probabilistic Safety Assessment and Management Conference and the Annual European Safety and Reliability Conference 2012, PSAM11 ESREL 2012; Helsinki, Finland (25-29 June 2012). ISBN: 978-162276436-5

5. **G. Ancione**, R. Lisi, D.G. Lister, G. Maschio, M.F. Milazzo. 2012. «Mappe di vulnerabilità per apparecchiature industriali in aree soggette a ricadute di ceneri vulcaniche». Proceedings of the GRICU 2012 - Conference of the GRuppo di Ingegneria Chimica dell'Università, Montesilvano (PE), Italy (16-19 September 2012) - pp. 223-226.

6. M.F. Milazzo, **G. Ancione,** E. Salzano, G. Maschio. 2013 «Vulnerability of Industrial Facilities to Potential Volcanic Ash Fallouts». *CHEMICAL ENGINEERING TRANSACTIONS*, Vol.31, pp. 901-906. ISSN:1974-9791. DOI: 10.3303/CET1331151.

7. M.F. Milazzo, **G. Ancione,** E. Salzano, G. Maschio. 2013. «Risks associated with volcanic ash fallout from Mt. Etna with reference to industrial filtration systems» *RELIABILITY ENGINEERING & SYSTEM SAFETY*. Vol.120, pp.106-110, ISSN: 09518320 DOI: 10.1016/j.ress.2013.05.008

8. **G. Ancione**, M.F. Milazzo, E. Salzano, G. Maschio. 2013 «Semi-automatic geo-processing procedure for the vulnerability mapping of industrial facilities in areas with the potential volcanic ash fallout». *JOURNAL OF POLISH SAFETY AND RELIABILITY ASSOCIATION* SUMMER SAFETY AND RELIABILITY SEMINARS. Vol.4, Num. 1 - pp. 1-8. ISSN: 2084-5316

9. **G. Ancione**, M.F. Milazzo, E. Salzano, G. Maschio. 2013. «A GIS-tool for the vulnerability mapping of industrial facilities» Proceedings of the ESREL 2013, Annual European Safety and Reliability Conference 2013, Amsterdam, Holland (29 September – 02 October 2013). pp.1881-1888, ISBN: 9781315815596

10. M.F. Milazzo, P. Primerano, **G. Ancione**, E. Salzano, G. Maschio. 2014. «Potential Damages of Atmospheric Storage Tanks due to Volcanic Ash Aggregations in Presence of Water». *CHEMICAL ENGINEERING TRANSACTIONS*, 36, 487-492. ISSN 2283-9216 DOI: 10.3303/CET1436082

11. **G. Ancione**, E. Salzano, G. Maschio, M.F. Milazzo. 2014. «Vulnerability of Wastewater Treatment Plants to Volcanic Na-Tech Events». *CHEMICAL ENGINEERING TRANSACTIONS*, 36, 433-438. ISSN: 2283-9216 DOI: 10.3303/CET1436073

12. **G. Ancione**, E. Salzano, G. Maschio, M.F. Milazzo. 2014. «An innovative GIS-based tool for the management of industrial accidents triggered by volcanic ash fallouts». Article in Press to *JOURNAL OF RISK RESEARCH*. ISSN: 13669877 DOI: 10.1080/13669877.2014.961515

13. M.F. Milazzo, **G. Ancione**, E. Salzano, G. Maschio. 2014. «Study of volcanic Na-Tech risks in primary wastewater treatments». Safety and Reliability: Methodology and Applications - Proceedings of the European Safety and Reliability Conference, ESREL 2014, pp. 1453-1461, Wroclaw, Poland, (14-18 September 2014). ISBN: 978-113802681-0

14. **G. Ancione**, M.F. Milazzo, G. Maschio. 2014. «The use of geoevents in the risk management of wastewater treatments». Safety and Reliability: Methodology and Applications - Proceedings of the European Safety and Reliability Conference, ESREL 2014, pp. 1431-1438, Wroclaw, Poland, (14-18 September 2014). ISBN: 978-113802681-0

15. M.F. Milazzo, **G. Ancione**, P. Primerano, E. Salzano, G. Maschio, 2014. «The impact of volcanic ash fallout on industrial facilities: Natural-Technological hazards in wastewater treatments (Part I - Screening processes)» Chapter in Press in *VOLCANIC ERUPTIONS: TRIGGERS, ROLE OF CLIMATE CHANGE AND ENVIRONMENTAL EFFECTS*, Nova publication.

16. **G. Ancione**, P. Primerano, E. Salzano, G. Maschio, M.F. Milazzo, 2014. «The impact of volcanic ash fallout on industrial facilities: Natural-Technological hazards in wastewater treatments (Grit removals)» Chapter in Press in *VOLCANIC ASH: CHEMICAL COMPOSITION, ENVIRONMENTAL IMPACT AND HEALTH RISKS*, Nova publication.

17. M.F. Milazzo, **G. Ancione,** P. Primerano, E. Salzano, G. Maschio, 2015 «Na-Tech in Wastewater Treatments due to Volcanic Ash Fallout: Characterisation of the Parameters Affecting the Screening Process Efficiency». *CHEMICAL ENGINEERING TRANSACTIONS*, proceeding of iCheap12 – 12th International Conference on Chemical and Process Engineering, Milan, Italy (19-22 May, 2015).

18. **G. Ancione,** M.F. Milazzo, R. Lisi, G. Maschio, 2015. «Consequences of liquid tank explosions caused by lava flow». *CHEMICAL ENGINEERING TRANSACTIONS*, proceeding of iCheap12 – 12th International Conference on Chemical and Process Engineering, Milan, Italy (19-22 May, 2015).

19. **G. Ancione,** M.F. Milazzo, E. Salzano, G. Maschio, 2015. «An overview of the methodologies to study Na-Tech events triggered by volcanic ash fallouts». Submitted to the ESREL 2015, The annual European Safety and Reliability Conference, Zürich, Switzerland (7-10 September, 2015).

ANNEX 2

TABLES

TABLE 4.1. AIR FILTER CLASSIFICATION (EN779:2012)..... 22

TABLE 4.2. CLASSIFICATIONS OF HIGH-EFFICIENCY FILTERS. 23

TABLE 4.3. DRAG AND TERMINAL SETTLING VELOCITY EQUATIONS [20]. 35

TABLE 4.4. K PARAMETER AND REGIME FLOW REGIONS. 36

TABLE 6.1. FINE SCREEN CHARACTERISTICS..... 51

TABLE 6.2. HORIZONTAL GRIT REMOVAL CHAMBER CHARACTERISTICS [87]. 52

TABLE 7.1. PROPERTIES OF BEDS OF SOME REGULAR-SHAPED MATERIALS [62]. 56

TABLE 8.1. DIAMETER OF PARTICLES (DRY SAMPLES). 60

TABLE 8.2. ASH DENSITIES..... 60

TABLE 8.3. SPECIFIC SURFACE AREA. 61

TABLE 8.4. WEIGHTED VALUES FOR S AND E FOR SAMPLE ID 1 AND 3. 61

TABLE 8.5. THRESHOLD LIMITS FOR DAMAGE TO A FIXED ROOF TANK 64

TABLE 8.6. CHARACTERISTICS AND FLOATATION STABILITY FOR THE IMMERSION IN WATER OF TWO LABORATORY BEAKERS AND THE MODEL FLOATING ROOF..... 64

TABLE 8.7. THRESHOLD LIMITS FOR SINKING AND CAPSIZING FOR THE MODEL DOUBLE DECK FLOATING ROOF. 66

TABLE 8.8. REYNOLDS NUMBERS AND REGIME FLOW (USING WEIGHTED S AND E)..... 77

TABLE 8.9. REYNOLDS NUMBERS AND REGIME FLOW (USING AVERAGE, MINIMUM AND MAXIMUM S). 78

TABLE 8.10. REYNOLDS NUMBERS AND REGIME FLOW (USING LITERATURE DATA FOR E). 78

TABLE 8.11. WEIGHTED AVERAGE CRITICAL THICKNESSES OF ASH DEPOSIT (USING WEIGHTED S AND E)..... 79

TABLE 8.12. THICKNESS OF ASH DEPOSIT (USING AVERAGE, MINIMUM AND MAXIMUM S). 80

TABLE 8.13. THICKNESS OF ASH DEPOSIT (USING LITERATURE DATA FOR E). 81

TABLE 8.14. TERMINAL SETTLING VELOCITY FOR THE SAMPLE ID 1 OF VOLCANIC ASH. 82

TABLE 8.15. TERMINAL SETTLING VELOCITY FOR THE SAMPLE ID 2 OF VOLCANIC ASH. 82

TABLE 8.16. TERMINAL SETTLING VELOCITY FOR THE SAMPLE ID 3 OF VOLCANIC ASH 82

TABLE 8.17. FRACTION OF REMOVED PARTICLES. 86

ANNEX 3

FIGURES

FIGURE 2.1. REPRESENTATION OF A VOLCANO [28]..... 7
FIGURE 2.2. VOLCANIC ACTIVITY TYPES [29]..... 8
FIGURE 2.3. VOLCANIC EXPLOSIVITY INDEX (VEI) SCHEME [32]. 9
FIGURE 2.4 EXAMPLE OF HOW A VOLCANIC ERUPTION CAN GENERATE A TSUNAMI.[38]..... 12
FIGURE 3.1. FLOW-SHEET FOR VULNERABILITY REPRESENTATION 16
FIGURE 3.2. QUANTITATIVE RISK ASSESSMENT 17
FIGURE 3.3. FLOW-CHART OF THE EXTENDED QRA PROCEDURE 18
FIGURE 4.1. (A) CONE ROOF, (B) DOME ROOF, (C) HANGING ROOFS, (D) UMBRELLA ROOF, (E,F) FIXED ROOFS (DOME OR CONE) WITH INTERNAL FLOATING ROOF..... 20
FIGURE 4.2. SECTION OF A GENERIC FLOATING ROOF TANKS. 21
FIGURE 4.3. AIR FILTER SYSTEM 22
FIGURE 4.4. WASTEWATER TREATMENT PLANT (ADAPTED FROM [48]). 24
FIGURE 4.5. COARSE SCREEN. 26
FIGURE 4.6. HORIZONTAL FLOW GRIT CHAMBERS. 27
FIGURE 4.7. THE FLOATING BODY 29
FIGURE 4.8. TERMINAL SETTLING VELOCITY AS A FUNCTION OF THE PARTICLE'S DIAMETER 36
FIGURE 4.9. RECTANGULAR SETTLING VESSEL. 38
FIGURE 5.1. GEOPROCESSING TOOLS [71]. 41
FIGURE 5.2. FLOWCHART OF THE DEVELOPED SEMI-AUTOMATIC PROCEDURE. 44
FIGURE 5.3. SCHEME OF THE PROPOSED METHODOLOGY FOR THE EMERGENCY MANAGEMENT. 45
FIGURE 6.1 LOCATION OF MT. ETNA (ITALY) AND MAIN CRATERS 47
FIGURE 6.2. CENSUS OF INDUSTRIES AT MAJOR RISK AND POWER PLANTS. 48
FIGURE 6.3. CENSUS OF WASTEWATER TREATMENT PLANTS. 49
FIGURE 6.4. VISCOSITY (BLACK LINE) AND DENSITY (RED LINE) OF THE DUSTY GAS VS. ASH CONCENTRATION (A) SCENARIO 1 AND (B) SCENARIO 2..... 50
FIGURE 6.5. SQUARE OPENING FINE SCREEN. 51
FIGURE 6.6. LOCATIONS OF THE COLLECTED ASH SAMPLES..... 53
FIGURE 7.1. PERMEAMETER AT CONSTANT HEAD. 57
FIGURE 8.1. SIZE DISTRIBUTION FOR SAMPLE ID 1. 58

FIGURE 8.2. SIZE DISTRIBUTION FOR SAMPLE ID 2. 59

FIGURE 8.3. SIZE DISTRIBUTION FOR SAMPLE ID 3. 59

FIGURE 8.4. SPECIFIC SURFACE AREA WITH RESPECT TO THE CLASS OF PARTICLES' SIZE. 62

FIGURE 8.5. VOIDAGE WITH RESPECT TO THE CLASS OF PARTICLES' SIZE. 62

FIGURE 8.6. VARIATION OF THE HEIGHT OF THE ASH DEPOSIT WITH RESPECT TO THE IMMERSION DEPTH FOR DIFFERENT LIQUID AND ASH DENSITIES. DEPTH OF THE ASH DEPOSIT TO SINK THE FLOATING ROOF FOR ρ_{LIQ} = 1,000 KG M^{-3}: (A) ρ_{ASH} = 1,000 KG M^{-3} (C) ρ_{ASH} = 2,000 KG M^{-3} AND ρ_{LIQ} = 800 KG M^{-3}: (B) ρ_{ASH} = 1,000 KG M^{-3} (D) ρ_{ASH} = 2,000 KG M^{-3}. THE RIGHT ORDINATE SHOWS THE RATIO M_{ASH}/M_{ROOF} FOR (E) ρ_{LIQ} = 1,000 KG M^{-3} AND (F) ρ_{LIQ} = 800 KG M^{-3} [93]. 65

FIGURE 8.7. POTENTIAL FAILURE MODES FOR FLOATING ROOF TANKS: (A) PARTIAL IMMERSION OF THE ROOF LEADING TO A RELEASE OF A LIQUID QUANTITY EQUAL TO ONE-FOURTH OF THE VOLUME OF THE ROOF, (B) ROOF SINKING AND (C) ROOF CAPSIZING. 66

FIGURE 8.8. EXCEEDANCE PROBABILITY AS A FUNCTION OF ASH LOAD. 68

FIGURE 8.9. EXCEEDANCE PROBABILITY AND THE TIME OF CLOGGING AS A FUNCTION OF ASH CONCENTRATION. 68

FIGURE 8.10. SPATIAL DISTRIBUTION OF POINTS. 70

FIGURE 8.11. VULNERABILITY MAP FOR LIGHT DAMAGE OF FIXED ROOF TANKS (INVERSE DISTANCE WEIGHTING APPROACH). 71

FIGURE 8.12. VULNERABILITY MAP FOR LIGHT DAMAGE OF FIXED ROOF TANKS (KRIGING APPROACH). 72

FIGURE 8.13. VULNERABILITY MAP FOR FILTERS' PARTIAL CLOGGING (INVERSE DISTANCE WEIGHTING APPROACH). 73

FIGURE 8.14. VULNERABILITY MAP FOR FILTERS' PARTIAL CLOGGING (KRIGING APPROACH). 74

FIGURE 8.15. VALIDATION OF PREDICTIONS FOR VULNERABILITY MAPS RELATED TO LIGHT DAMAGE OF FIXED ROOF TANKS: (A) IDW METHOD AND (B) KRIGING METHOD. 75

FIGURE 8.16. VALIDATION OF PREDICTIONS FOR VULNERABILITY MAPS RELATED TO PARTIAL CLOGGING OF FILTERS: (A) IDW METHOD AND (B) KRIGING METHOD. 75

FIGURE 8.17. ERROR ESTIMATION FOR PREDICTIONS RELATED TO LIGHT DAMAGE OF FIXED ROOF TANKS: (A) IDW METHOD AND (B) KRIGING METHOD. 76

FIGURE 8.18. ERROR ESTIMATION FOR PREDICTIONS RELATED TO PARTIAL CLOGGING OF FILTERS: (A) IDW METHOD AND (B) KRIGING METHOD. 77

FIGURE 8.19. HEAD LOSSES FOR FINE SCREENS VS. STREAM VELOCITY. 79

FIGURE 8.20. CRITICAL THICKNESSES OF ASH DEPOSIT WITH RESPECT TO THE PARTICLES' DIAMETER FOR (USING WEIGHTED S AND E). 80

FIGURE 8.21 TERMINAL SETTLING VELOCITY OF VOLCANIC ASH PARTICLES VERSUS PARTICLES' DIAMETER. 83

FIGURE 8.22. WEIGHT FRACTION REMAINING AT EACH SIEVE VERSUS TERMINAL SETTLING VELOCITY OF PARTICLES..... 84

FIGURE 8.23 FRACTION OF ASH WITH SETTLING VELOCITY LESS THAN $U_{T,P}$ VERSUS SETTLING VELOCITY (SAMPLE ID 1)..... 84

FIGURE 8.24. FRACTION OF ASH WITH SETTLING VELOCITY LESS THAN $U_{T,P}$ VERSUS SETTLING VELOCITY (SAMPLE ID 2)..... 85

FIGURE 8.25. FRACTION OF ASH WITH SETTLING VELOCITY LESS THAN $U_{T,P}$ VERSUS SETTLING VELOCITY (SAMPLE ID 3)..... 85

ANNEX 4

SYMBOLS

Symbol	Parameter
A_D	projected area of the particle in the flow direction
A_f	area of submerged screen
A_{gr}	cross section of the horizontal grit chamber
Am	average filter Arrestance
A_{pm}	cross section of the porous medium
A_s	effective open area of submerged screen
A_{tot}	cross-sectional area
B	centre of buoyancy
b_1	Bar spacing for the fine screen
b_2	Bar thickness for the fine screen
c	ash concentrations
C	opening size for the fine screen
C_D	drag coefficient
C_{disch}	coefficient of discharge for the fine screen
C_p	concentration of particle
d	reference particle's diameter (size) for the grain class
D_{eq}	equivalent diameter of the pore space
d_f	average equivalent diameter of the filter
d_i	distance between the i-th point and S_o
d_o	reference diameter for the particle
d_p	particle's diameter
e	voidage or porosity
Em	average filter Efficiency
e_w	weighted average voidage
ϕ	Krumbein parameter
G	centre of gravity
g	gravity acceleration
g	gravitational constant
GIS	Geographic Information System
G_o	specific mass flow rate of the dusty gas
h	height of ash deposit
H_v	vessel height
I	moment of inertia of the body

k	constant for the permability
K	parameter for the identification of the flow regime of a particle settling in a liquid
k_i	intrinsic permeability
L	lenght of the filtering surface
l	thickness of the porous medium
l_1	thickness of the ash deposit causing a pressure drop equal to ΔP_1
l_2	thickness of the ash deposit causing a pressure drop equal to ΔP_2
L_{pm}	length of the porous medium
L_v	vessel length
M	metacentre
M1	threshold limit of ash deposit causing a partial clogging of the filter
M2	threshold limit of ash deposit causing the rupture of the filter
M_{ash}	ash mass
m_{ash}	mass of ash deposit on the filter surface
M_{beaker}	beaker mass
MPPS	Most Penetrating Particle Size
M_{roof}	floating roof tank mass
n	empirical exponent dependent on Re
N	number of locations used for the estimation
$p(y)$	probability distribution of y
$p(y\|x)$	probability of occurence of y conditioned by the occurence of x
P_L	final pressure drop on the filtering surface
P_o	initial pressure drop on the filtering surface
Q	volumetric flow rate
Q_e	volcanic emission flow rate
QRA	Quantitative Risk Analysis
R	radius of the floating roof tank
R'	component of the drag force per unit area of particle surface in the direction of motion
Re	Reynolds number
S	specific surface area
S	filtering surface
S_1	specific surface area for Sample ID 1
S1	load threshold limit for light damage of the fixed roof
S_2	specific surface area for Sample ID 2
S2	load threshold limit for structural damage of the fixed roof
S_3	specific surface area for Sample ID 3
S3	load threshold limit for the collapse of the fixed roof
S_{av}	avarage specific surface area (calculated using the weighted average diameter)

S_{BET}	specific surface area measured with the BET method
S_{max}	maximum specific surface area (calculated using the minimum diameter)
S_{min}	minimum specific surface area (calculated using the maximum diameter)
S_o	predicition point
S_w	weighted average specific surface area
t	time
T1	load threshold limit for the partial immersion of a floating roof
T2	load threshold limit for thefloating roof sinking
T3	load threshold limit for the floating roof capsizing
t_o	retention time in vessel
u	average velocity
U_1	vertical opening distance for the fine screen
U_2	horizontal opening distance for the fine screen
u_f	sewage velocity
u_l	average velocity through the pore channels
u_o	critical settling velocity
u_s	the settling velocity
u_t	terminal settling velocity
$u'_{t,\mathrm{p}}$	final settling velocity of the particle
$u_{t,p}$	terminal settling velocity of a particle with a diameter d_p
$u_{t,p\|Cp}$	terminal settling velocity in hindered condition
V	vessel's volume
V_{disp}	volume of displaced liquid
VEI	Volcanic Explositivity Index
V_{imm}	immersed volume
v_o	velocity of the *dusty-gas* at the inlet
V_p	effective volume of the particle
V_{water}	volume of water collected during the time *t*
w_i	weight coefficient for the measured value at the i-th location
W_v	vessel width
WWT	Waste Water Treatment
x	indipendent variable
X	fraction of particles with less than the stated velocity
X_o	fraction particles with $u_{t,p} \leq u_o$
X_r	fraction removed of particles with a terminal settling velocity less than u_o or equal to u_o
$X_{r,total}$	total fraction of removed particles
X_w	weight fraction of ash sample remaining to a sieve
y	dipendent variable

Y	notation for the probability
$z_{(Si)}$	measured value of the variable at the i-th location
$z_{(So)}$	value to be predicted associated with the location S_o
z_B	height of the buoyancy centre
z_M	metacentre height
δ	depth of the floating roof tank
Δh	head load
δ_{imm}	depth of immersion
ΔP	pressure drop
ΔP_1	pressure drop for the dirty screen
ΔP_2	pressure drop for the very dirty screen
ΔP_o	initial screen's pressure drop
δ_{roof}	immersion depth of the floating roof tank in the absence of ash
ε	filter void fraction
λ_i	weight assigned to each measured value at the i-th location
μ	viscosity
π	pi greco constant
ρ	density
ρ_{ash}	ash density
ρ_{liquid}	liquid density
$\rho_{loose\ bulk}$	density of not compressed dried particles
ρ_s	particle density
ρ_{solid}	density of particles without inter-particles void